Title

The role of hepatic mitochondrial biliverdin exporter ABCB10 in non-alcoholic fatty liver disease (NAFLD) and alcoholic liver disease (ALD)

Author

Gutierrez, Vincent Manuel

Publication Date

2023

Peer reviewed|Thesis/dissertation

UNIVERSITY OF CALIFORNIA

Los Angeles

The role of hepatic mitochondrial biliverdin exporter ABCB10 in non-alcoholic fatty liver disease (NAFLD) and alcoholic liver disease (ALD)

A dissertation submitted in partial satisfaction of the requirements for the degree Doctor of Philosophy in Molecular, Cellular, and Integrative Physiology

by

Vincent Manuel Gutierrez

2023

ABSTRACT OF THE DISSERTATION

The role of hepatic mitochondrial biliverdin exporter ABCB10 in hepatic non-alcoholic fatty liver disease (NAFLD) and alcoholic liver disease (ALD)

by

Vincent Manuel Gutierrez

Doctor of Philosophy in Molecular, Cellular, and Integrative Physiology

University of California, Los Angeles, 2023

Professor Orian Shirihai, Chair

Non-alcoholic fatty liver disease (NAFLD) and alcoholic liver disease (ALD) are both characterized by altered mitochondrial respiratory capacity, steatosis, increased oxidative stress, and inflammation. ATP-binding cassette B10 (ABCB10) is an inner mitochondrial membrane protein that has been shown to participate in redox protection in hematopoietic cells and cardiomyocytes. While it is highly expressed in the liver, it is unknown if ABCB10 has a role in pathogenesis of NAFLD or ALD. Here I address these gaps in knowledge by first describing ABCB10 transport cargo. We find that ABCB10 exports the heme by-product biliverdin (BV) for subsequent reduction to lipophilic antioxidant bilirubin (BR), confirming the mechanism by which ABCB10 exerts antioxidant activity. Moreover, we find that ABCB10 content is differentially altered in

NAFLD versus ALD. Here, I describe how increased hepatic ABCB10 promotes NAFLD by decreasing mitochondrial respiration and promoting redox-mediated insulin resistance, both of which lead to hepatosteatosis. Conversely, severe alcoholic hepatitis in mice and patients results in decreased hepatic ABCB10 content. However, hepatic ABCB10 in both mild alcoholic steatohepatitis (ASH) and severe AH does not exert similar effects on mitochondrial respiration and steatosis as in NAFLD. Here I demonstrate that hepatic ABCB10 is not the pivot point which determines progression of ALD nor is it determinative of hepatic mitochondrial respiratory function in ASH or AH but rather mitigates the formation of hepatotoxic neutrophil extracellular traps (NETs) in severe ALD. Future research understanding the role of ABCB10-mediated BR generation and its role redox signaling/homeostasis can provide novel therapeutic approaches to treating liver disease.

ABCB10 exports mitochondrial biliverdin, driving metabolic maladaptation in obesity

While the impact of hydrophilic antioxidants on hepatic insulin resistance and non-alcoholic fatty liver disease (NAFLD) is well understood, the function of lipophilic antioxidants in these conditions is not as clear. Bilirubin, a lipophilic antioxidant known for scavenging hydrogen peroxide (H2O2), undergoes oxidation to biliverdin within mitochondria. This biliverdin is then exported to the cytosol and reduced back to bilirubin by cytosolic biliverdin reductase (BLVRA). The process of biliverdin export from mitochondria is crucial for the regeneration of bilirubin and its role in intracellular H2O2 scavenging. Our research identified ABCB10 as the transporter responsible for exporting biliverdin from mitochondria. We observed that ABCB10 assists in

transporting biliverdin and that its deletion leads to biliverdin build-up inside mitochondria. In mice, obesity and insulin resistance were found to increase ABCB10 expression in the liver, boosting both cytosolic and mitochondrial bilirubin levels in an ABCB10-dependent way. Surprisingly, deleting ABCB10 in the livers of obese mice led to protection against steatosis and high blood sugar. This was accompanied by improved insulin regulation of glucose production and reduced expression of the lipogenic enzyme SREBP-1c. This protective effect correlated with better mitochondrial performance and increased deactivation of PTP1B, an enzyme that interferes with insulin signaling and boosts SREBP-1c expression. Reintroducing bilirubin in ABCB10 knockout hepatocytes negated these beneficial effects, highlighting bilirubin's detrimental role associated with ABCB10 activity. Therefore, we've uncovered a vital transport mechanism that magnifies the effects of intracellular bilirubin in insulin resistance and steatosis during obesity.

The mitochondrial biliverdin exporter ABCB10 mitigates the formation of neutrophil extracellular traps in alcoholic hepatitis

Effective treatment for acute liver failure due to alcoholic hepatitis (AH) is currently limited to liver transplantation. AH-affected livers exhibit a distinct molecular pattern, marked by impaired redox metabolism in hepatocytes and the presence of neutrophils that produce myeloperoxidase (MPO) and create neutrophil extracellular traps (NETs). Enhanced NET formation and MPO activity are known to aggravate liver damage in AH, both in mice and as a predictor of poor outcomes in human patients. Understanding the mechanisms that inappropriately trigger NET formation in the liver could lead to new treatments for AH. It

remains uncertain if the redox imbalances in AH hepatocytes directly promote NET formation. Our research indicates that in AH, both human and mouse livers show reduced levels of the mitochondrial biliverdin exporter ABCB10, which is essential for producing the ROS-neutralizing agent bilirubin within hepatocytes. We found that increasing ABCB10 expression in the hepatocytes of mice with AH effectively reduced MPO gene expression and histone H3 citrullination, an indicator of NET formation. This anti-inflammatory action appears to be due to ABCB10’s role in lessening ROS-induced effects in the liver. Specifically, increasing ABCB10 activity led to a decrease in hepatic 4-HNE protein adducts without notably impacting mitochondrial fat metabolism or reducing steatosis and hepatocyte death. Therefore, our findings suggest that ABCB10's role in managing ROS within hepatocytes can alleviate the harmful activation of neutrophils to form NETs in AH. Enhancing ABCB10 function in hepatocytes might thus reduce acute liver failure in humans by curbing the inflammatory response triggered by excessive NET formation.

The dissertation of Vincent Gutierrez is approved.

Ambre Marguerite Bertholet

Anthony J. Covarrubias

Aldons J. Lusis

Marc Liesa-Roig

Orian S. Shirihai, Committee Chair

University of California, Los Angeles

2023

DEDICATION

I would like to dedicate this work to:

My parents Cynthia and Martin Gutierrez, my sister Alexandria Gutierrez, my brother Xavier for their understanding throughout my lengthy academic journey

My partner Kelli Malott for her patience and caring during our graduate school adventures

Our dogs (Xochi, Gordie, and Keanu) for all their unconditional love

TABLE OF CONTENTS

LIST OF FIGURES AND TABLES

ACKNOWLEDGMENTS

I would like to thank my mentor Marc Liesa for his time, insight and expertise in thoughtfully planning experiments, discussions how to interpret data, and advice on how to be an effective communicator. He taught me that data doesn't have emotions, that what is more important than your hypothesis being right or wrong is learning how to read what the data is telling you. I'm proud to share a piece of this scientific journey together.

I would like to thank my co-mentor, Orian Shirihai, for his guidance and support. Though we had long lab meetings, I am grateful for the time and dedication he displayed to get us to be creative but logical, showing us how to use literature, our own expertise, and the skillsets in the lab to identify important gaps in knowledge as well as novel methods of testing these hypotheses. I'm especially grateful for the open and collaborative environment he has fostered not only within the lab but within the theme space.

Lastly, I would like to thank all the members of the Shirihai/Liesa lab, for all their insight, advice, laughs, and memories, which have made training in the lab such a fruitful experience.

Published work included in this thesis

Chapter one is from Shum et al. ABCB10 exports mitochondrial biliverdin, driving metabolic maladaptation in obesity. *Sci Transl Med* 2021; 13(594), DOI: 10.1126/scitranslmed.abd1869

Chapter 2 is adapted from Gutierrez et al. The mitochondrial biliverdin exporter ABCB10 mitigates the formation of neutrophil extracellular traps in alcoholic hepatitis. Redox Biology (submitted).

Author contributions - V.G. Conceptualization; formal analysis; validation; investigation; methodology; writing – original draft; writing – review and editing. D.K.V. formal analysis; validation; investigation. M.S. formal analysis; supervision; validation; investigation; methodology. Q.Y. methodology. O.S.S. supervision. H.T. methodology; supervision. M.L. Conceptualization; resources; funding acquisition; supervision; formal analysis; validation; investigation; methodology; writing – original draft; writing – review and editing;

CURRICULUM VITAE

Education

INSTITUTION AND LOCATION	DEGREE	Completion Date MM/YYYY	FIELD OF STUDY
Salisbury University, Salisbury, MD	B.S	06/2012	Exercise Science

Positions and Employments:

2008-2012 Undergraduate Research Assistant in Dr. Scott Mazzetti's Lab, Department of Exercise Science, Salisbury University, Salisbury, MD

2010-2010 Summer Research Assistant in Dr. Yisang Yoon's Lab, Summer Scholars Research Program, University of Rochester, Rochester, NY

2011-2011 Summer Research Assistant in Dr. Orian Shirihai's Lab, Graduate Medical Sciences Summer Undergraduate Research Program, Boston University, Boston, MA

2012-2015 Intramural Research Training Award (IRTA) Postbaccalaureate Fellow in Dr. Rafael deCabo's Lab, Translational Gerontology Branch, National Institute on Aging, Baltimore, MD

Since 2019 Graduate Student, Department of Molecular, Cellular, and Integrative Physiology, University of California, Los Angeles

Other Experience and Professional Memberships:

2020 Organizer, UCLA Mitochondria Symposium
2021 Student Member,
2021 Student Member,

Honors:

2012 Outstanding Contribution to Student Life – Salisbury University Office of Student Activities, Organizations, and Leadership
2013 Scientific Director's Award Postbaccalaureate Poster Day (NIH/NIA)
2013 Outstanding Poster Award - NIH Postbaccalaureate Poster Day 2013
2013 American Aging Association Student Data Blitz – 3rd Place

2020 22nd SoCal Center for ALPD & Cirrhosis Symposia – Best Abstract Award

Publications (in reverse chronological order)

Ngo J, Choi DW, Stanley IA, Stiles L, Molina AJ, Chen P, Lako A, Han Sung IC, Goswami R, Kim M, Miller N, Baghdasarian S, Kim-Vasquez D, Jones AE, Roach B, **Gutierrez V**, Erion K, Divakaruni AS, Liesa M, Danial NN, Shirihai OS. Mitochondrial morphology controls fatty acid utilization by changing CPT1 sensitivity to malonyl-CoA. *EMBO J.* 2023;42(11):e111901.

Shum M, Shintre C, Althoff T, **Gutierrez V**, Segawa M, Saxberg AD, Martinez M, Adamson R, Young MR, Faust B, Gharakhanian R, Su S, Krishnan, KC, Mahdaviani, K, Veliova, M, Wolf DM, Ngo J, Nocito L, Stiles L, Abramson J, Lusis AD, Hevener, AL, Zhogbi ME, Carpenter EP, Liesa M. Export of mitochondrial biliverdin in liver drives metabolic maladaptation in obesity. *Sci Transl Med*. 2021;13(594):eabd1869.

Palliyaguru DL, Teixeira CVL, Duregon E, di Germanio C, Alfaras I, Mitchell SJ, Navas-Enamorado I, Shiroma EJ, Studenski S, Bernier M, Camandola S, Price NL, Ferrucci L, de Cabo R, **SLAM Investigators**. Study of Longitudinal Aging in Mice: Presentation of Experimental Techniques (SLAM POET). *J Gerontol A Biol Sci Med Sci*. 2020;76(4):552-560.

Bernier M, Mitchel SJ, Singh A, Price N, Diaz A, Wahl D, Ali A, Petr M, Cai H, Warren A, Kaiser T, Wang M, Zhang J, Zhang L, Wang Y, Mach J, **Guiterrez VM,** Navas-Enamorado I, Kim EY, Zhang Y, Becker K, Lakatta E, Egan J, Le Couteur D, Cogger V, Fernandez-Hernando C, Cuervo AM, de Cabo R. Disulfiram Treatment Normalizes Body Weight in Obese Mice. *Cell Metab.* 2020;32(2):203-214.e4.

Mitchell SJ, Madrigal-Matute J, Scheibye-Knudsen M, Fang E, Aon M, González-Reyes JA, Cortassa S, Kaushik S, Gonzalez-Freire M, Patel B, Wahl D, Ali A, Calvo-Rubio M, Burón MI, **Guiterrez V**, Ward TM, Palacios HH, Cai H, Frederick DW, Hine C, Broeskamp F, Habering L, Dawson J, Beasley TM, Wan J, Ikeno Y, Hubbard G, Becker KG, Zhang Y, Bohr VA, Longo DL, Navas P, Ferrucci L, Sinclair DA, Cohen P, Egan JM, Mitchell JR, Baur JA, Allison DB, Anson RM, Villalba JM, Madeo F, Cuervo AM, Pearson KJ, Ingram DK, Bernier M, and de Cabo R. Effects of Sex, Strain, and Energy Intake on Hallmarks of Aging in Mice. *Cell Metab.* 2016;23(6):1093-1112.

Martin-Montalvo A, Sun Y, Ali A, **Gutierrez V**, Palacios HH, Curtis JM, Siendones E, Ariza J, Abulwerdi G, Sun X, Pearson KJ, Fishbein KW, Spencer RG, Wang M, Han X, Scheibye-Knudsen M, Baur JA, Navas P, Villalba JM, Bernier M, de Cabo R. Cytochrome b_5 reductase and the control of lipid metabolism and healthspan. *NPJ Aging Mech Dis*. 2016;2:16006.

Ortega-Molina A, Lopez-Guadamillas E, Mattison JA, Mitchell SJ, Muñoz-Martin M, Iglesias G, **Gutierrez VM,** Vaughan KL, Szarowicz MD, Cebrián D, Martinez S, Pastor J, de Cabo R, and Serrano M. Pharmacological inhibition of PI3K reduces adiposity and metabolic syndrome in obese mice and rhesus monkeys. *Cell Metab.* 2015;21(4):558-570.

INTRODUCTION

Heme function and metabolism

Heme is an essential and complex molecule with a critical role in oxygen transport, cellular respiration, and enzymatic reactions. It is a vital component of hemoglobin, myoglobin, and many enzymes involved in redox reactions and cellular respiration. Heme is a cyclic, organic molecule consisting of a porphyrin ring at its core. This porphyrin ring contains four nitrogen atoms coordinated with a central iron (Fe) atom. The iron atom can exist in two oxidation states: ferrous (Fe^{2+}) and ferric (Fe^{3+})[1].

Heme is a critical component of oxygen transport via hemoglobin, a protein found in red blood cells. Hemoglobin binds to oxygen in the lungs and carries oxygen throughout the body. The iron atom at the center of the heme molecule can reversibly bind to oxygen. When oxygen binds to heme, it forms oxyhemoglobin. This enables the efficient transport of oxygen from the respiratory system to cells, where it is needed for energy production through aerobic respiration. In addition to hemoglobin, heme is also found in myoglobin, a protein primarily found in muscle tissue. Myoglobin acts as an oxygen reservoir (oxymyoglobin) in muscles, storing oxygen and releasing it when needed during periods of increased oxygen demand, such as during physical activity[1].

Heme is also a cofactor for several inactive apo-heme proteins that are converted to active hemoproteins when heme is incorporated. The ability of the iron core at the center of heme to change oxidation states, allows these hemoproteins to participate in oxido-reducing reactions[2]. While hemoglobin and myoglobin are used to transport and store oxygen, hemoproteins are used for a wide array of biological

functions. Cytochrome P450 enzymes play a crucial role in detoxification of drugs, xenobiotics, and endogenous compounds in the liver. In addition, heme is used in both catalases and peroxidases, which are responsible for breaking down hydrogen peroxide (H_2O_2) into water and oxygen, protecting cells from oxidative damage caused by excess hydrogen peroxide[3]. Nitric oxide synthase (NOS) enzymes also use heme to produce nitric oxide (NO), a signaling molecule involved in regulating blood vessel dilation and neurotransmission[4]. Finally, heme-containing proteins are integral components of the electron transport chain (ETC) in mitochondria, where they participate in the transfer of electrons during cellular respiration to produce adenosine triphosphate (ATP), the cell's primary source of energy[5].

In addition to being a site of high concentration of hemoproteins, the mitochondria also serve as the site of heme biosynthesis[5]. Heme biosynthesis occurs primarily in the liver and bone marrow in humans and involves multiple enzymatic reactions. Biosynthesis begins with the condensation of succinyl-CoA and glycine, a reaction catalyzed by the enzyme δ-aminolevulinate synthase (ALAS), the rate-limiting enzyme in heme production. This reaction results in the formation of δ-aminolevulinic acid (ALA). Intermediary steps involve the assembly of the porphyrin ring and the incorporation of iron into the ring. Once heme is synthesized, it can be incorporated into hemoglobin, myoglobin, and other hemoproteins. It is important to note that the regulation of heme biosynthesis is tightly controlled to ensure that de novo heme production is proportional to the demand of de novo hemoproteins. This is achieved through transcriptional regulation of heme biosynthetic and degradative enzymes via heme response elements (HREs)[6]. These motifs are located in enhancer regions and

have been shown to bind heme. HREs have also been shown to contain an antioxidant response element (ARE) binding motif, allowing for co-regulation by NF-E2 transcription factors (NF-E2, Nrf2, Nrf2)[7]. NF-E2 transcription factors have been shown to coordinate the expression of cytoprotective genes involved in antioxidant defense, phase II detoxification, and xenobiotic stress during oxidative insult.

While heme has many beneficial functions, heme excess can induce cellular damage via the formation of ROS. Heme is normally sequestered within hemoglobin in red blood cells, myoglobin in muscle cells, and within various hemoproteins as previously described[1,2]. Sources of unbound, labile heme include: excess de novo synthesis or oxidative-stress induced liberation from hemoproteins[3]. Free heme provides an abundance of redox-active iron. This free iron is highly reactive and can participate in Fenton and Haber-Weiss reactions, interacting with hydrogen peroxide (H_2O_2), leading to the production of free radicals like superoxide anion (O_2•−) and hydroxyl radicals (•OH). Excessive ROS production overwhelms antioxidant defense systems, which include enzymes like catalase, superoxide dismutase, glutathione peroxidase, and thioredoxin[8]. These enzymes act as secondary antioxidants by converting hydroperoxides into stable, non-radical by-products. Primary antioxidants are molecules that act to scavenge ROS, which includes Vitamins C and E in addition to minerals like Selenium and Zinc[8]. Lipid-soluble Vitamins C and E are components of the plasma membrane redox system responsible for extracellular electron transfer[9]. Zinc is required for antioxidant enzyme superoxide dismutase to detoxify singlet oxygen radials and can inhibit ROS-generating NADPH oxidases[10,11]. Selenium is a necessary component of antioxidant selenoproteins glutathione peroxidase and thioredoxin[12].

When these defense mechanisms are unable to neutralize the excess ROS, oxidative stress can lead to a range of deleterious cellular consequences. Lipophilic heme can intercalate into the phospholipid bilayer, where redox-active iron can catalyze the formation of lipid peroxides leading to increased membrane permeability and subsequent lytic cell death[13,14]. Heme-induced oxidative stress can also alter proteins via oxidative post-translational modifications (OPTMs)[15]. While some OPTMs are reversible (like sulfenation, nitrosylation, and gluathionylation), abundant oxidative stress can induce irreversible modifications (like carbonylation). While reversible OPTMs are not uniformly deleterious as these modifications can participate in crucial redox signaling cascades (i.e. insulin signaling), excess heme can induced irreversible modifications, leading to proteolysis or intracellular protein aggregation[16–18]. Additionally, free heme can damage DNA leading to base modifications, strands breaks, and cross-links[3]. Heme-induced oxidative stress is associated with various pathologies, such as hemolytic disorders, ischemia-reperfusion injury, inflammatory diseases, and neurodegenerative diseases[19,20].

In addition to primary and secondary antioxidants, there are heme-specific extracellular and intracellular mechanisms to protect from heme-induced oxidiatve stress. Molecules such as haptoglobin and hemopexin act as extracellular heme chelators. Haptoglobin will bind free heme for transportation to and degradation by macrophages in the reticuloendothelial system[21]. However, hemoglobin in circulation can be easily oxidized to methemoglobin when plasma haptoglobin buffering capacity is exceeded, thus releasing free heme. Hemopexin is a high-affinity heme scavenger able

to reduce heme toxicity by maintaining heme lipophilicity, decreasing heme's ability to catalyze radical formation as well as sequestering iron essential to microorganisms[22]. Though there are cellular antioxidant defense mechanisms and hemoglobin/heme chelators, the final protection mechanism from heme-induced oxidative stress is intracellular enzymatic degradation. Though the heme-hemopexin complex is recognized by the ubiquitous LDL receptor-related protein 1 (LRP1)[23], suggesting that extracellular heme can be recycled, hepatic delivery is essential for complete heme detoxification. The enzyme responsible for heme degradation is heme oxygenase, which is located in the endoplasmic reticulum and consists of three isoforms (HO-1, HO-2, HO-3)[19,24]. HO converts heme to hydrophilic biliverdin (BV), vasodilatory carbon monoxide (CO), and ferrous iron ($Fe2^{+}$). In hepatocytes, BV can be further reduced to lipophilic antioxidant bilirubin (BR) by the cytosolic enzyme biliverdin reductase (BLVR)[25]. BR can then undergo conjugation to glucuronic acids via UGT1A1 in the endoplasmic reticulum and subsequent excretion into bile acid, urine, or feces[24],

Thus, HO confers protection from heme-induced oxidative stress via two mechanisms: decreased pro-oxidant heme content as well as increasing production of the antioxidant metabolite unconjugated BR. While HO-2 is ubiquitously expressed, HO-1 is highly inducible. Stimuli such as heme (the most potent inducer), hypoxia, ischemia-reperfusion, inflammation, and heat shock have been shown to increase HO-1 expression in a variety of tissues but specifically in the liver[19,24,26]. BR has been shown to not only scavenge H_2O_2 and peroxyl radicals, preventing lipid peroxidation, but also to increase nuclear Nrf2 transcription factor aggregation, upregulating HO-1 expression in hepatocytes[25,27,28]. Reduction of BV to BR and interconversion of BR back to BV via

ROS-induced oxidation produces a powerful physiologic antioxidant cycle. Lipophilic BR has been shown to diffuse across cell membranes including mitochondria, where high concentrations decrease ATP production. Conversely, intramitochondrial BR can be beneficial in reducing ROS at a site of high oxidative potential. This poses a potential problem as scavenging intramitochondrial ROS can lead to trapping if hydrophilic BV in the mitochondrial matrix. Studies have evinced that a plasma membrane BV exporter is necessary for BV export to the bile as patients with BLVR mutations present with hyperbiliverdinemia, producing a green jaundice[29]. Identifying a mitochondrial BV exporter is key to understanding this redox cycle as BLVR is only expressed cytosolically. Control of cellular BR is key to balancing beneficial antioxidant effects with the detrimental decrease in mitochondrial ATP production.

Heme plays a crucial role in oxygen transport, cellular respiration, drug detoxification, and various redox reactions. Heme biosynthesis involves multiple steps and is tightly regulated to match the body's needs. However, excess heme can lead to cellular damage by forming ROS. These ROS can overwhelm the body's antioxidant defenses, leading to oxidative stress and cellular damage. Fortunately, the body has mechanisms to mitigate heme-induced oxidative stress, including antioxidant defenses and heme-specific chelators like haptoglobin and hemopexin. Additionally, heme is degraded by heme oxygenase enzymes, which convert it into less harmful by-products, playing a critical role in protecting against heme-induced oxidative stress. Understanding the balance between heme's beneficial and harmful effects, particularly in relation to cellular energy production and antioxidant capabilities, is crucial for comprehending its role in various oxidative and inflammatory pathologies.

ATP-Binding Cassette (ABC) proteins and their role in disease.

ATP-binding cassette (ABC) proteins constitute a large and diverse family of membrane transport proteins that are found in all forms of life, from bacteria to humans. In the 1970s, researchers discovered proteins in bacteria that were involved in the active transport of a wide range of substrates, including ions, sugars, amino acids, and peptides. The name "ATP-binding cassette" was coined in the 1980s to describe these proteins due to their shared feature of binding and hydrolyzing ATP to transport substrates across cellular membranes[30,31]. The first characterized ABC transporter in bacteria was the histidine permease, discovered in the bacterium Salmonella typhimurium[32]. Subsequent research led to the identification of numerous ABC transporters in bacteria, including those involved in the import and export of essential nutrients and toxins. It became evident that ABC transporters were not limited to bacteria but were also present in eukaryotic organisms, including humans. The first eukaryotic ABC transporter, P-glycoprotein (P-gp/MDR1), was discovered in the early 1980s[30,31]. As more ABC transporters were identified in various organisms, they were classified into different subfamilies based on sequence homology and function. The classification included ABCA to ABCG subfamilies[33]. These transporters were found to play crucial roles in diverse processes such as lipid transport, drug resistance, antigen presentation, and many other cellular functions[30,31].

Over time, researchers began to elucidate the structure and mechanism of ABC transporters. They found that these proteins typically consist of two transmembrane domains (TMDs) and two nucleotide-binding domains (NBDs). The TMDs are

responsible for substrate binding and transport across the membrane, while the NBDs bind and hydrolyze ATP, providing the energy necessary for substrate translocation. Understanding ABC transporters became particularly important in medicine due to their role in drug resistance and various genetic diseases. ABC transporters, particularly MDR1, are involved in multidrug resistance. In cancer cells, these export anticancer drugs, reducing their effectiveness and contributing to cell invasion, metastasis, and eventually treatment failure[30,31]. Mutations in ABC transporters also lead to disease, such as cystic fibrosis. The mutated CFTR (Cystic Fibrosis Transmembrane Conductance Regulator) gene encodes an ABC transporter. CFTR is responsible for transporting chloride ions across cell membranes, and defective CFTR channels result in thick, sticky mucus in the airways, leading to respiratory problems.

Several ABC transporters have been linked to metabolic diseases due to their involvement in the transport of lipids, cholesterol, and other metabolites. ABC proteins involved in cholesterol transport have been linked with atherosclerosis and cardiovascular disease. ABCA1 is crucial for the efflux of cholesterol and phospholipids from cells to form high-density lipoprotein (HDL) particles, increasing the risk for cardiovascular disease. Mutations in the ABCA1 gene are associated with Tangier disease and familial hypoalphalipoproteinemia, which are characterized by low levels of HDL cholesterol[34]. Mutations in ABCG5 and ABCG8 (Sterolin-1 and Sterolin-2) can lead to sitosterolemia, a rare autosomal recessive disorder characterized by the accumulation of plant sterols in the body and increased risk of atherosclerosis[35]. Additionally, many ABC transporters in the liver assist in the formation of bile. ABCB4 is responsible for the translocation of phospholipids into the bile, a crucial step in the

formation of bile micelles. Mutations in the ABCB4 gene can result in progressive familial intrahepatic cholestasis (PFIC) or low-phospholipid-associated cholelithiasis (LPAC), both of which are associated with liver and gallbladder dysfunction[36]. ABCB11 is primarily expressed in the liver and is essential for the secretion of bile salts into the bile. Mutations in ABCB11 (Bile Salt Export Pump, BSEP) can lead to progressive familial intrahepatic cholestasis type 2 (PFIC2) and benign recurrent intrahepatic cholestasis (BRIC), both of which affect bile flow and can result in hepatic metabolic disturbances[37–39].

Though ABC transporters are prevalent in the liver and involved in lipid metabolism, ABC proteins have yet to be linked with major liver diseases, such as non-alcoholic fatty liver disease (NAFLD) or alcoholic liver disease (ALD). Four mitochondrial ABC proteins have been discovered: ABCB6, ABCB7, ABCB8, and ABCB10[40]. ABCB10 forms homodimers inner mitochondrial membrane and is highly expressed in hematopoietic and cardiac tissues. The processes of erythropoiesis as well as cardiac ischemia-reperfusion injury both challenge the mitochondria with increased oxidative stress. Treatment of homozygous ABCB10 knockout (ABCB10 -/-) erythroid progenitors with a mitochondrial specific super oxide dismutase (SOD) mimetic prevented heme-induced oxidative stress and restored hemoglobin synthesis. This rescue effect was not seen when treating with cytosolic antioxidant N-acetyl-cysteine, suggesting ABCB10 functions to decrease mitochondrial oxidative stress during heme synthesis and erythrocyte differentiation[41]. Additionally, heterozygous ABCB10 deletion (ABCB10 +/-) in cardiac tissue was shown to increase susceptibility to oxidative stress during ischemia-reperfusion injury, leading to reduced recovery of

hemodynamic function and oxidative damage of both the mitochondria and sarcoplasmic reticulum calcium ATPase (SERCA). These markers of cardiac damage and dysfunction post-reperfusion were restored to wild-type levels when treating with a superoxide dismutase/catalase mimetic (EUK-207)[42]. In addition to cardiac and hematopoietic tissues, ABCB10 is also highly expressed in hepatocytes, which have the 2nd highest rate of heme production. While it was thought that ABCB10 would play a role in export of ALA or heme from the mitochondria, two rate-limiting steps in heme synthesis, these studies suggest ABCB10 functions to protect against mitochondrial oxidative stress. NAFLD and ALD have both been shown to have abhorrent lipid/cholesterol metabolism and increased oxidative stress, processes that have been shown to involve ABC proteins[43,44].

ATP-binding cassette (ABC) proteins form a large family of membrane transport proteins found in all life forms. They are known for binding and hydrolyzing ATP to transport various substrates across cellular membranes. ABC transporters are divided into subfamilies (ABCA to ABCG) and play roles in lipid transport, drug resistance, antigen presentation, and other cellular functions. These transporters are significant in medicine, particularly in drug resistance in cancer (e.g., MDR1 transporter) and genetic diseases like cystic fibrosis, caused by mutations in the CFTR transporter. ABC transporters are also implicated in metabolic diseases through their role in lipid and cholesterol transport, with mutations in certain transporters leading to conditions like Tangier disease, sitosterolemia, and progressive familial intrahepatic cholestasis. Although prevalent in the liver, a link between hepatic ABC proteins and major liver diseases like NAFLD or ALD has not yet been established. While ABCB10 has been

studied for their role in reducing oxidative stress during erythropoiesis and protecting cardiac tissue from ischemia-reperfusion injury, ABCB10 mutations in humans have not been identified or linked with any pathological states. Understanding the role of ABCB10 in NAFLD and ALD may offer crucial insights into new therapeutic strategies for two prevalent liver pathologies characterized by increased mitochondrial oxidative stress.

REFERENCES

1. Gell DA. Structure and function of haemoglobins. *Blood Cells Mol Dis*. 2018;70:13-42. doi:10.1016/j.bcmd.2017.10.006

2. Celis AI, DuBois JL. Making and breaking heme. *Curr Opin Struct Biol*. 2019;59:19-28. doi:10.1016/j.sbi.2019.01.006

3. Kumar S, Bandyopadhyay U. Free heme toxicity and its detoxification systems in human. *Toxicology Letters*. 2005;157(3):175-188. doi:10.1016/j.toxlet.2005.03.004

4. Thomas DD, Miranda KM, Colton CA, Citrin D, Espey MG, Wink DA. Heme proteins and nitric oxide (NO): the neglected, eloquent chemistry in NO redox signaling and regulation. *Antioxid Redox Signal*. 2003;5(3):307-317. doi:10.1089/152308603322110887

5. Kim HJ, Khalimonchuk O, Smith PM, Winge DR. Structure, function, and assembly of heme centers in mitochondrial respiratory complexes. *Biochim Biophys Acta*. 2012;1823(9):1604-1616. doi:10.1016/j.bbamcr.2012.04.008

6. Ogawa K, Sun J, Taketani S, et al. Heme mediates derepression of Maf recognition element through direct binding to transcription repressor Bach1. *The EMBO Journal*. 2001;20(11):2835-2843. doi:10.1093/emboj/20.11.2835

7. Inamdar NM, Ahn YI, Alam J. The Heme-Responsive Element of the Mouse Heme Oxygenase-1 Gene Is an Extended AP-1 Binding Site That Resembles the Recognition Sequences for MAF and NF-E2 Transcription Factors. *Biochemical and Biophysical Research Communications*. 1996;221(3):570-576. doi:10.1006/bbrc.1996.0637

8. He F, Li J, Liu Z, Chuang CC, Yang W, Zuo L. Redox Mechanism of Reactive Oxygen Species in Exercise. *Front Physiol*. 2016;7. doi:10.3389/fphys.2016.00486

9. de Grey ADNJ. The plasma membrane redox system: a candidate source of aging-related oxidative stress. *Age (Dordr)*. 2005;27(2):129-138. doi:10.1007/s11357-005-1630-1

10. Mondola P, Damiano S, Sasso A, Santillo M. The Cu, Zn Superoxide Dismutase: Not Only a Dismutase Enzyme. *Front Physiol*. 2016;7:594. doi:10.3389/fphys.2016.00594

11. Prasad AS, Bao B, Beck FWJ, Kucuk O, Sarkar FH. Antioxidant effect of zinc in humans. *Free Radic Biol Med*. 2004;37(8):1182-1190. doi:10.1016/j.freeradbiomed.2004.07.007

12. Tinggi U. Selenium: its role as antioxidant in human health. *Environ Health Prev Med*. 2008;13(2):102-108. doi:10.1007/s12199-007-0019-4

13. Balla G, Jacob HS, Eaton JW, Belcher JD, Vercellotti GM. Hemin: a possible physiological mediator of low density lipoprotein oxidation and endothelial injury. *Arterioscler Thromb*. 1991;11(6):1700-1711. doi:10.1161/01.atv.11.6.1700

14. Ryter SW, Tyrrell RM. The heme synthesis and degradation pathways: role in oxidant sensitivity: Heme oxygenase has both pro- and antioxidant properties. *Free Radical Biology and Medicine*. 2000;28(2):289-309. doi:10.1016/S0891-5849(99)00223-3

15. Cai Z, Yan LJ. Protein Oxidative Modifications: Beneficial Roles in Disease and Health. *J Biochem Pharmacol Res*. 2013;1(1):15-26.

16. Vasconcellos LRC, Dutra FF, Siqueira MS, et al. Protein aggregation as a cellular response to oxidative stress induced by heme and iron. *Proceedings of the National Academy of Sciences*. 2016;113(47):E7474-E7482. doi:10.1073/pnas.1608928113

17. Bader N, Grune T. Protein oxidation and proteolysis. *Biol Chem*. 2006;387(10-11):1351-1355. doi:10.1515/BC.2006.169

18. Gáll T, Pethő D, Nagy A, et al. Heme Induces Endoplasmic Reticulum Stress (HIER Stress) in Human Aortic Smooth Muscle Cells. *Frontiers in Physiology*. 2018;9. Accessed December 1, 2023. https://www.frontiersin.org/articles/10.3389/fphys.2018.01595

19. Chiabrando D, Vinchi F, Fiorito V, Mercurio S, Tolosano E. Heme in pathophysiology: a matter of scavenging, metabolism and trafficking across cell membranes. *Front Pharmacol*. 2014;5:61. doi:10.3389/fphar.2014.00061

20. Canesin G, Muralidharan AM, Swanson KD, Wegiel B. HO-1 and Heme: G-Quadruplex Interaction Choreograph DNA Damage Responses and Cancer Growth. *Cells*. 2021;10(7):1801. doi:10.3390/cells10071801

21. Schaer DJ, Buehler PW. Cell-Free Hemoglobin and Its Scavenger Proteins: New Disease Models Leading the Way to Targeted Therapies. *Cold Spring Harb Perspect Med*. 2013;3(6):a013433. doi:10.1101/cshperspect.a013433

22. Tolosano E, Fagoonee S, Morello N, Vinchi F, Fiorito V. Heme Scavenging and the Other Facets of Hemopexin. *Antioxidants & Redox Signaling*. 2010;12(2):305-320. doi:10.1089/ars.2009.2787

23. Hvidberg V, Maniecki MB, Jacobsen C, Højrup P, Møller HJ, Moestrup SK. Identification of the receptor scavenging hemopexin-heme complexes. *Blood*. 2005;106(7):2572-2579. doi:10.1182/blood-2005-03-1185

24. Dutt S, Hamza I, Bartnikas TB. Molecular Mechanisms of Iron and Heme Metabolism. *Annu Rev Nutr*. 2022;42:311-335. doi:10.1146/annurev-nutr-062320-112625

25. Barañano DE, Rao M, Ferris CD, Snyder SH. Biliverdin reductase: A major physiologic cytoprotectant. *Proc Natl Acad Sci U S A*. 2002;99(25):16093-16098. doi:10.1073/pnas.252626999

26. Llesuy SF, Tomaro ML. Heme oxygenase and oxidative stress. Evidence of involvement of bilirubin as physiological protector against oxidative damage. *Biochim Biophys Acta*. 1994;1223(1):9-14. doi:10.1016/0167-4889(94)90067-1

27. Sedlak TW, Snyder SH. Bilirubin Benefits: Cellular Protection by a Biliverdin Reductase Antioxidant Cycle. *Pediatrics*. 2004;113(6):1776-1782. doi:10.1542/peds.113.6.1776

28. Vasavda C, Kothari R, Malla AP, et al. Bilirubin links heme metabolism to neuroprotection by scavenging superoxide. *Cell Chem Biol*. 2019;26(10):1450-1460.e7. doi:10.1016/j.chembiol.2019.07.006

29. Nytofte NS, Serrano MA, Monte MJ, et al. A homozygous nonsense mutation (c.214C->A) in the biliverdin reductase alpha gene (BLVRA) results in accumulation of biliverdin during episodes of cholestasis. *J Med Genet*. 2011;48(4):219-225. doi:10.1136/jmg.2009.074567

30. Holland IB, Cole SPC, Kuchler K, Higgins CF. *ABC Proteins: From Bacteria to Man*. Elsevier; 2003.

31. Higgins CF. ABC Transporters: From Microorganisms to Man. *Annual Review of Cell Biology*. 1992;8(1):67-113. doi:10.1146/annurev.cb.08.110192.000435

32. Zolnerciks JK, Andress EJ, Nicolaou M, Linton KJ. Structure of ABC transporters. *Essays Biochem*. 2011;50(1):43-61. doi:10.1042/bse0500043

33. Thomas C, Tampé R. Structural and Mechanistic Principles of ABC Transporters. *Annual Review of Biochemistry*. 2020;89(1):605-636. doi:10.1146/annurev-biochem-011520-105201

34. Oram J. Tangier disease and ABCA1. *Biochimica et Biophysica Acta (BBA) - Molecular and Cell Biology of Lipids*. 2000;1529(1-3):321-330. doi:10.1016/S1388-1981(00)00157-8

35. Yu XH, Qian K, Jiang N, Zheng XL, Cayabyab FS, Tang CK. ABCG5/ABCG8 in cholesterol excretion and atherosclerosis. *Clinica Chimica Acta*. 2014;428:82-88. doi:10.1016/j.cca.2013.11.010

36. Sticova E, Jirsa M. ABCB4 disease: Many faces of one gene deficiency. *Ann Hepatol*. 2020;19(2):126-133. doi:10.1016/j.aohep.2019.09.010

37. Hayashi H, Sugiyama Y. Bile salt export pump (BSEP/ABCB11): trafficking and sorting disturbances. *Curr Mol Pharmacol*. 2013;6(2):95-103. doi:10.2174/18744672113069990036

38. Hayashi H, Takada T, Suzuki H, Akita H, Sugiyama Y. Two common PFIC2 mutations are associated with the impaired membrane trafficking of BSEP/ABCB11. *Hepatology*. 2005;41(4):916-924. doi:10.1002/hep.20627

39. Arthur Lorio E, Valadez D, Alkhouri N, Loo N. Cholestasis in Benign Recurrent Intrahepatic Cholestasis 2. *ACG Case Reports Journal*. 2020;7(6):e00412. doi:10.14309/crj.0000000000000412

40. Liesa M, Qiu W, Shirihai OS. Mitochondrial ABC transporters function: The role of ABCB10 (ABC-me) as a novel player in cellular handling of reactive oxygen species. *Biochimica et Biophysica Acta (BBA) - Molecular Cell Research*. 2012;1823(10):1945-1957. doi:10.1016/j.bbamcr.2012.07.013

41. Hyde BB, Liesa M, Elorza AA, et al. The mitochondrial transporter ABC-me (ABCB10), a downstream target of GATA-1, is essential for erythropoiesis in vivo. *Cell Death Differ*. 2012;19(7):1117-1126. doi:10.1038/cdd.2011.195

42. Liesa M, Luptak I, Qin F, et al. The mitochondrial transporter ABC-me (ABCB10) is a novel gene required for cardiac recovery after ischemia-reperfusion. *Circulation*. 2011;124(7):806-813. doi:10.1161/CIRCULATIONAHA.110.003418

43. Teschke R. Alcoholic Liver Disease: Alcohol Metabolism, Cascade of Molecular Mechanisms, Cellular Targets, and Clinical Aspects. *Biomedicines*. 2018;6(4). doi:10.3390/biomedicines6040106

44. Shum M, Ngo J, Shirihai OS, Liesa M. Mitochondrial oxidative function in NAFLD: Friend or foe? *Mol Metab*. 2020;50:101134. doi:10.1016/j.molmet.2020.101134

Chapter 1: ABCB10 exports mitochondrial biliverdin, driving metabolic maladaptation in obesity.

REPRINT

HHS Public Access

Author manuscript

Sci Transl Med. Author manuscript; available in PMC 2021 November 19.

Published in final edited form as:

Sci Transl Med. 2021 May 19; 13(594): . doi:10.1126/scitranslmed.abd1869.

ABCB10 exports mitochondrial biliverdin, driving metabolic maladaptation in obesity[$]

Michael Shum[1,2,3,13], **Chitra A. Shintre**[4], **Thorsten Althoff**[5], **Vincent Gutierrez**[1,2,3], **Mayuko Segawa**[1,2,3], **Alexandra D. Saxberg**[6], **Melissa Martinez**[6], **Roslin Adamson**[4], **Margaret R. Young**[4], **Belinda Faust**[4,14], **Raffi Gharakhanian**[1,2], **Shi Su**[7], **Karthickeyan Chella Krishnan**[8,9], **Kiana Mahdaviani**[1,7], **Michaela Veliova**[2], **Dane M. Wolf**[1,7], **Jennifer Ngo**[1,2,3,10], **Laura Nocito**[7], **Linsey Stiles**[1,2], **Jeff Abramson**[5], **Aldons J. Lusis**[3,8,11,12], **Andrea L. Hevener**[1], **Maria E. Zoghbi**[#6], **Elisabeth P. Carpenter**[#4,14], **Marc Liesa**[1,2,3,*]

[1]Department of Medicine, Division of Endocrinology, David Geffen School of Medicine at UCLA. 650 Charles E. Young Dr., Los Angeles, CA 90095 USA.

[2]Department of Molecular and Medical Pharmacology, David Geffen School of Medicine at UCLA. 650 Charles E. Young Dr., Los Angeles, CA 90095 USA.

[3]Molecular Biology Institute at UCLA, 611 Charles E. Young Dr., Los Angeles, CA 90095 USA.

[4]Center for Medicines Discovery, University of Oxford, Oxfordshire, OX3 7DQ, UK.

[5]Department of Physiology, University of California, Los Angeles, 650 Charles E. Young Dr., Los Angeles, CA 90095 USA.

[6]University of California Merced, School of Natural Sciences, 5200 North Lake Rd. Merced, CA 95343.

[7]Evans Biomedical Research Center, Boston University School of Medicine, 650 Albany st., Boston, MA 02118 USA.

[8]Department of Human Genetics, David Geffen School of Medicine at UCLA. 650 Charles E. Young Dr., Los Angeles, CA 90095 USA.

[9]Department of Pharmacology and Systems Physiology, University of Cincinnati College of Medicine, 231 Albert Sabin Way, Cincinnati, OH 45267-0575 USA.

[10]Department of Chemistry & Biochemistry, University of California, Los Angeles, CA 90095.

---

[*]Corresponding author: mliesa@mednet.ucla.edu.

Author contributions: M.L., M.Sh., C.A.S and E.P.C conceptualized the project. M.Sh., C.A.S., T.A., V.G., M.Se., M.L., R.A., M.Y., B.F., E.P.C., A.D.S., M.M., M.E.Z., T.A., J.A., A.H. and A.J.L. provided methods. M.Sh., M.L., C.A.S., T.A., V.G., M.Se., E.P.C., A.D.S., M.M., M.E.Z., R.G., K.C.K., A.H. and M.V analyzed data. M.Sh., T.A., M.L., C.A.S., V.G., M.Se., A.D.S., M.M., M.E.Z., R.G., S.S., K.M., A.H., M.V., D.M.W., J.N., L.N and L.S. performed experiments. M.L., E.P.C., M.Z., A.H., A.J.L. and J.A provided resources. M.Sh. and M.L. wrote the original draft. M.L., E.P.C and M.E.Z. supervised the project and acquired funds.

Competing interests: The following competing interests are not related to this study: E.P.C and B.F. are currently employed by Vertex Pharmaceuticals and M.L. is a co-founder and consultant of Enspire Bio LLC. The authors declare that they have no competing interests.

[11]Department of Medicine, Division of Cardiology, David Geffen School of Medicine at UCLA. 650 Charles E. Young Dr., Los Angeles, CA 90095 USA.

[12]Department of Microbiology, Immunology and Molecular Genetics, David Geffen School of Medicine at UCLA. 650 Charles E. Young Dr., Los Angeles, CA 90095 USA.

[13]Present address, Department of Molecular Medicine, Faculty of Medicine, Université Laval, Québec City, G1V 0A6, Canada

[14]Present address, Vertex Pharmaceuticals Ltd., Jubilee Drive, Milton Park, Abingdon, OX14 4RZ, UK.

[#] These authors contributed equally to this work.

Abstract

Although the role of hydrophilic antioxidants in the development of hepatic insulin resistance and non-alcoholic fatty liver disease (NAFLD) has been well studied, the role of lipophilic antioxidants remains poorly characterized. A known lipophilic H_2O_2 scavenger is bilirubin, which can be oxidized to biliverdin and then reduced back to bilirubin by cytosolic biliverdin reductase (BLVRA). Oxidation of bilirubin to biliverdin inside mitochondria must be followed by the export of biliverdin to the cytosol, where biliverdin is reduced back to bilirubin. Thus, the putative mitochondrial exporter of biliverdin is expected to be a major determinant of bilirubin regeneration and intracellular H_2O_2 scavenging. Here, we identified ABCB10 as a mitochondrial biliverdin exporter. ABCB10 reconstituted into liposomes transported biliverdin and ABCB10 deletion caused accumulation of biliverdin inside mitochondria. Obesity with insulin resistance upregulated hepatic ABCB10 expression in mice and elevated cytosolic and mitochondrial bilirubin content in an ABCB10-dependent manner. Revealing a maladaptive role of ABCB10 driven bilirubin synthesis, hepatic ABCB10 deletion protected diet-induced obese mice from steatosis and hyperglycemia, improving insulin-mediated suppression of glucose production and decreasing lipogenic SREBP-1c expression. Protection was concurrent with enhanced mitochondrial function and increased inactivation of PTP1B, a phosphatase disrupting insulin signaling and elevating SREBP-1c expression. Restoration of cellular bilirubin content in ABCB10 KO hepatocytes reversed the improvements in mitochondrial function and PTP1B inactivation, demonstrating that bilirubin was the maladaptive effector linked to ABCB10 function. Thus, we identified a fundamental transport process that amplifies intracellular bilirubin redox actions, which can exacerbate insulin resistance and steatosis in obesity.

One Sentence Summary:

ABCB10 in liver promotes hyperglycemia and steatosis.

INTRODUCTION:

H_2O_2 produced by mitochondria not only can damage cells, but it is a central molecule participating in signaling transduction as well (1). Consequently, pro- and anti-oxidant systems are key regulators of metabolism and can play tissue-specific roles. Liver is one of the tissues with the highest antioxidant capacity and largest variety of antioxidant systems. Both pro-oxidants and antioxidants are concurrently elevated in insulin resistant and

steatotic livers and are distributed to distinct microdomains based on their chemical properties. A well-studied antioxidant of the hydrophilic environment is glutathione. The lipophilic environment, which includes membranes, has its own antioxidant systems that are less studied. Among them are ubiquinol, melatonin, α-lipoic acid, and bilirubin (2). Bilirubin is a particularly interesting antioxidant due to its lipophilicity, cell-autonomous and ubiquitous production from heme degradation and its presence in different organelles (3, 4).

Heme is an essential cofactor present in all cell types, as it is part of mitochondrial cytochromes and oxygen carrier proteins. However, free heme is toxic, as it can cause oxidative damage (5). Consequently, all cells prevent heme-induced toxicity by degrading heme to biliverdin. Biliverdin is soluble and is transformed by cytosolic biliverdin reductase (BLVRA) to lipophilic bilirubin (6, 7). Bilirubin and biliverdin are both released from the cytosol to the bloodstream. Plasma bilirubin concentrations are higher (1–25 μM) than biliverdin (0.12–0.01 μM), which is explained by the efficient and ubiquitous conversion of biliverdin to bilirubin and the faster excretion of biliverdin. Indeed, biliverdin can be directly excreted to the bile (8), whereas solubilization of bilirubin is required for its efficient excretion. Bilirubin solubilization is achieved by conjugating bilirubin to glucuronic acids, a reaction catalyzed by UGT1A1 in the endoplasmic reticulum (ER) lumen of hepatocytes (9).

The lipophilicity of unconjugated bilirubin allows its passive diffusion through cellular membranes, including mitochondrial membranes (10). Kernicterus, a neurological disease resulting from excessive plasma bilirubin concentrations (>300μM), damages brain mitochondria (11). The detrimental effect of high bilirubin concentrations on mitochondrial function can be reproduced *in vitro*, as 100 μM bilirubin added to isolated mitochondria completely blocks their ATP synthesis capacity (12). In contrast, 100 μM biliverdin has no effects on isolated mitochondrial function (12). Moreover, bilirubin decreases mitochondrial OXPHOS efficiency (12), scavenges lipid peroxides and decreases H_2O_2 content at low micromolar, even nanomolar concentrations (6, 7).

Consequently, the intracellular pool of free bilirubin must be tightly regulated to prevent the toxic actions of bilirubin on mitochondria and execute its beneficial actions when needed. The lipophilic nature of bilirubin and higher hydrophilicity of biliverdin impose a mechanistic challenge on the regulation of their intracellular pools. Bilirubin can cross membranes by passive diffusion and equilibrate across the ER, mitochondria, and cytosol (10). When bilirubin scavenges H_2O_2, it is oxidized to form biliverdin, which cannot cross membranes easily. Indeed, there is functional evidence that an uncharacterized biliverdin exporter is present in the plasma membrane of hepatocytes and is required to export biliverdin to the bile (8). However, whether mitochondria export biliverdin is unknown. Biliverdin cannot be converted back to bilirubin in the mitochondrial matrix, as BLVRA is absent (13, 14). Therefore, mitochondria can regulate bilirubin synthesis by controlling the export of biliverdin. The regulation of mitochondrial biliverdin export and its consequences on the cellular pool of bilirubin, as well as on mitochondrial bilirubin content, are currently undefined.

The ATP binding cassette (ABC) transporter ABCB10 is located in the inner mitochondrial membrane (15–18) and is highly expressed in the liver and bone marrow. ABCB10 is

essential for hemoglobinization during primitive erythropoiesis and ABCB10 deletion causes defects in hemoglobin synthesis that are rescued by treatments with antioxidants. This rescue by antioxidants demonstrates that ABCB10 is not essential for heme synthesis *per se*, but rather protects from oxidative stress induced by high heme content (16). Hepatocytes are ranked second after differentiating erythrocytes as the cells with the highest rates of heme synthesis in their mitochondria (19). Disturbed heme homeostasis and changes in mitochondrial function in liver are associated with insulin resistance and fatty liver disease (20), and *ABCB10* is the only gene that encodes for a mitochondrial transporter related to heme homeostasis with intronic variants associated with type 2 diabetes (21, 22). However, the function of ABCB10 in liver, its role in insulin resistance, and the cargo transported by ABCB10 are unknown.

Here, we demonstrate that ABCB10 is a mitochondrial biliverdin exporter that increases bilirubin production. We find that ABCB10 upregulation is necessary for the increase in mitochondrial bilirubin content induced by obesity, which leads to a redox state that promotes hepatic steatosis and insulin resistance. In all, we define a mitochondrial transport process that becomes maladaptive in obesity.

RESULTS

ABCB10 exports biliverdin, which increases bilirubin synthesis

ABCB10 has been mostly studied in differentiating red blood cells (15–18, 23). As the substrate exported by ABCB10 is unknown, the mechanism by which ABCB10 protected from oxidative damage is uncharacterized (16). However, previous data provided key insights about the nature of ABCB10 cargo. Treating ABCB10 knockout (KO) red blood cell precursors with antioxidants rescues heme biosynthesis, showing that ABCB10 is not essential to transport heme intermediates and heme itself (16, 24). Instead, the cargo transported by ABCB10 is expected to counteract oxidative stress and to be produced during heme synthesis.

In this context, the next logical molecules to test as ABCB10 cargo were the products of heme metabolism, biliverdin and its redox pair bilirubin (fig. S1A). ABC transporters harness energy from the hydrolysis of ATP to facilitate the conformational changes necessary to execute transport cycles. Thus, ABCB10 ATPase activity is expected to increase in the presence of its cargo (24, 25). We found that biliverdin, but not bilirubin, caused a 2-fold increase in ABCB10 ATPase activity in purified human ABCB10 reconstituted into nanodiscs (Fig. 1A). Maximal ATPase activation was achieved at biliverdin concentrations of 2.5–5 μM with a Km of 143.6 nmols biliverdin/mg protein/min and a Vmax of 323 nmols Pi/mg protein/min (Fig. 1B). Moreover, other heme-related molecules previously hypothesized to be transported by ABCB10, including heme precursors aminolevulinic acid (ALA) and protoporphyrin IX, as well as hemin, did not change ABCB10 ATPase activity (26, 27). Altogether, these results support that biliverdin is the only heme-related candidate as cargo transported by ABCB10.

To directly determine whether ABCB10 transports biliverdin across membranes, we reconstituted human ABCB10 into sealed liposomes. For ABC transporters that carry a

substrate away from the ATP domain, cargo accumulation inside liposomes can be achieved by adding ATP in the incubation media. The reason is that ATP cannot cross the membrane of a sealed liposome and thus ATP is not accessible to transporters inserted in the opposite orientation. As a result, ABCB10 molecules with their ATP binding domain facing the incubation media will be the only ABCB10 molecules transporting cargos, allowing the cargo to accumulate inside liposomes (Fig. 1C).

With ATP in the media, we observed a linear increase in radioactive biliverdin accumulation in ABCB10-liposomes, approaching a plateau 15–30 minutes after adding radioactive biliverdin (Fig. 1D). In the absence of ATP, we detected a minor and linear increase in radioactive biliverdin content in liposomes. We attributed the ATP-independent increase in biliverdin accumulation to the expected binding of biliverdin to lipids and maybe to ABCB10 itself, but without being transported. This ATP-independent increase in biliverdin accumulation was subtracted to calculate the maximal amount of biliverdin transported by ABCB10. After 60 minutes of incubation, 135 nmols of biliverdin/mg ABCB10 protein accumulated into the liposomes (Fig. 1D). To further confirm the specificity of ABCB10-mediated biliverdin transport, we tested the ability of the heme-related molecules, as well as unlabeled biliverdin, to compete for ABCB10-mediated labeled biliverdin uptake. As expected, un-labelled biliverdin (1 μM, 3-fold higher than labelled) blocked labelled biliverdin uptake, whereas the other physiological heme-related molecules did not (fig. S2). In all, these data support that the only heme-related molecule transported by ABCB10 is biliverdin.

As bilirubin is synthesized in the cytosol from biliverdin by BLVRA, our expectation was that ABCB10-mediated biliverdin export would increase cytosolic bilirubin production and availability (fig. S3). If this expectation was correct, ABCB10 gain-of-function would increase bilirubin content in the cytosol of hepatocytes. Then, higher cytosolic bilirubin availability would lead to an increase in mitochondrial bilirubin through passive diffusion across mitochondrial membranes (10). The availability of a fluorescent and reversible bilirubin sensor, the eel protein UnaG (4, 28) (Fig. 1E), allowed us to perform real-time measurements of cytosolic and mitochondrial bilirubin in live cells. UnaG was successfully targeted to the mitochondrial matrix of mouse primary hepatocytes, as shown by its co-localization with TMRE (Fig. 1E). UnaG fluorescence successfully reported mitochondrial bilirubin content, as shown by the increase in UnaG fluorescence after adding bilirubin to the media (fig. S4A–B) (3, 4). Increasing ABCB10 expression in AML12 murine hepatocytes elevated both cytosolic and mitochondrial bilirubin content (Fig. 1F and fig. S5), supporting that ABCB10-mediated biliverdin export was sufficient to increase bilirubin synthesis.

Hepatic ABCB10 expression is higher in diet-induced obese mice and is associated with greater steatosis and insulin resistance

As insulin resistance induces hepatic redox stress and intronic *ABCB10* variants are associated with type 2 diabetes in humans (21, 22), we analyzed hepatic *Abcb10* expression in the Western diet-fed Hybrid Mouse Diversity Panel (HMDP). The HMDP is a collection of 102 mouse strains with obesity, insulin resistance, and hepatic steatosis (29). *Abcb10*

mRNA content in liver is elevated by Western diet feeding in 68 of the 102 HMDP strains, with 68 being the number of strains with matched chow diet feeding. The increase in ABCB10 expression ranged 2–10-fold depending on the strain (Fig. 1G). Analyzing the 102 Western diet fed HMDP strains, we found a positive correlation between hepatic *Abcb10* expression and the severity of steatosis and insulin resistance (Fig. 1H and fig. S6A,B). Accordingly, liver *Abcb10* expression showed positive and significant correlations with liver triglyceride content ($p=0.0033$), HOMA-IR values ($p=0.0057$), and fasting insulin concentrations ($p=0.0008$) (Fig. 1H and fig. S6A–C). Correlations were determined via midweight bicorrelation analyses as reported (29). No significant ($p>0.05$) correlations of liver *Abcb10* expression with gonadal fat mass were detected (Fig. 1I and fig. S6D). Thus, hepatic ABCB10 upregulation was not a reflection of the different susceptibility among HMDP strains to develop obesity. Last, ABCB10 protein was also increased in liver from C57BL/6J mice fed a 45% high-fat diet (Fig. 1J).

ABCB10 is dispensable for normal hepatocyte function in mice

Liver is ranked second in the list of tissues with the highest ABCB10 content and heme synthesis rates (30). To determine the physiological relevance of ABCB10-mediated biliverdin export in hepatocytes, we first tested the effects of deleting ABCB10 in hepatocytes from control lean mice by generating *Abcb10* liver-specific KO mice (LKO) (fig. S7). *Abcb10* excision was confirmed by amplification of the Cre-excised *Abcb10* genomic sequence and elimination of ABCB10 protein from primary hepatocytes isolated from LKO mice (Fig. 2A,B). Phenotypically, LKO mice were healthy with normal body weight, glucose tolerance, hepatic lipid content, and mitochondrial function (Fig. 2C–G). In marked contrast to erythroid cells (16), ABCB10 is not essential for viability, mitochondrial function, or heme homeostasis in hepatocytes. If ABCB10 exported biliverdin in hepatocytes *in vivo*, biliverdin would accumulate in ABCB10 KO mitochondria. Relative quantifications of mitochondrial biliverdin content revealed a 79% increase in isolated mitochondria from LKO mice, showing that the absence of ABCB10 caused accumulation of biliverdin in mitochondria (Fig. 2H). As expected from a decrease in bilirubin synthesis induced by an abrogation of ABCB10-mediated biliverdin export, ABCB10 deletion decreased both cytosolic and mitochondrial bilirubin content in primary hepatocytes (Fig. 2I,J). These data indicate that mitochondrial biliverdin export by ABCB10 contributes to bilirubin production in mouse hepatocytes, and that neither ABCB10 deletion nor elevated mitochondrial biliverdin are deleterious for normal liver function in mice.

Hepatic ABCB10 deletion protects diet-induced obese mice from insulin resistance

The positive correlation between hepatic ABCB10 expression and insulin resistance suggested two possible roles for ABCB10: either ABCB10 exacerbates insulin resistance or ABCB10 ineffectively counteracts insulin resistance. Supporting the first role, ABCB10 liver-specific KO (LKO) mice were protected from glucose intolerance induced by high-fat diet (HFD) and showed improved glucose clearance during a GTT without changes in insulinemia (Fig. 3A–B), as well as a prolonged action of insulin maintaining lower glycemia during an ITT (Fig. 3C). ABCB10 deletion decreased fasting glucose concentrations, without changing fasting insulin (Fig. 3D–E). A 7.2% decrease in body

weight without changes in food intake was observed in HFD-fed LKO mice, which was explained by lower fat mass (Fig. 3F–H).

The improvement in the glycemic profiles of LKO mice could be a result of a decrease in hepatic glucose production and an improvement in insulin action suppressing hepatic glucose production. Consequently, to test whether changes in hepatic glucose production in LKO mice were independent of decreased body weight, we used weight-matched HFD-fed LKO and WT mice (Fig. 3I) to perform hyperinsulinemic-.euglycemic clamps (Fig. 3J). These clamp experiments revealed that glucose infusion rates in weight-matched HFD-fed LKO mice were 48% higher than in WT littermates (Fig. 3K). Hepatic glucose production was markedly decreased and the ability of insulin to suppress hepatic glucose production was improved in HFD-fed LKO mice (Fig. 3L–M). Higher suppression of hepatic glucose production by insulin, without a change in insulin-stimulated glucose disappearance rates (Fig. 3N), indicated that protection from insulin resistance in LKO mice was largely restricted to the liver. Thus, these data support that ABCB10 deletion in liver might not protect muscle from insulin resistance.

ABCB10 impairs insulin signaling in primary human and mouse hepatocytes

Although hepatic glucose production rates can be determined by extrahepatic tissues, impaired insulin signal transduction in liver can augment hepatic glucose production and is a reliable biomarker of hepatocyte-autonomous insulin resistance (31–33). To determine whether ABCB10 deletion improved insulin sensitivity in a hepatocyte-autonomous manner, we isolated primary hepatocytes from weight-matched HFD-fed WT and ABCB10 LKO mice and determined insulin action *ex vivo*. To this end, we measured the effects of insulin treatment on the insulin receptor (INSR) and AKT phosphorylation in cultured primary hepatocytes. After five minutes treatment of 10 nM insulin, HFD-fed LKO primary hepatocytes showed a 2-fold improvement in the action of insulin increasing INSR Tyr1162/1163 and AKT Ser473 phosphorylation, when compared to hepatocytes from HFD-fed WT littermates (Fig. 4A). In healthy primary human hepatocytes with ABCB10 knocked down (40%) (fig. S8A), a similar improvement in insulin action on INSR Tyr1162/1163 phosphorylation was observed (Fig. 4B).

To test whether elevated ABCB10 function was sufficient to decrease insulin signaling in human hepatocytes, we used adenoviral transduction to increase ABCB10 expression (fig. S8B). The ability of insulin (10 nM) to induce INSR and AKT phosphorylation was decreased both in mouse AML12 and primary human hepatocytes with increased ABCB10 expression (Fig. 4C,D). Last, we restored ABCB10 expression *ex vivo* via adenoviral transduction of primary hepatocytes isolated from HFD-fed ABCB10 LKO mice. We found that the improvement in insulin action phosphorylating INSR and AKT in LKO hepatocytes was reversed by ABCB10 re-expression (fig. S9).

Our data show that high ABCB10 expression promotes a hepatocyte-autonomous disruption in insulin signaling in mouse and human hepatocytes. Accordingly, ABCB10 deletion in HFD-fed mice improved insulin signaling, decreased hepatic glucose production, and increased the action of insulin suppressing hepatic glucose production in HFD-fed mice.

Hepatic ABCB10 deletion increases mitochondrial respiration, protects from steatosis, and counteracts hyperlipidemia in diet-induced obese mice

To investigate why HFD-fed ABCB10 LKO mice showed decreased fat mass, we measured their energy balance using CLAMS. No significant changes ($p > 0.05$) were detected in their food intake, fecal lipids (Fig. 5A, B), or total physical activity (fig. S10A). In contrast, we detected a significant ($p < 0.05$) increase in oxygen consumption (VO_2) and energy expenditure (EE) in HFD-fed LKO mice at night (fed state) when using co-variate statistics to model VO_2 and EE values at an equal body weight between genotypes (Fig. 5C, D). HFD-fed LKO mice showed an elevation in carbohydrate oxidation, revealed by higher respiratory exchange rates (RER) at night (Fig. 5E). Thus, increased RER showed that the decrease in body fat in LKO mice was associated with increased carbohydrate expenditure, rather than elevated fat expenditure. Accordingly, we did not observe changes in circulating FGF21 in ABCB10 LKO mice (fig. S10B), a factor secreted by the liver that increases systemic energy expenditure by promoting fat oxidation (34).

Higher mitochondrial oxidative function in hepatocytes was previously shown to improve insulin signaling (20, 35). To test whether ABCB10 deletion increased mitochondrial function in diet-induced obese mice, we isolated mitochondria and primary hepatocytes from livers of HFD-fed ABCB10 LKO mice and measured their respiratory capacity. Respiration coupled to ATP synthesis was increased both in isolated mitochondria and in primary hepatocytes isolated from HFD-fed ABCB10 LKO mice (Fig. 5F, G). Maximal respiratory capacity was increased in primary hepatocytes from HFD-fed LKO mice as well (Fig. 5H). These changes in mitochondrial function occurred in the absence of changes in mitochondrial biogenesis markers, such as PGC-1α (PPARγ coactivator-1 alpha) or TFAM (Transcription factor A, mitochondrial) (fig. S10C), and without a coordinated upregulation in the subunits of mitochondrial complexes I, III, IV and V (Fig. 5I, J). Altogether, our data showed that ATP-synthesizing capacity (OXPHOS) was improved per unit of mitochondria with ABCB10 deleted. In this regard, we observed a 50% upregulation exclusively in complex II content (Fig. 5I, J). The specific upregulation of complex II in ABCB10 KO mitochondria suggests that bilirubin might not just be decreasing electron transfer activity as previously reported (12), but might decrease the total content of complex II as well. These data support that the regulation of complex II content could be an additional mechanism by which bilirubin is decreasing mitochondrial function and ROS production.

As hepatic steatosis is associated with insulin resistance and metabolic dysfunction, we measured lipid content and lipogenic gene expression in livers from HFD-fed LKO mice. Liver histology revealed decreased lipid droplet area in livers from HFD-fed LKO mice (Fig. 5K), which was confirmed by the 40% reduction in total triglyceride (TG) content (Fig. 5L). Moreover, HFD-fed LKO mice showed a significant ($p<0.05$) reduction in plasma TG and VLDL concentrations and a non-significant ($p>0.05$) decrease in plasma cholesterol content (Fig. 5M–O). Last, HFD-fed LKO mice showed a 50% decrease in the mRNA content of the master regulator of lipogenesis *Srebp1c* and its downstream target, fatty acid synthase (*Fasn*) (Fig. 5P). Altogether, these data support that decreased hepatic triglyceride synthesis can contribute to protection from steatosis and hyperlipidemia in LKO mice.

ABCB10 expression induced by high-fat diet hinders cytosolic and mitochondrial H_2O_2-redox signaling by elevating cellular bilirubin content

Our data show that ABCB10 gain of function was sufficient to increase mitochondrial bilirubin content in hepatocytes. However, the effects on obesity and insulin resistance on mitochondrial bilirubin content have not been measured. Consistent with the increase in ABCB10 expression induced by high-fat diet (HFD), HFD feeding elevated both mitochondrial and cytosolic bilirubin content by 50%in isolated primary hepatocytes, and these HFD-induced increases were completely prevented by ABCB10 deletion (Fig. 6A, B). In addition, we validated that the total content of the bilirubin sensor UnaG was not altered by ABCB10 deletion (fig. S11), as expected given that UnaG was delivered via viral transduction. Furthermore, ABCB10 deletion did not change the content of proteins involved in heme catabolism (HMOX1), bilirubin synthesis (BLVRA) (fig. S12), or excretion (ABCC2) (fig. S13A). Moreover, the expression of the main enzyme involved in free bilirubin conjugation, UGT1A1, was not changed by ABCB10 deletion (fig. S13B). UGT activity, mostly determined by UGT1A1, showed a non-significant ($p>0.05$) decrease in ABCB10 KO livers, which could be reflecting an unsuccessful compensation trying to preserve free bilirubin content (fig. S13C). Altogether, these data support that a major driver of increased intrahepatic bilirubin content induced by HFD was bilirubin synthesis from mitochondrial biliverdin exported by ABCB10.

A major action of bilirubin is to decrease H_2O_2 content as well as mitochondrial OXPHOS, a source of H_2O_2. H_2O_2 released by mitochondria generates signals that improve insulin signaling and prevent hepatic steatosis (20, 36). Thus, as expected from decreased bilirubin content in ABCB10 KO hepatocytes, we explored whether ABCB10 deletion caused an increase in mitochondrial H_2O_2 release and H_2O_2-mediated actions regulating the activity of redox-sensitive proteins. Using ratiometric roGFP2 probes, we measured H_2O_2 and its action on the glutathione redox state (GSSG/GSH) in live primary murine hepatocytes. Concurrently with higher mitochondrial and cytosolic H_2O_2 content (Fig. 6C–D), both mitochondrial and cytosolic GSSG/GSH were increased in live hepatocytes isolated from HFD-fed LKO mice (Fig. 6E–F). The magnitude of the elevation in H_2O_2 content and in the GSSG/GSH ratio (ranging 25–40%), together with improved mitochondrial respiration, show that the increase in H_2O_2 induced by hepatic ABCB10 deletion was not in the toxic range.

Protein Tyrosine Phosphatase 1B is increased by HFD-feeding and plays a dual maladaptive action: PTP1B directly dephosphorylates Tyr1162/1163 in INSR, blocking insulin signaling, and activates a different signaling cascade that increases *Srebp1c* expression (37–39). Furthermore, PTP1B oxidative inactivation is one of the mechanisms by which mitochondrial H_2O_2 release was demonstrated to protect from insulin resistance and hepatic steatosis (20). Consequently, we determined the effects of ABCB10 deletion in HFD fed mice on PTP1B activity. By immunoprecipitating endogenous PTP1B from total lysates of primary hepatocytes, we found that HFD-fed ABCB10 LKO mice showed a ~30% decrease in PTP1B phosphatase activity (Fig. 6G).

In sum, ABCB10 driven increases in cellular bilirubin content generate a redox state favoring insulin resistance and steatosis, by disrupting mitochondrial H_2O_2 actions on

insulin signaling (fig. S14). To determine the causal role of bilirubin in these redox changes, we next aimed to restore bilirubin content in ABCB10 KO hepatocytes and test its effects on redox and PTP1B activity (Fig. 7A).

Bilirubin supplementation reverses the redox benefits induced by ABCB10 deletion in diet-induced obese mice

Supplementing primary hepatocytes isolated from HFD-fed LKO mice with physiological bilirubin concentrations (10 μM) effectively restored mitochondrial and cytosolic bilirubin to WT concentrations (Fig. 7A and fig. S4C). Moreover, the slope of the fold increase in UnaG fluorescence over time after adding bilirubin was the same in WT and LKO hepatocytes (fig. S4A,B), supporting that the capacity of extracellular bilirubin to reach both the cytosol and the mitochondrial matrix was not changed by ABCB10 deletion. One could hypothesize that the lower content of bilirubin in LKO could accelerate the entry of bilirubin into hepatocytes. However, our data showing the absence of an acceleration suggests that the occupancy of bilirubin acceptor(s) by other competing molecules could be increased by ABCB10 deletion, or that intracellular bilirubin content is not a parameter strongly determining bilirubin entry rates.

We next tested the relationship between decreased bilirubin and the redox changes induced by ABCB10 deletion. Restoring bilirubin in HFD-fed LKO hepatocytes brought mitochondrial H_2O_2 content and GSSG/GSH back to HFD-fed WT values (Fig. 7B, C). In WT hepatocytes, HFD-feeding significantly ($p<0.05$) increased only cytosolic H_2O_2 content and, accordingly, bilirubin supplementation significantly ($p<0.05$) decreased only cytosolic H_2O_2 in HFD-fed WT hepatocytes (Figs. 6C, 7B).

As ABCB10 deletion increased mitochondrial OXPHOS, which can elevate H_2O_2 release, we tested whether restoring bilirubin content could reverse the positive effects on mitochondrial respiration observed in ABCB10 KO hepatocytes. Bilirubin 10 μM reversed the increase in mitochondrial OXPHOS observed in primary hepatocytes from HFD-fed ABCB10 LKO mice without changing OXPHOS in WT hepatocytes (Fig. 7D–E). The acute nature of bilirubin actions on mitochondria was further supported by the reversal of increased respiration when bilirubin was added to liver mitochondria isolated from HFD-fed LKO mice (Fig. 7F).

We determined whether bilirubin-mediated reversal of ABCB10 KO actions on mitochondrial redox impacted PTP1B activity. Bilirubin induced a non-significant ($p > 0.05$) increase in PTP1B activity in WT hepatocytes from HFD mice (Fig. 7G), consistent with bilirubin decreasing cytosolic H_2O_2 content (Fig. 7B) and thus PTP1B oxidative inactivation (40). Last, the same bilirubin treatments completely reversed the reduction of PTP1B activity observed in ABCB10 KO hepatocytes isolated from HFD-fed mice (Fig. 7G). Altogether, these results show that bilirubin is the major effector of ABCB10-mediated redox actions in hepatocytes from HFD-fed mice (fig. S15).

DISCUSSION

We have identified that ABCB10 exports biliverdin out of the mitochondria to amplify bilirubin synthesis. Our cell-free approach using human ABCB10 reconstituted in vesicles demonstrates that ABCB10 transports biliverdin from the matrix to the intermembrane space (IMS) domain of ABCB10. Mitochondrial biliverdin export was confirmed *in vivo* by the accumulation of biliverdin in ABCB10 KO mitochondria isolated from mouse liver. Up to this study, it was known that ABCB10 supported hemoglobin synthesis in differentiating erythrocytes, by preventing oxidative damage associated with heme synthesis (16, 30). Thus, how does biliverdin export then protect from oxidative damage?

We find that mitochondrial biliverdin export executed by ABCB10 increases the availability of biliverdin destined for bilirubin synthesis, as the enzyme transforming biliverdin to bilirubin is located in the cytosol (BLVRA). Bilirubin is an effective antioxidant that scavenges H_2O_2 and, due to its lipophilic nature, effectively crosses mitochondrial membranes (10). Accordingly, elevating ABCB10 expression is sufficient to increase cytosolic and mitochondrial bilirubin content. Indeed, BLVRA can be associated with the cytosolic side of the ER (41, 42), an organelle with tight interactions with mitochondria in liver from insulin resistant mice (43). This tight interaction means that biliverdin exported by mitochondria can be readily transformed to bilirubin in ER-mitochondria contact areas, a microdomain that could facilitate a preferential trafficking of bilirubin to mitochondria.

Initially, we expected that hepatic ABCB10 deletion would exacerbate insulin resistance and steatosis in obese mice by increasing oxidative damage and disrupting insulin signaling (44, 45). However, we obtained the opposite results. Mitochondrial OXPHOS and insulin signaling were improved in hepatocytes from diet-induced obese ABCB10 LKO mice, concurrent with mild increases in mitochondrial and cytosolic H_2O_2 content. Our study is not the first example showing that a protein that hinders H_2O_2 actions in hepatocytes promotes insulin resistance and steatosis. Hepatocyte-specific deletion of glutathione peroxidase 1 (GPX1 LKO mice), a mitochondrial and cytosolic enzyme that removes H_2O_2, and hepatocyte-specific decreases in cytosolic biliverdin production achieved by deleting heme oxygenase 1 (HMOX1 LKO mice) induced the same benefits as ABCB10 deletion. In GPX1 LKO and HMOX1 LKO mice, an improvement in insulin sensitivity was explained by the post-translational oxidative inactivation of the phosphatase PTP1B (20, 36).

PTP1B is maladaptive in obesity, as it blocks insulin signaling transduction and promotes lipid synthesis in liver (37, 46). The increase in mitochondrial H_2O_2 release as a result of GPX1 and HMOX1 deletion leads to the oxidative inactivation of the catalytic cysteine in PTP1B. Hepatocyte-specific deletion or 50% downregulation of PTP1B activity is sufficient to protect mice from diet-induced obesity insulin resistance and steatosis (37, 46). Accordingly, we found that ABCB10 deletion decreased PTP1B phosphatase activity (30%) in hepatocytes from HFD fed mice, similarly to what was reported for GPX1 and HMOX1 deletion. However, the benefits induced by hepatic ABCB10 deletion on metabolic health are greater when compared to PTP1B deletion (37). These phenotypic differences support that ABCB10 deletion induces additional benefits beyond PTP1B inactivation. We propose that the increase in mitochondria function and energy expenditure observed in ABCB10

LKO mice are responsible for these additional benefits. In this regard, we demonstrated that decreased mitochondrial bilirubin content induced by ABCB10 deletion is responsible for improved mitochondrial function, a benefit that is not expected when PTP1B is deleted.

Other approaches inducing systemic increases in heme catabolism or in plasma bilirubin were shown to protect from metabolic dysfunction in obesity (47). However, mitochondrial bilirubin content was not measured in this study, meaning that it is possible that mitochondrial bilirubin was decreased by these other approaches. In this regard, bilirubin generated from mitochondrial biliverdin might preferentially act on different subcellular sites than imported bilirubin or bilirubin generated from cytosolic biliverdin. This preferential action could be achieved by confining bilirubin to a microdomain (ER-mitochondria contact areas) to restrict its action on specific targets. Thus, we propose that mechanisms controlling BLVRA trafficking to different cytosolic microdomains might be a major determinant of adapative and maladaptive bilirubin actions.

Controversy exists on whether bilirubin can be synthesized in the mitochondrial matrix, with one study detecting BLVRA in the inner mitochondrial membrane (48). This study did not determine whether the catalytic domain of BLVRA responsible for bilirubin synthesis was facing the matrix or the intermembrane space (IMS) (48). Indeed, the authors showed that isolated liver mitochondria can transform exogenous biliverdin to bilirubin. The transformation of exogenously added biliverdin supports that, if BLVRA was located in the inner membrane, the domain responsible for bilirubin synthesis could be facing the IMS to access exogenous biliverdin more easily. Moreover, it is unknown how BLVRA translocates from the cytosol to the inner membrane, as no mitochondrial targeting sequence is present in BLVRA. Last, other independent studies could not reproduce BLVRA detection in mitochondria, including MitoCarta (13, 14). Our data showing the existence of an active mitochondrial biliverdin export supports that bilirubin is not synthesized in the matrix. Lack of matrix bilirubin synthesis or in the inner membrane face of the IMS could be justified by the need to prevent bilirubin bursts damaging the mitochondrial inner membrane. Bilirubin is a lipophilic molecule that can strongly bind to membranes and fatty acid binding proteins. Indeed, bilirubin can make the membrane leaky to protons at low concentrations and completely block electron transfer at higher concentrations (12).

The maladaptive and non-essential role of hepatic ABCB10 function further supports that bilirubin is the major effector of ABCB10 actions. Bilirubin availability in hepatocytes *in vivo* cannot be severely impaired by eliminating ABCB10-mediated biliverdin export. ABCB10 KO hepatocytes can still synthesize bilirubin from biliverdin generated in the cytosol and import bilirubin from the blood (70% of bilirubin synthesis is extrahepatic) (9). Moreover, our data show that biliverdin accumulation in liver mitochondria induced by ABCB10 deletion is not toxic in mice. This conclusion can apply to erythroid cells as well, as the essential role of ABCB10 supporting heme synthesis in erythroid cells was rescued by antioxidant treatments (16). Consequently, heme biosynthesis and respiration occur in ABCB10 KO erythroid mitochondria accumulating biliverdin when oxidative damage is prevented. The role of bilirubin actions in erythroid cells remains largely uncharacterized, as the assumption is that heme molecules synthesized in erythroid mitochondria are all

exported to produce hemoglobin and none of them are degraded. Our study could potentially change our understanding of mitochondrial heme fate during erythroid differentiation.

As ABCB10 is dispensable for mouse liver function, is maladaptive in murine obesity, and its role exporting biliverdin and modulating insulin signaling is conserved in humans, we propose that hepatocyte-restricted targeting of ABCB10 holds promise as an approach to be tested to counteract hepatic insulin resistance and steatosis. The main limitation of our study is that the role of ABCB10 in mouse models of more severe forms of liver disease was not determined. Thus, it is a possibility that ABCB10 could be playing a protective role when liver damage is induced by something different than a high-fat diet model of obesity. In addition, the mechanism by which bilirubin slows down OXPHOS directly in mitochondria remains unidentified, but should involve saturable binding sites.

Materials and Methods

Study design.

The aim of this study was to examine the substrate transported by ABCB10, as well as the role of ABCB10 in the development of insulin resistance and steatosis. To this end, we used ABCB10 reconstituted into liposomes and nanodiscs, hepatocyte-specific ABCB10 KO mice, isolated mouse primary hepatocytes, human primary hepatocytes, and AML12 murine hepatocytes. We used fluorescent sensors to quantify bilirubin, H_2O_2, and GSSG/GSH in intact hepatocytes to determine the role of ABCB10 regulating the redox state and bilirubin compartmentalization in live cells. All experiments were approved by IACUC at Boston University and by ARC at UCLA. For mouse studies, a power analysis was used to calculate the sample sizes required. For *in vitro* studies, a minimum of three independent experiments were performed and the numbers of independent experiments (n) are presented in the figure legends.

Abcb10$^{Wt/flox}$ mice generation.

Targeted C57BL/6J ES cells with *Abcb10* containing loxP sites flanking exons 2–3 and a neomycin cassette flanked by Frt sites were generated by Genoway. Targeted ES cells were injected and implanted in C57BL/6J-Tyrc-2J/J (albino) females at the Boston University Mouse Transgenic Core, directed by Gregory L. Martin and Katya Ravid. Seven male chimeras containing floxed ABCB10 were identified by coat color and bred with C57BL/6J FLP recombinase females from Jackson (B6.Cg-Tg(ACTFLPe)9205Dym/J) to excise the neomycin cassette. The offspring were bred with wild type C57BL/6J, to obtain *Abcb10*$^{wt/flox}$ mice without FLP recombinase. *Abcb10*$^{wt/flox}$ mice were paired with B6.Cg-Tg(Alb-cre)21Mgn/J purchased from Jackson, to generate ABCB10 liver-specific KO mice. Groups analyzed were offspring littermates from breeding pairs between *Abcb10*$^{flox/flox}$; *Alb-Cre*$^{-/-}$ with *Abcb10*$^{wt/flox}$; *Alb-Cre*$^{+/-}$. Wild type mice (WT) are *Abcb10*$^{flox/flox}$ and *Abcb10*$^{wt/flox}$ mice (no Cre) and ABCB10-LKO are *Abcb10*$^{flox/flox}$; *Alb-Cre*$^{+/-}$.

Mice, diets, metabolic and body composition measurements

Mice were provided with water and food *ad libitum*, housed 2–5 mice per cage, 12h light:dark cycle and at a room temperature of 22–24ºC. Obesity and insulin resistance were

induced by high-fat diet feeding (D12451, Research Diets, 45 kcal % fat). Lean controls were mice fed a chow diet for the same period of time. Male mice were introduced to the diets after weaning (3–4 weeks of age). Body weight and food intake were monitored weekly. Glucose tolerance tests (GTT), Insulin tolerance tests (ITT) and metabolic cage measurements (CLAMS) were sequentially performed in the same cohorts of mice. Mice were left 2 weeks to recover between GTT and ITT measurements. ITTs were performed at 26 weeks and GTTs at 28 weeks of diet. At 30 weeks of diet, lean and fat mass were measured using Echo MRI, using a known mass of canola oil for calibration purposes, followed by 5 days of metabolic cage measurements. Additional cohorts of mice were used at 30 weeks to perform hyperinsulinemic-euglycemic clamps and isolate primary hepatocytes. Mice were left to recover from the metabolic cage analyses for 1 week and then euthanized, with plasma and tissues harvested for biochemical analyses. Body weight, GTT, ITT, and hyperinsulinemic clamps confirmed that protection from high-fat diet in LKO mice was preserved between 26–32 weeks of HFD feeding.

Statistical analyses

Data were tested for normality using Shapiro-Wilk. Excel, Graph Pad 8, and Sigma Plot 14.0 were used for statistical analyses, which included Student's t-tests or Mann-Whitney when comparing two groups, one-way ANOVA with Tukey or two-way ANOVA with Tukey or Holm-Sidak post hoc, when comparing multiple groups of samples. ANCOVA was performed with Sigma Plot 14, Systat Software Inc. using the MMPC website: https://www.mmpc.org/shared/regression.aspx. Chemical structures of bilirubin and biliverdin were taken from PubChem and drawn with ChemDoodle software.

Supplementary Material

Refer to Web version on PubMed Central for supplementary material.

ACKNOWLEDGEMENTS

We thank Daniel Braas and Thomas Graeber at the UCLA Metabolomics core for the LC/MS measurements of biliverdin. We thank Shinobu Matsuura, Gregory Martin, and Katya Ravid from the Transgenic Core at Boston University for the generation of ABCB10 floxed mice. We thank Tom Balon from Boston University for help with CLAMS. We thank Tobias Dick for the roGFP2 constructs, and thank Jong-Seok Park and Hyun-Woo Rhee for the UnaG construct. We thank Barbara E. Corkey, Marcus Fernandes de Oliveira, Susan K. Fried, and Orian S. Shirihai for input and discussions, and Sam B. Sereda, Eleni Ritou, and Nate Miller for technical assistance.

Funding:

M.L. is funded by the Department of Medicine at UCLA, pilot grants from P30 DK 41301 (UCLA:DDRC NIH), P50 AA011999 (USC-ALPD), UL1TR001881 (CTSI), P30 DK063491 (UCSD-UCLA DERC), P30 DK046200 (BNORC), and NIH-1R01AA026914-01A1. M.E.Z is funded by NIH-1R15GM131289-01. M.Sh. is funded by the Canadian Diabetes Association. C.A.S, R.A., M.R.Y, B.F. and E.P.C. were in the SGC, a registered charity funded by AbbVie, Bayer Pharma AG, Boehringer Ingelheim, Canada Foundation for Innovation, Genome Canada, Janssen, Merck KGaA, Merck & Co., Novartis, Ontario Ministry of Economic Development and Innovation, Pfizer, São Paulo Research Foundation-FAPESP, Takeda, Innovative Medicines Initiative Joint Undertaking ULTRA-DD grant 115766 and Wellcome Trust (106169/Z/14/Z). TA and JA were funded by by NIH 1R35GM135175-01, A.J.L by NIH-P01HL028481 and DK120342, and K.C.K by K99 DK120875 and AHA18POST33990256.

Data availability:

All data associated with this study are present in the paper or supplementary materials. The hybrid mouse diversity panel (HMDP) data is available at https://systems.genetics.ucla.edu. roGFP2 constructs were obtained under an MTA with Dr. Tobias Dick.

References and notes

1. Shadel GS, Horvath TL, Mitochondrial ROS signaling in organismal homeostasis. Cell 163, 560–569 (2015); published online EpubOct 22 (10.1016/j.cell.2015.10.001). [PubMed: 26496603]
2. Mironczuk-Chodakowska I, Witkowska AM, Zujko ME, Endogenous non-enzymatic antioxidants in the human body. Adv Med Sci 63, 68–78 (2018); published online EpubMar (10.1016/j.advms.2017.05.005). [PubMed: 28822266]
3. Sedlak TW, Saleh M, Higginson DS, Paul BD, Juluri KR, Snyder SH, Bilirubin and glutathione have complementary antioxidant and cytoprotective roles. Proc Natl Acad Sci U S A 106, 5171–5176 (2009); published online EpubMar 31 (10.1073/pnas.0813132106). [PubMed: 19286972]
4. Park JS, Nam E, Lee HK, Lim MH, Rhee HW, In Cellulo Mapping of Subcellular Localized Bilirubin. ACS Chem Biol 11, 2177–2185 (2016); published online EpubAug 19 (10.1021/acschembio.6b00017). [PubMed: 27232847]
5. Chiabrando D, Vinchi F, Fiorito V, Mercurio S, Tolosano E, Heme in pathophysiology: a matter of scavenging, metabolism and trafficking across cell membranes. Front Pharmacol 5, 61 (2014)10.3389/fphar.2014.00061).
6. Baranano DE, Rao M, Ferris CD, Snyder SH, Biliverdin reductase: a major physiologic cytoprotectant. Proc. Natl. Acad. Sci. U. S. A 99, 16093–16098 (2002); published online Epub12/10/2002 (10.1073/pnas.252626999 [doi];252626999 [pii]). [PubMed: 12456881]
7. Stocker R, Yamamoto Y, McDonagh AF, Glazer AN, Ames BN, Bilirubin is an antioxidant of possible physiological importance. Science 235, 1043–1046 (1987); published online Epub2/27/1987 ([PubMed: 3029864]
8. Nytofte NS, Serrano MA, Monte MJ, Gonzalez-Sanchez E, Turner Z, Ladefoged K, Briz O, Marin JJ, A homozygous nonsense mutation (c.214C->A) in the biliverdin reductase alpha gene (BLVRA) results in accumulation of biliverdin during episodes of cholestasis. J Med Genet 48, 219–225 (2011); published online EpubApr (10.1136/jmg.2009.074567). [PubMed: 21278388]
9. Erlinger S, Arias IM, Dhumeaux D, Inherited disorders of bilirubin transport and conjugation: new insights into molecular mechanisms and consequences. Gastroenterology 146, 1625–1638 (2014); published online Epub6/2014 (S0016–5085(14)00444–2 [pii];10.1053/j.gastro.2014.03.047 [doi]). [PubMed: 24704527]
10. Zucker SD, Goessling W, Hoppin AG, Unconjugated bilirubin exhibits spontaneous diffusion through model lipid bilayers and native hepatocyte membranes. J Biol Chem 274, 10852–10862 (1999); published online EpubApr 16 (10.1074/jbc.274.16.10852). [PubMed: 10196162]
11. Schutta HS, Johnson L, Neville HE, Mitochondrial abnormalities in bilirubin encephalopathy. J Neuropathol Exp Neurol 29, 296–305 (1970); published online EpubApr (10.1097/00005072-197004000-00010). [PubMed: 5435823]
12. Mustafa MG, Cowger ML, King TE, Effects of bilirubin on mitochondrial reactions. J. Biol. Chem 244, 6403–6414 (1969); published online Epub12/10/1969 ([PubMed: 4982202]
13. Slebos DJ, Ryter SW, van der Toorn M, Liu F, Guo F, Baty CJ, Karlsson JM, Watkins SC, Kim HP, Wang X, Lee JS, Postma DS, Kauffman HF, Choi AM, Mitochondrial localization and function of heme oxygenase-1 in cigarette smoke-induced cell death. Am J Respir Cell Mol Biol 36, 409–417 (2007); published online EpubApr (10.1165/rcmb.2006-0214OC). [PubMed: 17079780]
14. Calvo SE, Clauser KR, Mootha VK, MitoCarta2.0: an updated inventory of mammalian mitochondrial proteins. Nucleic Acids Res 44, D1251–1257 (2016); published online EpubJan 4 (10.1093/nar/gkv1003). [PubMed: 26450961]
15. Chen W, Paradkar PN, Li L, Pierce EL, Langer NB, Takahashi-Makise N, Hyde BB, Shirihai OS, Ward DM, Kaplan J, Paw BH, Abcb10 physically interacts with mitoferrin-1 (Slc25a37) to

enhance its stability and function in the erythroid mitochondria. Proc. Natl. Acad. Sci. U. S. A 106, 16263–16268 (2009); published online Epub9/22/2009 (0904519106 [pii];10.1073/pnas.0904519106 [doi]). [PubMed: 19805291]

16. Hyde BB, Liesa M, Elorza AA, Qiu W, Haigh SE, Richey L, Mikkola HK, Schlaeger TM, Shirihai OS, The mitochondrial transporter ABC-me (ABCB10), a downstream target of GATA-1, is essential for erythropoiesis in vivo. Cell Death. Differ 19, 1117–1126 (2012); published online Epub7/2012 (cdd2011195 [pii];10.1038/cdd.2011.195 [doi]). [PubMed: 22240895]
17. Yamamoto M, Arimura H, Fukushige T, Minami K, Nishizawa Y, Tanimoto A, Kanekura T, Nakagawa M, Akiyama S, Furukawa T, Abcb10 role in heme biosynthesis in vivo: Abcb10 knockout in mice causes anemia with protoporphyrin IX and iron accumulation. Mol. Cell Biol 34, 1077–1084 (2014); published online Epub3/2014 (MCB.00865–13 [pii];10.1128/MCB.00865-13 [doi]). [PubMed: 24421385]
18. Tang L, Bergevoet SM, Bakker-Verweij G, Harteveld CL, Giordano PC, Nijtmans L, de Witte T, Jansen JH, Raymakers RA, van der Reijden BA, Human mitochondrial ATP-binding cassette transporter ABCB10 is required for efficient red blood cell development. Br J Haematol 157, 151–154 (2012); published online EpubApr (10.1111/j.1365-2141.2011.08936.x). [PubMed: 22085049]
19. Bonkowsky HL, Sinclair PR, Sinclair JF, Hepatic heme metabolism and its control. Yale J Biol Med 52, 13–37 (1979); published online EpubJan-Feb ([PubMed: 222077]
20. Jais A, Einwallner E, Sharif O, Gossens K, Lu TT, Soyal SM, Medgyesi D, Neureiter D, Paier-Pourani J, Dalgaard K, Duvigneau JC, Lindroos-Christensen J, Zapf TC, Amann S, Saluzzo S, Jantscher F, Stiedl P, Todoric J, Martins R, Oberkofler H, Muller S, Hauser-Kronberger C, Kenner L, Casanova E, Sutterluty-Fall H, Bilban M, Miller K, Kozlov AV, Krempler F, Knapp S, Lumeng CN, Patsch W, Wagner O, Pospisilik JA, Esterbauer H, Heme oxygenase-1 drives metaflammation and insulin resistance in mouse and man. Cell 158, 25–40 (2014); published online EpubJul 3 (10.1016/j.cell.2014.04.043). [PubMed: 24995976]
21. Mahajan A, Taliun D, Thurner M, Robertson NR, Torres JM, Rayner NW, Payne AJ, Steinthorsdottir V, Scott RA, Grarup N, Cook JP, Schmidt EM, Wuttke M, Sarnowski C, Magi R, Nano J, Gieger C, Trompet S, Lecoeur C, Preuss MH, Prins BP, Guo X, Bielak LF, Below JE, Bowden DW, Chambers JC, Kim YJ, Ng MCY, Petty LE, Sim X, Zhang W, Bennett AJ, Bork-Jensen J, Brummett CM, Canouil M, Ec Kardt KU, Fischer K, Kardia SLR, Kronenberg F, Lall K, Liu CT, Locke AE, Luan J, Ntalla I, Nylander V, Schonherr S, Schurmann C, Yengo L, Bottinger EP, Brandslund I, Christensen C, Dedoussis G, Florez JC, Ford I, Franco OH, Frayling TM, Giedraitis V, Hackinger S, Hattersley AT, Herder C, Ikram MA, Ingelsson M, Jorgensen ME, Jorgensen T, Kriebel J, Kuusisto J, Ligthart S, Lindgren CM, Linneberg A, Lyssenko V, Mamakou V, Meitinger T, Mohlke KL, Morris AD, Nadkarni G, Pankow JS, Peters A, Sattar N, Stancakova A, Strauch K, Taylor KD, Thorand B, Thorleifsson G, Thorsteinsdottir U, Tuomilehto J, Witte DR, Dupuis J, Peyser PA, Zeggini E, Loos RJF, Froguel P, Ingelsson E, Lind L, Groop L, Laakso M, Collins FS, Jukema JW, Palmer CNA, Grallert H, Metspalu A, Dehghan A, Kottgen A, Abecasis GR, Meigs JB, Rotter JI, Marchini J, Pedersen O, Hansen T, Langenberg C, Wareham NJ, Stefansson K, Gloyn AL, Morris AP, Boehnke M, McCarthy MI, Fine-mapping type 2 diabetes loci to single-variant resolution using high-density imputation and islet-specific epigenome maps. Nat Genet 50, 1505–1513 (2018); published online EpubNov (10.1038/s41588-018-0241-6). [PubMed: 30297969]
22. Morris AP, Voight BF, Teslovich TM, Ferreira T, Segre AV, Steinthorsdottir V, Strawbridge RJ, Khan H, Grallert H, Mahajan A, Prokopenko I, Kang HM, Dina C, Esko T, Fraser RM, Kanoni S, Kumar A, Lagou V, Langenberg C, Luan J, Lindgren CM, Muller-Nurasyid M, Pechlivanis S, Rayner NW, Scott LJ, Wiltshire S, Yengo L, Kinnunen L, Rossin EJ, Raychaudhuri S, Johnson AD, Dimas AS, Loos RJ, Vedantam S, Chen H, Florez JC, Fox C, Liu CT, Rybin D, Couper DJ, Kao WH, Li M, Cornelis MC, Kraft P, Sun Q, van Dam RM, Stringham HM, Chines PS, Fischer K, Fontanillas P, Holmen OL, Hunt SE, Jackson AU, Kong A, Lawrence R, Meyer J, Perry JR, Platou CG, Potter S, Rehnberg E, Robertson N, Sivapalaratnam S, Stancakova A, Stirrups K, Thorleifsson G, Tikkanen E, Wood AR, Almgren P, Atalay M, Benediktsson R, Bonnycastle LL, Burtt N, Carey J, Charpentier G, Crenshaw AT, Doney AS, Dorkhan M, Edkins S, Emilsson V, Eury E, Forsen T, Gertow K, Gigante B, Grant GB, Groves CJ, Guiducci C, Herder C, Hreidarsson AB, Hui J, James A, Jonsson A, Rathmann W, Klopp N, Kravic J, Krjutskov K, Langford C, Leander K, Lindholm E, Lobbens S, Mannisto S, Mirza G, Muhleisen TW, Musk B, Parkin M,

Rallidis L, Saramies J, Sennblad B, Shah S, Sigurethsson G, Silveira A, Steinbach G, Thorand B, Trakalo J, Veglia F, Wennauer R, Winckler W, Zabaneh D, Campbell H, van Duijn C, Uitterlinden AG, Hofman A, Sijbrands E, Abecasis GR, Owen KR, Zeggini E, Trip MD, Forouhi NG, Syvanen AC, Eriksson JG, Peltonen L, Nothen MM, Balkau B, Palmer CN, Lyssenko V, Tuomi T, Isomaa B, Hunter DJ, Qi L, Wellcome C Trust Case Control, G. Meta-Analyses of, I. Insulin-related traits Consortium, A. T. C. Genetic Investigation of, C. Asian Genetic Epidemiology Network-Type 2 Diabetes, C. South Asian Type 2 Diabetes, Shuldiner AR, Roden M, Barroso I, Wilsgaard T, Beilby J, Hovingh K, Price JF, Wilson JF, Rauramaa R, Lakka TA, Lind L, Dedoussis G, Njolstad I, Pedersen NL, Khaw KT, Wareham NJ, Keinanen-Kiukaanniemi SM, Saaristo TE, Korpi-Hyovalti E, Saltevo J, Laakso M, Kuusisto J, Metspalu A, Collins FS, Mohlke KL, Bergman RN, Tuomilehto J, Boehm BO, Gieger C, Hveem K, Cauchi S, Froguel P, Baldassarre D, Tremoli E, Humphries SE, Saleheen D, Danesh J, Ingelsson E, Ripatti S, Salomaa V, Erbel R, Jockel KH, Moebus S, Peters A, Illig T, de Faire U, Hamsten A, Morris AD, Donnelly PJ, Frayling TM, Hattersley AT, Boerwinkle E, Melander O, Kathiresan S, Nilsson PM, Deloukas P, Thorsteinsdottir U, Groop LC, Stefansson K, Hu F, Pankow JS, Dupuis J, Meigs JB, Altshuler D, Boehnke M, McCarthy MI, Replication DIG, Meta-analysis C, Large-scale association analysis provides insights into the genetic architecture and pathophysiology of type 2 diabetes. Nat Genet 44, 981–990 (2012); published online EpubSep (10.1038/ng.2383). [PubMed: 22885922]

23. Seguin A, Takahashi-Makise N, Yien YY, Huston NC, Whitman JC, Musso G, Wallace JA, Bradley T, Bergonia HA, Kafina MD, Matsumoto M, Igarashi K, Phillips JD, Paw BH, Kaplan J, Ward DM, Reductions in the mitochondrial ABC transporter Abcb10 affect the transcriptional profile of heme biosynthesis genes. J Biol Chem 292, 16284–16299 (2017); published online EpubSep 29 (10.1074/jbc.M117.797415). [PubMed: 28808058]
24. Qiu W, Liesa M, Carpenter EP, Shirihai OS, ATP Binding and Hydrolysis Properties of ABCB10 and Their Regulation by Glutathione. PLoS One 10, e0129772 (2015)10.1371/journal.pone.0129772). [PubMed: 26053025]
25. Shintre CA, Pike AC, Li Q, Kim JI, Barr AJ, Goubin S, Shrestha L, Yang J, Berridge G, Ross J, Stansfeld PJ, Sansom MS, Edwards AM, Bountra C, Marsden BD, von Delft F, Bullock AN, Gileadi O, Burgess-Brown NA, Carpenter EP, Structures of ABCB10, a human ATP-binding cassette transporter in apo- and nucleotide-bound states. Proc Natl Acad Sci U S A 110, 9710–9715 (2013); published online EpubJun 11 (10.1073/pnas.1217042110). [PubMed: 23716676]
26. Martinez M, Fendley GA, Saxberg AD, Zoghbi ME, Stimulation of the human mitochondrial transporter ABCB10 by zinc-mesoporphrin. PLoS One 15, e0238754 (2020)10.1371/journal.pone.0238754). [PubMed: 33253225]
27. Saxberg AD, Martinez M, Fendley GA, Zoghbi ME, Production of a human mitochondrial ABC transporter in E. coli. Protein Expr Purif 178, 105778 (2021); published online EpubFeb (10.1016/j.pep.2020.105778). [PubMed: 33069825]
28. Kumagai A, Ando R, Miyatake H, Greimel P, Kobayashi T, Hirabayashi Y, Shimogori T, Miyawaki A, A bilirubin-inducible fluorescent protein from eel muscle. Cell 153, 1602–1611 (2013); published online EpubJun 20 (10.1016/j.cell.2013.05.038). [PubMed: 23768684]
29. Bennett BJ, Davis RC, Civelek M, Orozco L, Wu J, Qi H, Pan C, Packard RR, Eskin E, Yan M, Kirchgessner T, Wang Z, Li X, Gregory JC, Hazen SL, Gargalovic PS, Lusis AJ, Genetic Architecture of Atherosclerosis in Mice: A Systems Genetics Analysis of Common Inbred Strains. PLoS Genet 11, e1005711 (2015); published online EpubDec (10.1371/journal.pgen.1005711). [PubMed: 26694027]
30. Shirihai OS, Gregory T, Yu C, Orkin SH, Weiss MJ, ABC-me: a novel mitochondrial transporter induced by GATA-1 during erythroid differentiation. EMBO J 19, 2492–2502 (2000); published online Epub6/1/2000 (10.1093/emboj/19.11.2492 [doi]). [PubMed: 10835348]
31. Perry RJ, Samuel VT, Petersen KF, Shulman GI, The role of hepatic lipids in hepatic insulin resistance and type 2 diabetes. Nature 510, 84–91 (2014); published online EpubJun 5 (10.1038/nature13478). [PubMed: 24899308]
32. Michael MD, Kulkarni RN, Postic C, Previs SF, Shulman GI, Magnuson MA, Kahn CR, Loss of insulin signaling in hepatocytes leads to severe insulin resistance and progressive hepatic dysfunction. Mol. Cell 6, 87–97 (2000); published online Epub7/2000 (S1097–2765(05)00015–8 [pii]). [PubMed: 10949030]

33. Perry RJ, Camporez JG, Kursawe R, Titchenell PM, Zhang D, Perry CJ, Jurczak MJ, Abudukadier A, Han MS, Zhang XM, Ruan HB, Yang X, Caprio S, Kaech SM, Sul HS, Birnbaum MJ, Davis RJ, Cline GW, Petersen KF, Shulman GI, Hepatic acetyl CoA links adipose tissue inflammation to hepatic insulin resistance and type 2 diabetes. Cell 160, 745–758 (2015); published online EpubFeb 12 (10.1016/j.cell.2015.01.012). [PubMed: 25662011]
34. Vernia S, Cavanagh-Kyros J, Garcia-Haro L, Sabio G, Barrett T, Jung DY, Kim JK, Xu J, Shulha HP, Garber M, Gao G, Davis RJ, The PPARalpha-FGF21 hormone axis contributes to metabolic regulation by the hepatic JNK signaling pathway. Cell Metab 20, 512–525 (2014); published online EpubSep 2 (10.1016/j.cmet.2014.06.010). [PubMed: 25043817]
35. Perry RJ, Kim T, Zhang XM, Lee HY, Pesta D, Popov VB, Zhang D, Rahimi Y, Jurczak MJ, Cline GW, Spiegel DA, Shulman GI, Reversal of hypertriglyceridemia, fatty liver disease, and insulin resistance by a liver-targeted mitochondrial uncoupler. Cell Metab 18, 740–748 (2013); published online EpubNov 5 (10.1016/j.cmet.2013.10.004). [PubMed: 24206666]
36. Merry TL, Tran M, Dodd GT, Mangiafico SP, Wiede F, Kaur S, McLean CL, Andrikopoulos S, Tiganis T, Hepatocyte glutathione peroxidase-1 deficiency improves hepatic glucose metabolism and decreases steatohepatitis in mice. Diabetologia 59, 2632–2644 (2016); published online EpubDec (10.1007/s00125-016-4084-3). [PubMed: 27628106]
37. Delibegovic M, Zimmer D, Kauffman C, Rak K, Hong EG, Cho YR, Kim JK, Kahn BB, Neel BG, Bence KK, Liver-specific deletion of protein-tyrosine phosphatase 1B (PTP1B) improves metabolic syndrome and attenuates diet-induced endoplasmic reticulum stress. Diabetes 58, 590–599 (2009); published online EpubMar (10.2337/db08-0913). [PubMed: 19074988]
38. Krishnan N, Bonham CA, Rus IA, Shrestha OK, Gauss CM, Haque A, Tocilj A, Joshua-Tor L, Tonks NK, Harnessing insulin- and leptin-induced oxidation of PTP1B for therapeutic development. Nat Commun 9, 283 (2018); published online EpubJan 18 (10.1038/s41467-017-02252-2). [PubMed: 29348454]
39. Shimizu S, Ugi S, Maegawa H, Egawa K, Nishio Y, Yoshizaki T, Shi K, Nagai Y, Morino K, Nemoto K, Nakamura T, Bryer-Ash M, Kashiwagi A, Protein-tyrosine phosphatase 1B as new activator for hepatic lipogenesis via sterol regulatory element-binding protein-1 gene expression. J Biol Chem 278, 43095–43101 (2003); published online EpubOct 31 (10.1074/jbc.M306880200). [PubMed: 12941932]
40. Mahadev K, Zilbering A, Zhu L, Goldstein BJ, Insulin-stimulated hydrogen peroxide reversibly inhibits protein-tyrosine phosphatase 1b in vivo and enhances the early insulin action cascade. J Biol Chem 276, 21938–21942 (2001); published online EpubJun 15 (10.1074/jbc.C100109200). [PubMed: 11297536]
41. Kutty RK, Maines MD, Purification and characterization of biliverdin reductase from rat liver. J. Biol. Chem 256, 3956–3962 (1981); published online Epub4/25/1981 ([PubMed: 7217067]
42. Yoshinaga T, Sassa S, Kappas A, The occurrence of molecular interactions among NADPH-cytochrome c reductase, heme oxygenase, and biliverdin reductase in heme degradation. J Biol Chem 257, 7786–7793 (1982); published online EpubJul 10 ([PubMed: 6806283]
43. Arruda AP, Pers BM, Parlakgul G, Guney E, Inouye K, Hotamisligil GS, Chronic enrichment of hepatic endoplasmic reticulum-mitochondria contact leads to mitochondrial dysfunction in obesity. Nat Med 20, 1427–1435 (2014); published online EpubDec (10.1038/nm.3735). [PubMed: 25419710]
44. Koliaki C, Szendroedi J, Kaul K, Jelenik T, Nowotny P, Jankowiak F, Herder C, Carstensen M, Krausch M, Knoefel WT, Schlensak M, Roden M, Adaptation of hepatic mitochondrial function in humans with non-alcoholic fatty liver is lost in steatohepatitis. Cell Metab 21, 739–746 (2015); published online EpubMay 5 (10.1016/j.cmet.2015.04.004). [PubMed: 25955209]
45. Sunny NE, Parks EJ, Browning JD, Burgess SC, Excessive hepatic mitochondrial TCA cycle and gluconeogenesis in humans with nonalcoholic fatty liver disease. Cell Metab 14, 804–810 (2011); published online EpubDec 7 (10.1016/j.cmet.2011.11.004). [PubMed: 22152305]
46. Agouni A, Mody N, Owen C, Czopek A, Zimmer D, Bentires-Alj M, Bence KK, Delibegovic M, Liver-specific deletion of protein tyrosine phosphatase (PTP) 1B improves obesity- and pharmacologically induced endoplasmic reticulum stress. Biochem. J 438, 369–378 (2011); published online Epub9/1/2011 (BJ20110373 [pii];10.1042/BJ20110373 [doi]). [PubMed: 21605081]

47. Liu J, Dong H, Zhang Y, Cao M, Song L, Pan Q, Bulmer A, Adams DB, Dong X, Wang H, Bilirubin Increases Insulin Sensitivity by Regulating Cholesterol Metabolism, Adipokines and PPARgamma Levels. Sci. Rep 5, 9886 (2015); published online Epub5/28/2015 (srep09886 [pii];10.1038/srep09886 [doi]). [PubMed: 26017184]

48. Converso DP, Taille C, Carreras MC, Jaitovich A, Poderoso JJ, Boczkowski J, HO-1 is located in liver mitochondria and modulates mitochondrial heme content and metabolism. FASEB J 20, 1236–1238 (2006); published online EpubJun (10.1096/fj.05-4204fje). [PubMed: 16672635]

49. Folch J, Lees M, Sloane Stanley GH, A simple method for the isolation and purification of total lipides from animal tissues. J Biol Chem 226, 497–509 (1957). [PubMed: 13428781]

50. Ribas V, Drew BG, Zhou Z, Phun J, Kalajian NY, Soleymani T, Daraei P, Widjaja K, Wanagat J, de Aguiar Vallim TQ, Fluitt AH, Bensinger S, Le T, Radu C, Whitelegge JP, Beaven SW, Tontonoz P, Lusis AJ, Parks BW, Vergnes L, Reue K, Singh H, Bopassa JC, Toro L, Stefani E, Watt MJ, Schenk S, Akerstrom T, Kelly M, Pedersen BK, Hewitt SC, Korach KS, Hevener AL, Skeletal muscle action of estrogen receptor alpha is critical for the maintenance of mitochondrial function and metabolic homeostasis in females. Science translational medicine 8, 334ra354 (2016).

51. Steele R, Influences of glucose loading and of injected insulin on hepatic glucose output. Annals of the New York Academy of Sciences 82, 420–430 (1959). [PubMed: 13833973]

52. Nocito L, Kleckner AS, Yoo EJ, Jones IV AR, Liesa M, Corkey BE, The extracellular redox state modulates mitochondrial function, gluconeogenesis, and glycogen synthesis in murine hepatocytes. PLoS. One 10, e0122818 (2015). [PubMed: 25816337]

53. Shum M, Bellmann K, St-Pierre P, Marette A, Pharmacological inhibition of S6K1 increases glucose metabolism and Akt signalling in vitro and in diet-induced obese mice. Diabetologia 59, 592–603 (2016). [PubMed: 26733005]

54. Meyer AJ, Dick TP, Fluorescent protein-based redox probes. Antioxid Redox Signal 13, 621–650 (2010). [PubMed: 20088706]

55. Mahdaviani K, Benador IY, Shu S, Gharakhanian RA, Stiles L, Trudeau KM, Cardamone M, Enríquez-Zarralanga V, Ritou E, Aprahamian T, Oliveira MF, Corkey BE, Liesa M, Shirihai OS, Mfn2 deletion in brown adipose tissue protects from insulin resistance and impairs thermogenesis. EMBO Rep 18, 1123–1138 (2017). [PubMed: 28539390]

56. Zoghbi ME, Cooper RS, Altenberg GA, The Lipid Bilayer Modulates the Structure and Function of an ATP-binding Cassette Exporter. J Biol Chem 291, 4453–4461 (2016). [PubMed: 26725230]

57. Geertsma ER, Nik Mahmood NA, Schuurman-Wolters GK, Poolman B, Membrane reconstitution of ABC transporters and assays of translocator function. Nat Protoc 3, 256–266 (2008). [PubMed: 18274528]

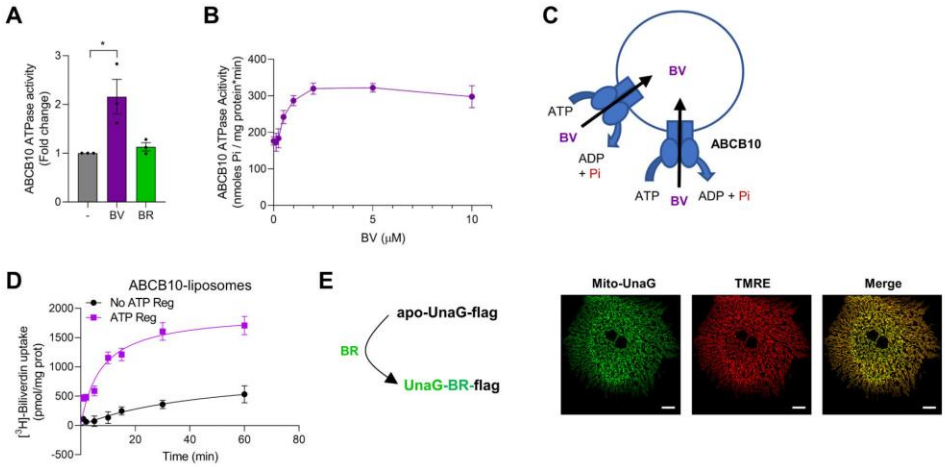

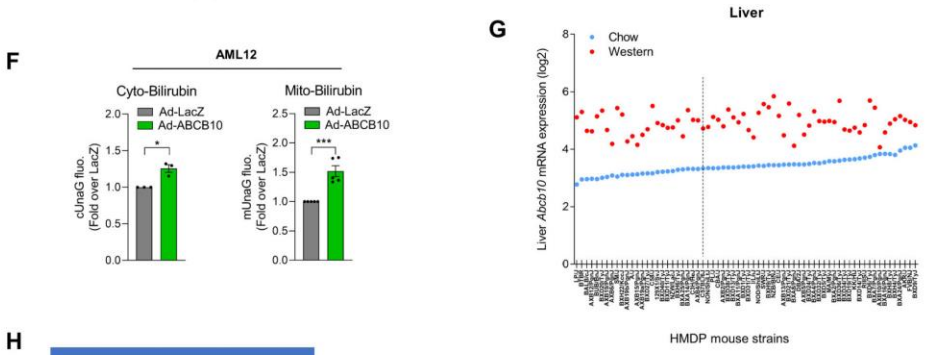

H

HMDP Western diet group		
Abcb10 expression-trait correlations		
Metabolic trait	Bi-correlation	P-value
HOMA-IR	0.288	0.0057
TG (liver)	0.285	0.0033
Fasting insulin	0.334	0.0008
gWAT	ND	>0.05

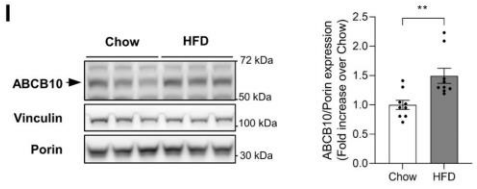

Fig. 1. ABCB10 exports mitochondrial biliverdin to increase bilirubin synthesis and is positively associated with insulin resistance and steatosis.

(**A**) ATPase activity of ABCB10 reconstituted into nanodiscs in the presence of biliverdin (BV, 5 μM) or bilirubin (BR, 5 μM). n=3 independent experiments. (**B**) Michaelis-Menten plot of ABCB10 ATPase activity with increasing biliverdin concentrations. N=7 independent experiments. (**C**) Scheme of ABCB10 orientation in sealed liposomes. (**D**) ^{3}[H]-biliverdin accumulation into sealed ABCB10-liposomes determined with or without ATP for the indicated times. Graph plotted using one-phase association equation, mean of n=5

independent transport experiments ± SEM, from two independent protein and liposome preparations. (**E**) UnaG-Flag protein fluorescence upon reversible binding to bilirubin, with high-resolution confocal images of primary mouse hepatocytes expressing the bilirubin sensor in mitochondria (Mito-UnaG or mUnaG) showing co-localization with the mitochondrial dye TMRE. Scale bar, 20 μm. (**F**) AML12 mouse hepatocytes co-transduced with adenovirus encoding LacZ or ABCB10 with cytosolic UnaG (cUnaG) or mUnaG to measure bilirubin, n=3–5 independent experiments. **(G)** Hepatic *Abcb10* mRNA content measured in 68 strains (x axis) of the Hybrid Mouse Diversity Panel (HMDP) fed chow (blue) or Western diet (red), including C57BL/6J (dashed line). (**H**) Biweight midcorrelation values between hepatic ABCB10 transcript content with the metabolic trait measured in the Western diet-fed HMDP mice, with nominal p values shown (n=102 strains). (**I**) ABCB10 expression in liver lysates from WT mice fed a HFD (45% Kcal as fat). n=9 mice per group; Mann-Whitney U test; *p<0.05; **p<0.01; ***p<0.001.

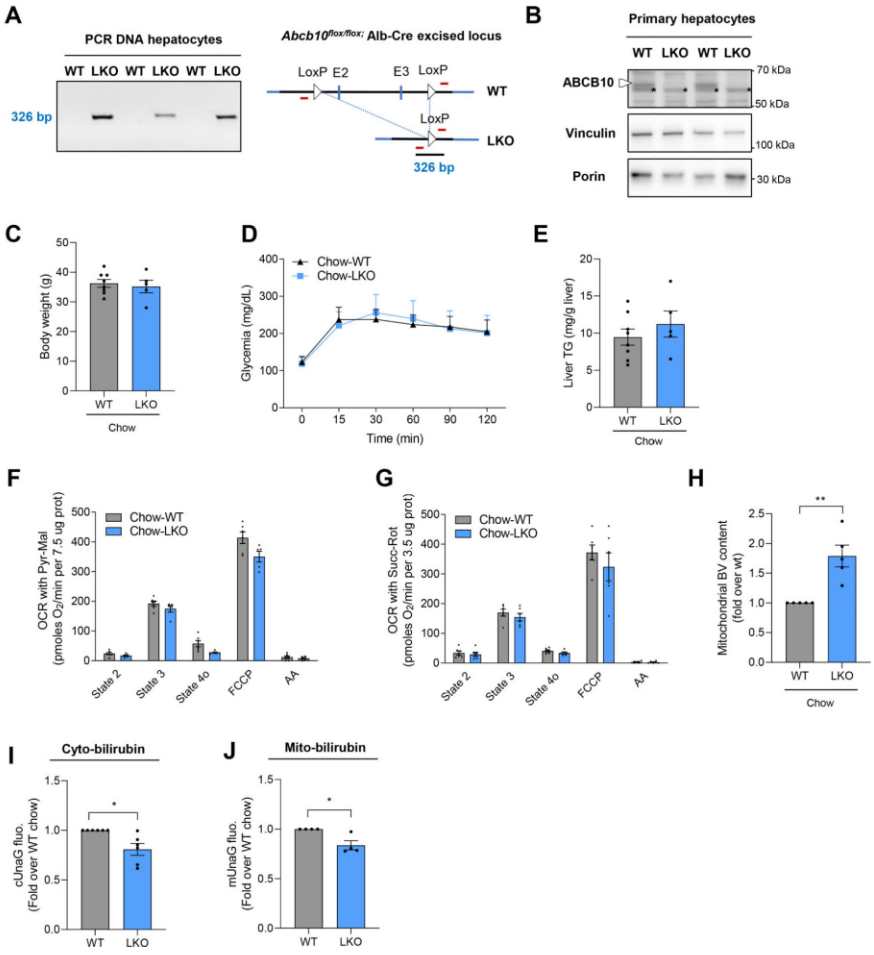

Fig. 2. ABCB10-mediated bilirubin synthesis is dispensable for normal hepatocyte function in control mice.

(**A**) PCR product of the genomic fragment resulting from Cre-mediated excision of *Abcb10*$^{flox/flox}$, determined in extracts of hepatocytes isolated from ABCB10-LKO mice; one mouse per lane. (**B**) ABCB10 protein measured in lysates from isolated primary hepatocytes, with an unspecific band close to ABCB10 marked with an asterisk*, one mouse per lane. Measurements in WT and ABCB10-LKO mice after 28 weeks of chow diet of (**C**) body weight and (**D**) blood glucose content during an i.p. glucose tolerance test (GTT) after 16h fast. n=5–8 male mice. (**E**) Liver triglyceride (TG) content in total liver lipid extracts. (**F-G**) Oxygen consumption rates (OCR) of isolated liver mitochondria from WT and ABCB10 LKO littermates under state 2 (leak), state 3 (maximal ATP synthesis), state 4o (leak after oligomycin injection), maximal respiratory capacity (FCCP), and non-respiration OCR (antimycin A, AA), fueled by pyruvate + malate (**F**) or by succinate + rotenone (**G**).

n=5–6 mice/group. **(H)** Mitochondrial biliverdin content measured by LC/MS in liver mitochondria isolated from WT and ABCB10 LKO. n=5 mice/group. Student's t-test **p<0.01 (**I**) Primary hepatocytes from lean (chow diet) WT or ABCB10-LKO mice transduced with adenovirus encoding cytosolic UnaG (cUnaG), to measure cytosolic bilirubin content (Student's t-test; *p<0.05) or (**J**) with adenovirus encoding mitochondrial matrix-targeted UnaG (mUnaG). Mann-Whitney U test; *p<0.05. n=4–6 mice. Results are presented as mean ± SEM.

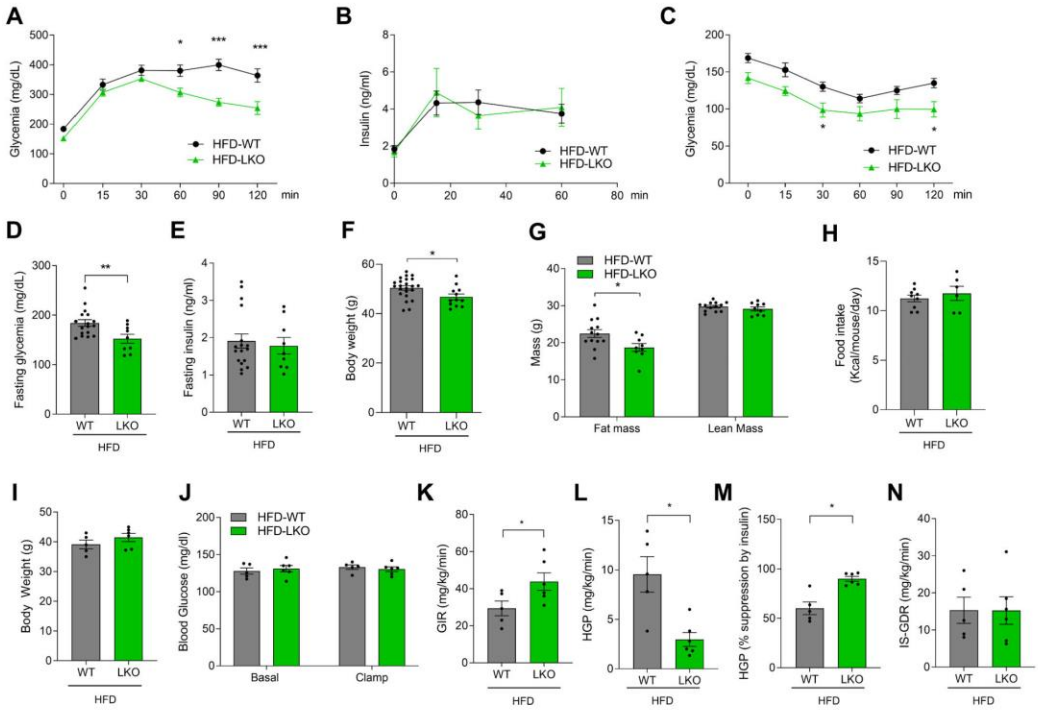

Fig. 3. Hepatic ABCB10 deletion protects from HFD-induced insulin resistance and increases insulin-mediated suppression of hepatic glucose production.

(A-N) WT and ABCB10 LKO male mice were fed a HFD and (**A**) blood glucose and (**B**) plasma insulin were measured after 16h fasting during GTT at 28 weeks of diet; Two-way ANOVA; *p<0.05, ***p<0.001, n=9–17 mice per group. (**C**) Insulin tolerance test (ITT) performed after a 6h fast at 26 weeks of HFD. Two-way ANOVA; *p<0.05, n=11–19 mice per group. (**D**) Fasting glycemia and (**E**), fasting insulinemia values from panels A and B. (**F**) Body weight of WT and LKO mice after 30 weeks of HFD. N=9–23 mice per group; Student's t-test, *p < 0.05 **p<0.01. (**G**) Lean and fat mass of HFD-fed WT and LKO mice determined by Echo-MRI at 30 weeks of diet. N=9–13 mice/group Student's t-test, *p < 0.05. (**H**) Daily food intake in WT or ABCB10 LKO mice. (**I-N**), Hyperinsulinemic-euglycemic clamps in weight-matched HFD-fed WT and ABCB10-LKO mice at 30 weeks of diet, n=5–6 mice/group. (**I**) Body weight of clamped mice with (**J**) blood glucose concentration at basal state and during the clamps. (**K**) Glucose infusion rates (GIR), Student's t-test, *p<0.05. (**L**) Hepatic glucose production (HGP), Student's t-test, *p<0.05. (**M**) Insulin suppression of HGP, Student's t-test, *p<0.05. (**N**), Insulin-stimulated glucose disappearance rate (IS-GDR). Results are presented as mean ± SEM.

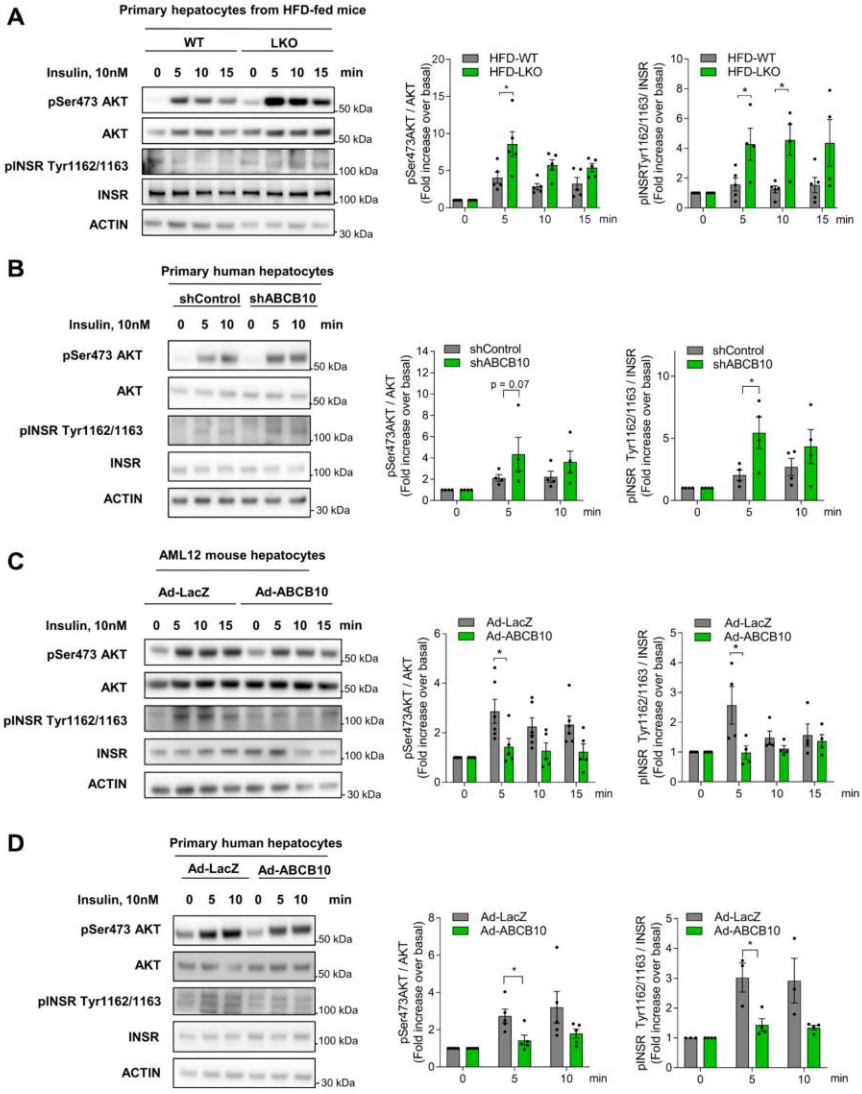

Fig. 4. ABCB10 is sufficient to impair insulin signaling in mouse and human primary hepatocytes.

(**A**) Western blots detecting pSer473 AKT and pTyr1162/1163 INSR in total lysates of primary hepatocytes isolated from HFD-fed WT and LKO mice. Hepatocytes were serum-starved (o/n) and treated with 10 nM insulin for the indicated times. n=4–5 independent experiments. (**B**) Human hepatocytes were transduced with lentivirus encoding shControl (sh001) or shABCB10. Two days after transduction, hepatocytes were serum-starved (6h) and treated with 10 nM insulin for the indicated times. Western blots of pSer473 AKT and

pIR Tyr1162/1163 in total lysates. n=4 independent experiments. (**C**) Mouse AML12 hepatocytes were transduced with Adenovirus (Ad) encoding LacZ or ABCB10. Two days after transduction, hepatocytes were serum-starved (6h) and treated with 10 nM insulin for the indicated times. Western blots of pSer473 AKT and pTyr1162/1163 INSR, n=4–6 independent experiments. (**D**) Human primary hepatocytes transduced with Ad-LacZ and Ad-ABCB10. Two days after transduction, hepatocytes were serum-starved (6h) and treated with 10 nM insulin for the indicated times. Western blots detecting pSer473 Akt and pTyr1162/1163 INSR in total lysates. n=3–5 independent experiments. Mean ± SEM, *p<0.05 One-way ANOVA.

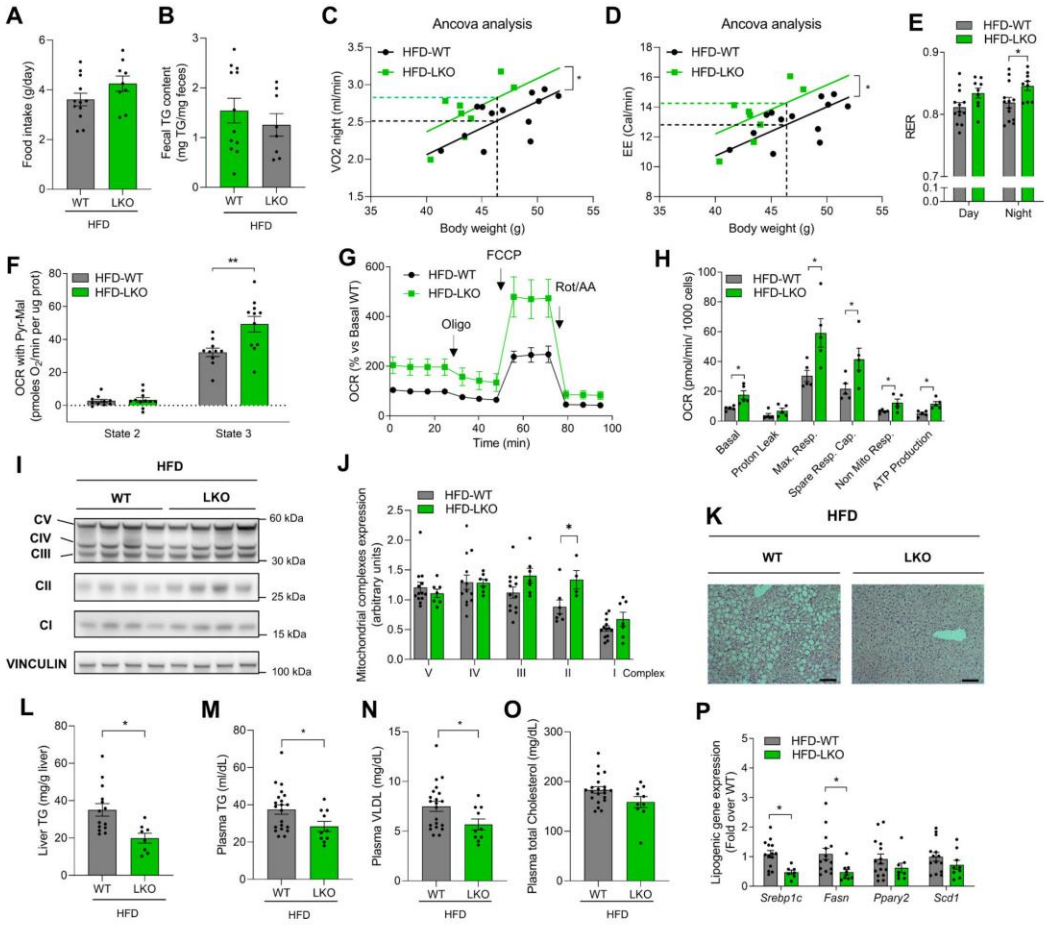

Fig. 5. Hepatic ABCB10 deletion increases mitochondrial energy expenditure and protects from hepatic steatosis and hyperlipidemia induced by high-fat diet.

(**A-O**) Measurements in WT and ABCB10-LKO male mice fed a high-fat diet (HFD) for 30–32 weeks. (**A**) Food intake of each individual mouse over a 48h period and (**B**) triglyceride (TG) content measured in feces collected in the metabolic cages (n=8–12 mice). (**C**) Co-variate analysis of VO_2 and (**D**) energy expenditure (EE) versus total body weight measured using CLAMS. Dashed lines represent the average body weight values modeled to determine VO_2 and EE in each group, *p<0.05 using ANCOVA, n=8–13 mice/group. (**E**) Respiratory exchange ratio (RER), *p<0.05, Student's t test; n=8–13 mice/group. (**F**) Oxygen consumption rates (OCR) from isolated liver mitochondria under state 2 (leak) and state 3 (maximal ATP synthesis) fueled by pyruvate (Pyr) and malate (Mal). n=10–12 mice/ group, **p<0.01, Student's t-test. (**G**) OCR traces showing basal, ATP-synthesizing (oligomycin sensitive), and maximal respiration (induced by FCCP) and (**H**) their bar graph quantification measured in intact primary hepatocytes isolated from n=5 mice/group;

*p<0.05, Student's t-test. (**I-J**) Mitochondrial complex I to V subunits protein content in total liver lysates, with vinculin as loading control. n=7–13 mice/group. *p<0.05, Student's t-test WT vs LKO. (**K**) Hematoxylin & eosin staining of liver sections. Scale bar, 100 μm. (**L**) Liver triglyceride content in total liver lipid extracts. n=8–14 mice/ group; *p<0.05, Student's t-test. (**M**) Plasma triglyceride, (**N**) plasma very-low-density lipoprotein (VLDL) and (**O**) plasma total cholesterol concentration. n=10–21 mice per group. *p<0.05, Student's t-test. (**P**) Expression of lipogenic genes *Srebp1c*, *Fasn, Atgl, Pparγ2, Scd1* measured by qPCR of cDNA retrotranscribed from HFD fed-WT and LKO mouse livers. n=7–15 mice/ group. *p<0.05, Student's t-test. Results presented as mean ± SEM.

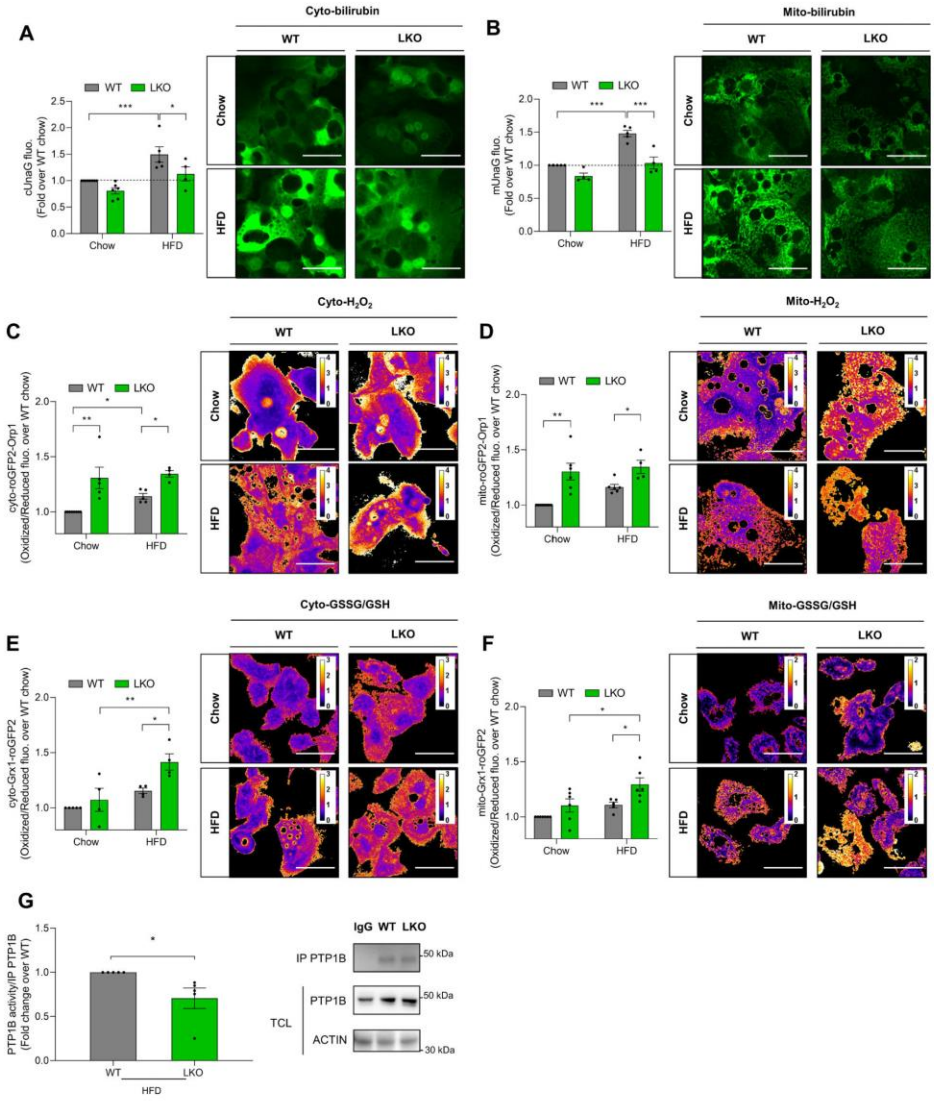

Fig. 6. Hepatic ABCB10 deletion increases mitochondrial H_2O_2 release and inactivates PTP1B, a phosphatase promoting hepatic insulin resistance and steatosis.

(**A-B**) Primary hepatocytes from lean (chow diet) and HFD-fed WT and ABCB10-LKO mice transduced with adenovirus encoding cytosolic UnaG (cUnaG), to measure cytosolic bilirubin content, or encoding mitochondrial matrix-targeted UnaG (mUnaG), to measure mitochondrial bilirubin. n=5–8 mice/group and independent experiments. Scale bar, 100 μm. Two-way ANOVA; *p<0.05, **p<0.01, ***p<0.001. (**C-F**) Primary hepatocytes isolated from WT and ABCB10-LKO mice fed a HFD for 30 weeks and transduced with adenovirus

encoding (**C**) Cyto-roGFP2-Orp1, measuring cytosolic H_2O_2 content, (**D**) Mito-roGFP2-Orp1, measuring mitochondrial matrix H_2O_2 content, (**E**) Cyto-Grx1-roGFP2 measuring cytosolic GSSG/GSH or (**F**) Mito-Grx1-roGFP2 measuring mitochondrial GSSG/GSH. The ratio of green fluorescence emitted by oxidized roGFP2 divided by reduced roGFP2 is proportional to H_2O_2 content (Orp1) and GSSG/GSH (Grx1) respectively. Scale bar, 100 μm. n=4–9 mice/group and independent isolations; *p<0.05, **p<0.01, Two-way ANOVA. (**G**) PTP1B activity measured in primary hepatocytes isolated from HFD-fed WT and ABCB10-LKO mice by immunoprecipitating PTP1B and measuring its phosphatase activity. n=5 mice/group and independent isolations; *p<0.05, Mann-Whitney U test. Results presented as mean ± SEM.

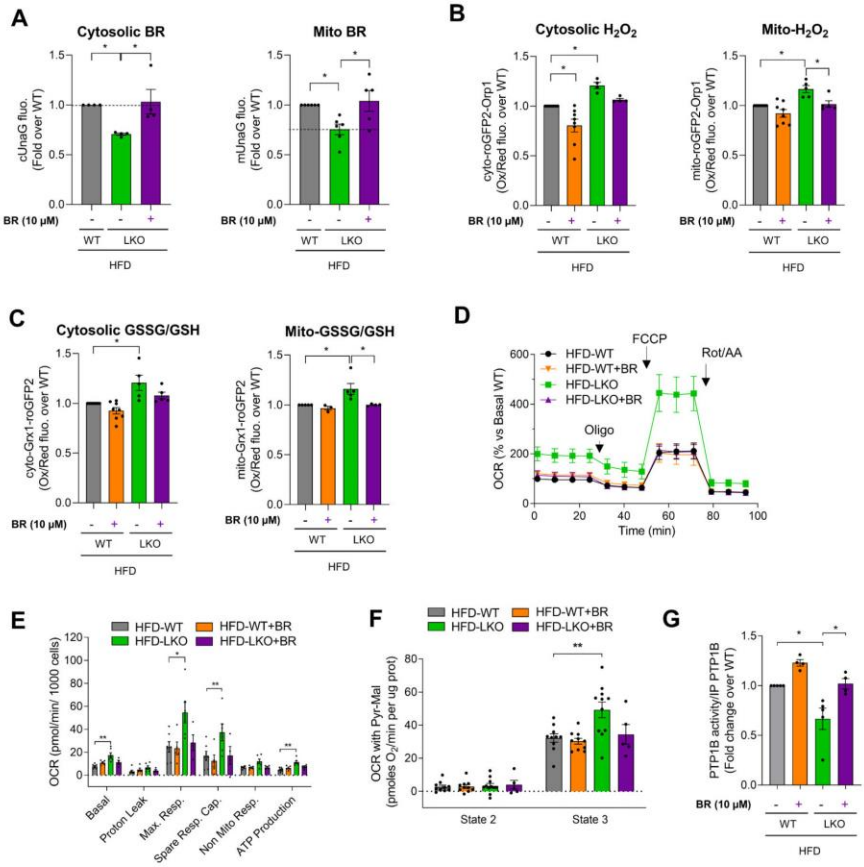

Fig. 7. Bilirubin supplementation reverses the redox benefits induced by hepatic ABCB10 deletion in diet-induced obese mice.

(**A**) Live imaging of cUnaG and mUnaG average fluorescence intensity to quantify cytosolic and mitochondrial bilirubin in hepatocytes isolated from HFD-fed ABCB10 LKO mice and then treated with vehicle (DMSO) and 10 μM bilirubin. Effects of the same bilirubin treatments on (**B**) cytosolic and mitochondrial matrix H_2O_2 content and (**C**) Grx1-roGFP2 and mito-Grx1-roGFP2 measuring cytosolic and mitochondrial GSSG/GSH. n = 3–8 mice/group. *p<0.05; Two-way ANOVA. (**D**) Respiration traces of primary hepatocytes treated with vehicle (DMSO) or 10 μM bilirubin (16h), isolated from HFD-fed WT and ABCB10 LKO mice. (**E**) Bar graph of respiration traces in (**D**) ± SEM. n=3–7 mice/group. Two-way ANOVA: *p<0.05 (**F**) Liver mitochondria isolated from HFD-fed WT and ABCB10 LKO mice respiring under state 2 (leak) and state 3 (maximal ATP synthesis) fueled by pyruvate (Pyr) and malate (Mal), with vehicle (DMSO) or 10 μM bilirubin (BR). n=5–11 mice/group. Two-way ANOVA; **p<0.01. (**G**) Phosphatase activity measured in immunoprecipitated PTP1B from primary hepatocytes treated with vehicle (DMSO) or 10 μM bilirubin (BR)

(16h) and isolated from HFD-fed WT and ABCB10 LKO mice. n= 4–5 mice/group. Two-way ANOVA, *p<0.05. Results presented as mean ± SEM.

SUPPLEMENTARY MATERIALS

Science Translational Medicine
AAAS

stm.sciencemag.org/cgi/content/full/13/594/eabd1869/DC1

Supplementary Materials for

ABCB10 exports mitochondrial biliverdin, driving metabolic maladaptation in obesity

Michael Shum, Chitra A. Shintre, Thorsten Althoff, Vincent Gutierrez, Mayuko Segawa, Alexandra D. Saxberg, Melissa Martinez, Roslin Adamson, Margaret R. Young, Belinda Faust, Raffi Gharakhanian, Shi Su, Karthickeyan Chella Krishnan, Kiana Mahdaviani, Michaela Veliova, Dane M. Wolf, Jennifer Ngo, Laura Nocito, Linsey Stiles, Jeff Abramson, Aldons J. Lusis, Andrea L. Hevener, Maria E. Zoghbi, Elisabeth P. Carpenter, Marc Liesa*

*Corresponding author: Email: mliesa@mednet.ucla.edu

Published 19 May 2021, *Sci. Transl. Med.* **13**, eabd1869 (2021)
DOI: 10.1126/scitranslmed.abd1869

The PDF file includes:

Table S1. Primer sequences.
Legend for data file S1

Other Supplementary Material for this manuscript includes the following:

(available at stm.sciencemag.org/cgi/content/full/13/594/eabd1869/DC1)

Data File S1 (Microsoft Excel format). Primary data for Figs. 1 to 7 in tabular format.

Supplementary material

Materials and Methods

Genotyping and PCR validating Cre-mediated excision

Mouse tails (0.5 cm) and primary hepatocytes were lysed with 200 µl and 50 µl of Viagen direct PCR lysis reagent with proteinase K respectively. One microliter of the lysate was used to amplify ABCB10 floxed alleles using primers r11: GCAGACTGTAGGGACAAAGGCATCAC and 12: CTGAGCCGTCAGAGGTAATCG, which concurrently amplify the floxed and WT allele. To detect Cre-mediated excision of floxed ABCB10, primers 27: AGAAGCCTTCCCTATTGAGCTCATGC and 26: GGAACTGCTCCCCAAAGTTTATGTATCG, amplified a 326 bp fragment only existing after excision. The WT allele fragment flanked by these primers being too long to be amplified (see **Fig. 2A**).

Glucose and insulin tolerance tests (GTT, ITT)

Mice were fasted overnight for GTT and 6h for ITT, with fasting blood glucose measured before intraperitoneal injection of glucose (1g/kg weight) or insulin (Humulin, 1 mU/g weight), in a blood drop obtained from a tail nick. Then, after injection of glucose or insulin respectively, additional blood glucose measures were performed at 15, 30, 60, 90, and 120 min using *Free style* (Abbot) glucometer and glucose strips. Additional blood was collected during GTT using glass capillaries containing EDTA (Sarstedt and Fisher brand) to obtain plasma and measure insulin at time 0, 15 and 30 min by ELISA (ALPCO).

Metabolic cage measurements

O_2 consumed, CO_2 produced and physical activity (XYZ, laser beam breaks counts) were determined using Oxymax Comprehensive Lab Animal Monitoring System (CLAMS, Columbus Instruments) at the Boston University Mouse Physiology core and at UCLA. Mice were housed for 5 days in CLAMS, with data analyzed for the last 2 days, when the 3 day-acclimation period to the metabolic cages passed. RER was calculated with CLAX software (Columbus Instruments) as VCO_2/VO_2. Energy expenditure in

cal/min was derived from the Lusk equation: $(3.815 + 1.232 \times RER) \times VO_2$, with VO_2 in ml/min. The system was calibrated with gas of a known O_2 and CO_2 % before every experiment.

Liver and feces triglycerides

Liver and feces triglycerides were quantified by extracting their lipid fraction using a variation of the Folch method (*48*). Briefly, 100 mg of crushed frozen liver powder or 60 mg feces were mixed with 6 ml of Chloroform : Methanol (2:1) in glass vials, homogenized for 30 seconds, capped and incubated overnight at 4ºC on a shaker. Then, 1.5 ml $MgCl_2$ (0.043%) was added, the mixture vortexed and centrifuged 15 min at 2000 rpm. The lower organic phase was collected with a glass pipette and transferred to a clean glass tube. The solvent was evaporated and lipids resuspended in 500 ml of 1% Triton X-100 in chloroform, with chloroform evaporated again. The lipids with Triton X-100 were finally resuspended in water, vortexing and incubating them at 65ºC for 20 min. Triglycerides were measured using a colorimetric assay as described (*29*).

Hyper-insulinemic euglycemic clamps

Glucose clamps were performed 3 days after implanting dual catheters in the right jugular vein of mice. Mice were fasted for 6h prior to the clamp. Basal glucose turnover was determined after 90 min of constant [3-^{3}H] D-glucose infusion (5.0 µCi/h, 0.12 ml/h, Perkin Elmer). After basal glucose turnover rate was assessed at steady state, insulin (8 $mU \cdot kg^{-1} \cdot min^{-1}$; Novo Nordisk) plus [3-^{3}H] D-glucose (5.0 µCi/h) were constantly infused (2 µl/min). Exogenous glucose was simultaneously infused at a rate to maintain blood glucose at fasting levels and thus match the decrease in glycemia induced by insulin. Blood glucose concentration was clamped at ~130 mg/dl using a variable glucose (50% dextrose; Abbott) infusion rate (GIR). As previously described and using the Steele equation for steady state metabolism (*49, 50*), a tracer dilution approach was used to determine the rate of endogenous hepatic glucose production (HGP) and the insulin-stimulated glucose disposal rate above basal (IS-GDR).

Hybrid Mouse Diversity Panel (HMDP) analyses

Liver and serum were collected from transgenic male mice carrying both human *CETP* and human *APOE3* Leiden variant, fed a "Western diet" starting at 8-weeks of age (33 % kcal fat from cocoa butter, 1% cholesterol, Research Diets D10042101) and euthanized after 8 weeks of diet. The control group were the same mouse strains without the human transgenes and fed a chow diet (Ralston Purina Company). The bicor (biweight midcorrelation) function implemented in the Weighted Gene Co-expression Network Analysis R package (WGCNA) was used to calculate hepatic *Abcb10* transcript-trait correlations in the Western diet group and obtain a nominal p value for the different correlations. Gene expression data in the liver was determined by hybridization to Affymetrix HT-MG_430 PM microarrays, with *Abcb10* mRNA quantified using probe 1416403_PM. Serum and liver triglycerides were measured in the HMDP strains as described (*29*).

Serum triglycerides, cholesterol, and VLDL measurements

TGs and total cholesterol were measured by colorimetric assays from Sigma according to the manufacturer's instructions. VLDL in plasma were quantified using the Friedewald calculation as described (*29*).

Primary mouse hepatocyte isolation and culture

This protocol was modified from our previous publication (*51*). Krebs-perfused livers of ketamine/xylazine anesthetized mice were digested by perfusing a type 4 collagenase solution (Worthington Biochemical Corp) through the inferior vena cava. Hepatocyte viability was determined by trypan blue exclusion, with isolations only over 70% viability being used. WT and LKO sibling pairs were used in each independent isolation experiment. Primary hepatocytes were plated in M199 medium supplemented with 100 U/ml penicillin, 100 µg/ml streptomycin, 0.1% bovine serum albumin, 500 nM dexamethasone (Sigma-Aldrich), 100 nM triiodothyronine (Sigma-Aldrich), 10 nM insulin (Actrapid, Novo Nordisk). Hepatocytes were seeded at a density of 2.5×10^5 cells/well on 6-well plates and 8000 cells/well on 96 well plates for XF96 respirometry and for live cell fluorescence imaging. After 2-4h of

seeding hepatocytes on a collagen-coated plate, media was replaced to remove unattached, dead hepatocytes with M199 medium supplemented with 100 U/ml penicillin, 100 µg/ml streptomycin, 0.1% bovine serum albumin, 500 nM dexamethasone.

AML12 and human primary hepatocytes culture

AML12 mouse hepatocytes were grown in DMEM/F12 media (Thermofisher Scientific) supplemented with 10% (vol./vol.) FBS, insulin (0.003 mg/ml), dexamethasone (40 ng/ml), transferrin (0.005 mg/ml) and sodium selenite (5 ng/ml). 48h later, AML12 were deprived of serum for 6h prior to insulin (10 nM) treatment for the indicated times. Human primary hepatocytes were purchased from Lonza and cultured in Williams E media supplemented with 10% (vol./vol.) FBS, dexamethasone (500 nM), penicillin/streptomycin 1% (vol./vol.), insulin (10 nM), triiodothyronine (200 nM) and HEPES (15 mM). 48h later, human primary hepatocytes were deprived of serum for 6h prior to insulin (10 nm) treatment for the indicated times. For adenoviral and lentiviral transductions, hepatocytes were exposed to the MOI indicated in each method section listed below, washed and analyzed 48h later.

PTP1B activity measurements

Primary hepatocytes were homogenized in lysis buffer 48h after their isolation (20 mM Tris pH 7.6, 150 mM NaCl, 0.5 mM EDTA, protease inhibitors, and 1% Triton X-100). Lysates were centrifuged for 10 min at 12.000xg, to discard the insoluble fraction. One milligram of protein from lysates was precleared for 10 min at 4°C by incubation with 20 µl protein A/G plus agarose beads (Santa Cruz). Precleared samples were incubated for 1 h at 4°C with anti-PTP1B (Proteintech). Next, 20 µl agarose beads were added to capture PTP1B complexed to the antibody and incubated for 2 h at 4°C. Samples were washed two times with immunoprecipitation buffer and two times with phosphatase assay buffer (25 mM HEPES pH 7.2, 50 mM NaCl, 2 mM EDTA, 3 mM DTT). PTP1B activity was measured using 50 mM of para-nitrophenylphosphate (New England BioLabs) as a phosphatase substrate, according to the manufacturer's instructions. Subsequently, immunoprecipitated PTP1B samples were boiled and

subjected to immunoblotting using rabbit anti-PTP1B (R&D System). Immunoprecipitated PTP1B content was quantified by blot densitometry and PTP1B phosphatase activity was normalized to the amount of immunoprecipitated PTP1B.

Insulin signaling analyses

This protocol was modified from our previous publication (*52*). Briefly, serum starved primary hepatocytes were treated, for the indicated times, with saline or 10 nM insulin (Actrapid, Novo Nordisk). Insulin action was quantified by measuring the fold increase in phosphorylation of AKT and the insulin receptor (INSR) induced by insulin over the saline group, detected by Western blot.

Primary mouse hepatocyte respirometry and bilirubin treatments

Freshly isolated hepatocytes were seeded at 8000 cells/well on 96 well-plate for Seahorse respirometry (Agilent), measured 48h after isolation. One hour prior and during the assay itself, hepatocytes were cultured in DMEM with low glucose. Mitochondrial stress test compounds were added at 2 μM oligomycin, 1 μM FCCP, 1 μM rotenone and 1 μM antimycin A. Bilirubin was added at 10 μM 16 hours prior running the respirometry assay, with bilirubin being present during respirometry.

Hepatocyte transduction and imaging of redox and bilirubin probes

The cDNAs for UnaG and roGFP2 sensors were obtained from Drs. Rhee (*4*) and Dick (*53*). Adenovirus were used to deliver ABCB10, Grx1-roGFP2 (GSSG/GSH), roGFP2-Orp1 (H_2O_2 probe) and UnaG (bilirubin probe) to primary hepatocytes, with the fluorescent probe proteins targeted either to the mitochondrial matrix or to the cytosol as described *(7,8)*. roGFP2 and ABCB10 adenoviruses (mouse cDNA) were generated *in house* using Gateway cloning (Invitrogen) into a pAdeno-CMV vector, while UnaG cDNA was cloned into adenovirus by Welgen. Hepatocytes were exposed to adenoviruses (MOI 1 for UnaG viruses and MOI 400 for roGFP2 viruses) for 2h the same day of isolation and imaged 48h after

transduction. Live cell imaging was performed in 96-well plates at 37°C, 5% CO_2, using the Operetta Spinning Disk Fluorescent Microscope imaging system (Perkin Elmer). A Xenon lamp with the following excitation filters was used for each probe: oxidized form of roGFP2 (roGFP2ox) with Ex 460 - 490 nm and Em 500 – 550 nm; reduced form of roGFP2 (roGFP2red) with Ex 410 - 480 nm and Em 500 – 550 nm and for UnaG, Ex 460 - 490 nm and Em 500 – 550 nm. To quantify fluorescence, Columbus Perkin Elmer software was used to select cells and threshold the images to remove background fluorescence. Average fluorescence intensity values were calculated per field, containing 20-30 cells. Results for roGFP2-Orp1 and Grx1-roGFP2 were expressed as oxidized/reduced probe fluorescence ratio.

Properties of UnaG to detect bilirubin

The domain of UnaG that binds unconjugated bilirubin to generate fluorescence is a FABP (fatty acid binding protein) (*28*). Thus, UnaG cannot report on bilirubin bound with stronger affinity to other FABP proteins and lipids. Purified UnaG is a highly sensitive and reversible bilirubin sensor, having a Kd with bilirubin of 98 pM and reporting on concentrations as low as 20-40 pM. UnaG detects real time changes in intracellular bilirubin content in live cells. UnaG reports relative amounts of bilirubin, as no internal standards could be reliably generated in intact live cells. UnaG fluorescence is insensitive to hypoxia and continues to fluoresce after fixation, still reporting differences in bilirubin content detected prior fixation.

UGT activity assay

Microsomes were isolated from frozen WT and ABCB10 KO livers and UGT activity was measured according to the manufacturer's protocol (Biovision).

Downregulation of ABCB10 expression by shRNA

Stable short hairpin RNA (shRNA)-mediated knockdown of ABCB10 expression in primary human hepatocytes was achieved using lentiviral transduction. Human control (sh001) and ABCB10 shRNA (TRCN0000060176) encoded in pLKO.1-Puro vector (Sigma-Aldrich) were used. Lentiviruses were

produced in HEK293T cells. Human primary hepatocytes were exposed to lentivirus overnight, then washed and analyzed 48h after transduction.

Isolated mitochondria respirometry and bilirubin treatments

A differential centrifugation protocol was used to isolate mitochondria as published (*54*). Mitochondria were diluted in Mitochondrial Assay buffer (MAS: 70 mM sucrose, 220 mM mannitol, 10 mM KH_2PO_4, 5 mM $MgCl_2$, 2 mM HEPES, 1 mM EGTA and 0.2% fatty acid-free BSA, pH 7.2) on ice. 25 µL of MAS with 3.5-4µg of mitochondrial protein fraction for succinate (5mM) + rotenone (4µM) or with 7-10µg for pyruvate (5mM) + malate (5mM)-driven respiration were plated in a XF96-well plate. The XF96 plate was then centrifuged at 4°C at 2000xg for 5 min to sediment mitochondria to the bottom of the well, then carefully adding the rest of MAS (110 µl) on top. For bilirubin treatments, bilirubin in DMSO (10mM) was diluted 1/1000 in MAS to 10 µM, which is a physiological plasma concentration of free bilirubin. The XF96 plate was incubated 5-8 min at 37°C before loading it to the instrument measuring respiration. State 3 was induced after injection of ADP (4mM final), State 4o after injection of oligomycin (3.5 µM final), maximal after injecting FCCP (4µM final) and antimycin A (4µM final) to block respiration.

Western blot analyses

This protocol was modified from our previous publication (*52*). Cells or tissues were homogenized in lysis buffer (50 mM Tris pH 7.5, 150 mM NaCl, 2 mM EDTA, 5 mM EGTA, 1% Triton X-100, 1% SDS, 1% sodium deoxycholate, 2 mM sodium orthovanadate, 50 mM sodium fluoride, 5 mM sodium pyrophosphate, 1 mM PMSF, 80 mM sodium β-glycerophosphate). Lysates were centrifuged for 10 min at 12.000xg. Protein concentration was determined with BCA Protein Assay Kit (Pierce). Equal amounts of proteins were separated by SDS-PAGE (4-12% (wt/vol.)) and transferred onto PVDF membrane. Membranes were blocked in 3% (wt/vol.) milk diluted in Tris pH 7.4 + 0.1% (vol./vol.) Tween (TBS-T) and incubated overnight at 4°C with the respective antibodies diluted in 3% (wt/vol.) BSA in TBS-T. Anti-phospho-INSR Tyr1162/1163 was from Invitrogen, phospho-AKT Ser 473, total AKT and INSR

were from Cell Signaling Technologies. Porin/VDAC1, vinculin and total OXPHOS complexes were from Abcam. ABCB10, PTP1B and anti-flag were from Proteintech. Anti-actin was from Millipore. BLVRA and HMOX1 were from SantaCruz.

qPCR analyses

Total RNA was extracted from liver tissues using RNeasy (QIAGEN) and TRIzol, (Invitrogen). 2 µg total RNA were reverse transcribed into cDNA (Applied Biosystems). qPCR reactions were performed using the iQ SYBR Green Supermix (Bio-Rad Laboratories). See table 1 for Primers list. Melting curve analysis was performed to control for unspecific products. *Ugt1a1* (Mm02603337_m1) and *Abcc2* (Mm00496899_m1) gene expression were measured using TaqMan probes and gene expression assay (Thermofisher). Results were normalized to acidic ribosomal phosphoprotein P0 (*Arbp*) within each sample to obtain sample-specific ΔCt values (Ct gene of interest - Ct Rplp0). 2_ΔΔCt values were calculated to obtain fold expression levels, where ΔΔCt = (ΔCt treatment - ΔCt control).

Confocal imaging

Zeiss LSM880 with Airyscan was used to image live primary hepatocytes at 37 ℃ and with humidified 5% CO_2 chamber, transduced with mito-UnaG and stained with 100nM TMRE. Super-resolution imaging was performed with 40x Apochromat oil-immersion lens and AiryScan super-resolution detector.

ATPase activity of ABCB10

The codon-optimized ABCB10 gene, without mitochondrial targeting sequence, was synthesized and inserted in the pET28a-TEV vector (Gene Script) within the NdeI and BamHI sites. The N-term His-tagged protein was expressed in Rosetta 2 (DE) (Novagen) cells, extracted from the membrane with 1 % dodecyl-maltoside (DDM) and 0.1 % cholesteryl hemi-succinate (CHS), and purified using Ni-NTA resin (Qiagen) in a Low-Pressure chromatography system (BioRad). Most concentrated fractions were pooled and treated with TEV protease during dialysis (300 mM NaCl, 10 % Glycerol, 20 mM Tris-HCl pH 7.5, 0.06 % DDM, and 0.5 mM DTT), followed by batch Ni-NTA purification. Purified His-tagged free

ABCB10 was recovered from the supernatant and stored at -80°C. For reconstitution in nanodiscs, ABCB10 in detergent was mixed with *E. coli* total or polar lipids and membrane scaffold protein MSP1D1, and detergent was removed by addition of absorbent Biobeads. The reconstituted protein sample was run through a size-exclusion chromatography column (Enrich 650, BioRad) to remove aggregates. ABCB10 concentration in ABCB10-nanodisc fractions was estimated by SDS-gel electrophoresis using purified ABCB10 in detergent as standard. The ATPase activity of reconstituted ABCB10 was measured by the linked-enzyme assay, following the decrease in NADH absorbance at 340 nm during 3 to 4 hours at 37°C (*55*). The buffer contained: 100 mM KCl, 5 mM NaCl, 20 mM Tris-HCl pH 7.5, 5 mM Na ATP, 10 mM $MgCl_2$, 3 mM phosphoenol pyruvate, 0.5 mM TCEP, 0.8 mM NADH, plus the enzymes pyruvate kinase and lactate dehydrogenase (Sigma). Biliverdin and Bilirubin (Chem Cruz) were dissolved in DMSO. See publications (*26, 27*) for more details on ABCB10 production and ATPase assays.

Biliverdin transport assays

ABCB10 was cloned and purified as published (*25*). ABCB10 was reconstituted using the method outlined in (*56*) with some modifications. Reconstitution was performed in a 1:1 (wt:wt) mixture of 1-palmitoyl-2-oleoyl-sn-glycero-3-phosphocholine (POPC) and 1-palmitoyl-2-oleoyl-sn-glycero-3-phosphoethanolamine (POPE) (Avanti Lipids). Chloroform solubilized lipids were dried into a glass flask under argon to form a film under vacuum for 1h. Reconstitution/ ATPase assay buffer (50 mM HEPES, 200 mM NaCl, 10 mM $MgSO_4$) was used to solubilize the lipids and form multilamellar vesicles, which were solubilized with 1% Triton-X100. Protein was added to the prepared lipids in a 1:10 ratio by weight and mixed. 0.1 g of SM2-Biobeads washed with ATPase buffer were added and the mixture was rotated overnight at 4°C. Fresh Biobeads were added and the incubation continued for 2h before removal of Biobeads to recover reconstituted ABCB10. Protein concentration was measured on a Coomassie blue-stained SDS/PAGE gel comparing protein staining to a BSA standard. Transport assay was performed using ABCB10-liposomes (6 µg) resuspended in 50 mM Tris, 10% Sucrose, 100 mM NaCl, pH 7.0. To

initiate the transport, no ATP buffer or ATP regenerating buffer (20 mM ATP, Creatine Kinase 2.5 mg/ml, 20mM $MgSO_4$, 25 mM Creatine Phosphate) in presence of ^{3}[H]-Biliverdin (34 pmols, 10 Ci/mmol) (American Radiolabeled Chemicals) was added to each sample at 37°C. At appropriate time points, 800 µl of cold no ATP buffer were added to each sample and filtered rapidly through 0.45-µm cellulose acetate filters. After washing the filters with another 3 ml of cold buffer, the filters were dissolved in 900 µl ethyl acetate and the radioactivity in the filter was determined by scintillation counting in 3 ml Ultima Gold XR scintillation cocktail (Perkin Elmer) in a Beckman LS6500 scintillation counter. Competition assay of ^{3}H-biliverdin transport in ABCB10-liposomes with or without ATP (ATP + regeneration buffer) was performed by using 3 mg of ABCB10-protein incubated with 34 pmols ^{3}H-biliverdin in a 110 ml reaction (0.3 µM), competing with unlabeled biliverdin, aminolevulinic Acid (ALA) (Sigma), protoporphyrin IX (PPIX) (Sigma) or hemin (Sigma) at 0.5 µM and 1 µM. Data was analyzed using the one-phase association equation, mean of independent transport experiments and ABCB10 proteoliposome batches ± SEM.

Biliverdin measurements in isolated mitochondria by LC/MS

A differential centrifugation protocol was used to isolate mitochondria. This method preserves the integrity of the inner membrane and thus the retention of metabolites, quantitatively shown by respiratory control ratio values (>5) (Figure 1). Polar metabolites were extracted from 500 µg of mitochondrial protein using 1 ml of ice-cold 80% MeOH. Extraction was performed by vortexing samples three times for 10 sec and then centrifuged at 10,000xg for 10 min at 4°C. Both Biliverdin IX alpha (1 nmol final) and D/L-norvaline (5 nmols final) were added for standard and extraction normalization purposes. Then, samples were dried using a *speedvac* centrifuge, and reconstituted in 50 µl of 70% acetonitrile (ACN). For mass spectrometry analysis, 5 µl of each sample was injected onto a Luna NH2 (150 mm x 2 mm, Phenomenex) column. Samples were analyzed with an UltiMate 3000RSLC (Thermo Scientific) coupled to a Q Exactive mass spectrometer (Thermo Scientific). The Q Exactive was run with polarity switching

(+3.00 kV / -3.00 kV) in full scan mode with an m/z range of 65–950. Separation was achieved using 5 mM NH_4 AcO (pH 9.9) and ACN. The gradient started with 15% NH_4 AcO and reached 90% over 18 min, followed by an isocratic step for 9 min and reversal to the initial 15% NH_4 AcO for 7 min. Biliverdin was detected at m/z=583 and relative quantities were calculated using El-Maven software.

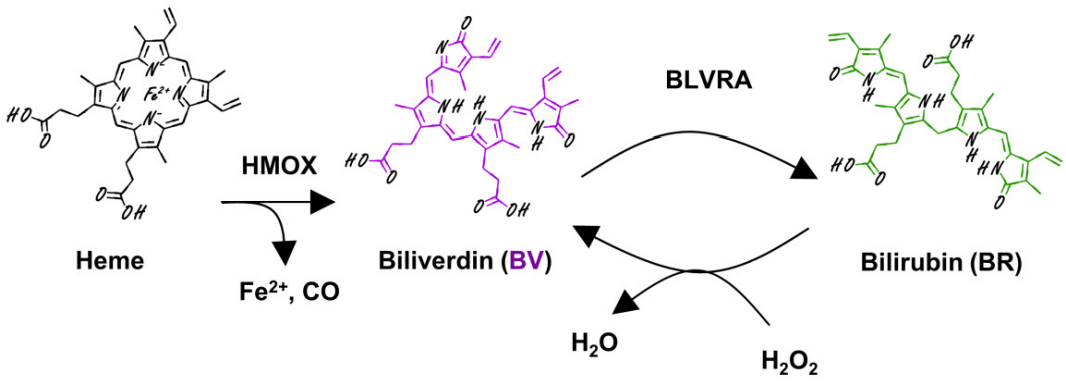

Fig. S1. Scheme summarizing heme catabolism to biliverdin and bilirubin. Heme is oxidized by heme oxygenases (HMOX) to biliverdin (BV), which is reduced to bilirubin (BR) by biliverdin reductase A (BLVRA). Hydrogen peroxide (H_2O2) was shown to oxidize bilirubin to generate biliverdin.

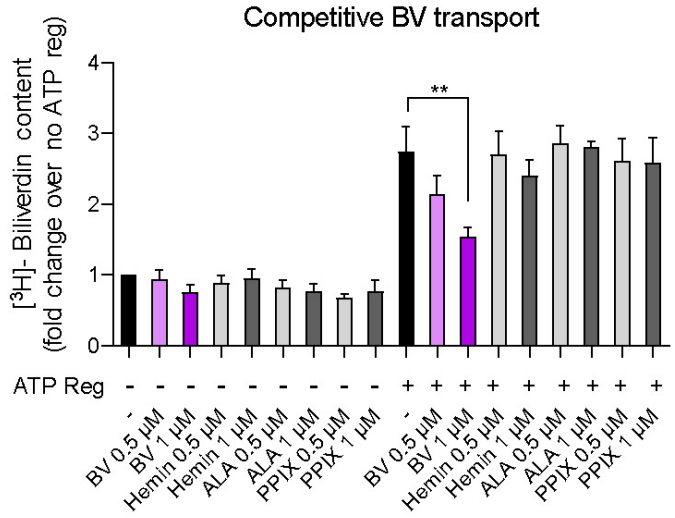

Fig. S2. Evidence excluding other heme-related molecules as ABCB10 cargos. Competition assay of ^{3}H-biliverdin transport in ABCB10-liposomes with or without ATP regenerating buffer (ATP reg) and incubated with unlabeled biliverdin (BV), aminolevulinic acid (ALA), protoporphyrin IX (PPIX) or hemin at 0.5 µM and 1 µM. n=4-5 independent transport assays. **p<0.01, one-way ANOVA.

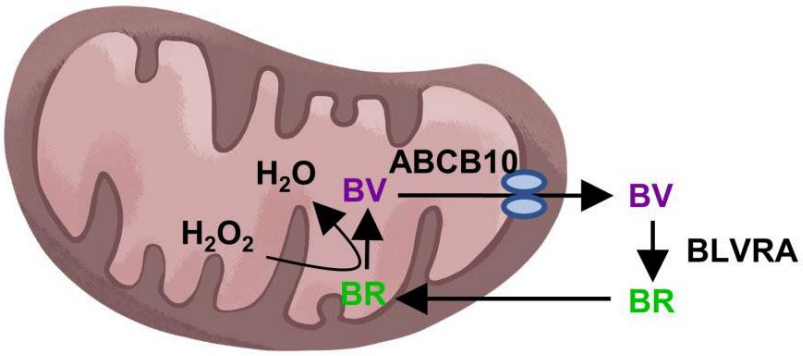

Fig. S3. ABCB10-mediated biliverdin export increases bilirubin synthesis. Scheme showing how biliverdin export increases bilirubin synthesis catalyzed by BLVRA.

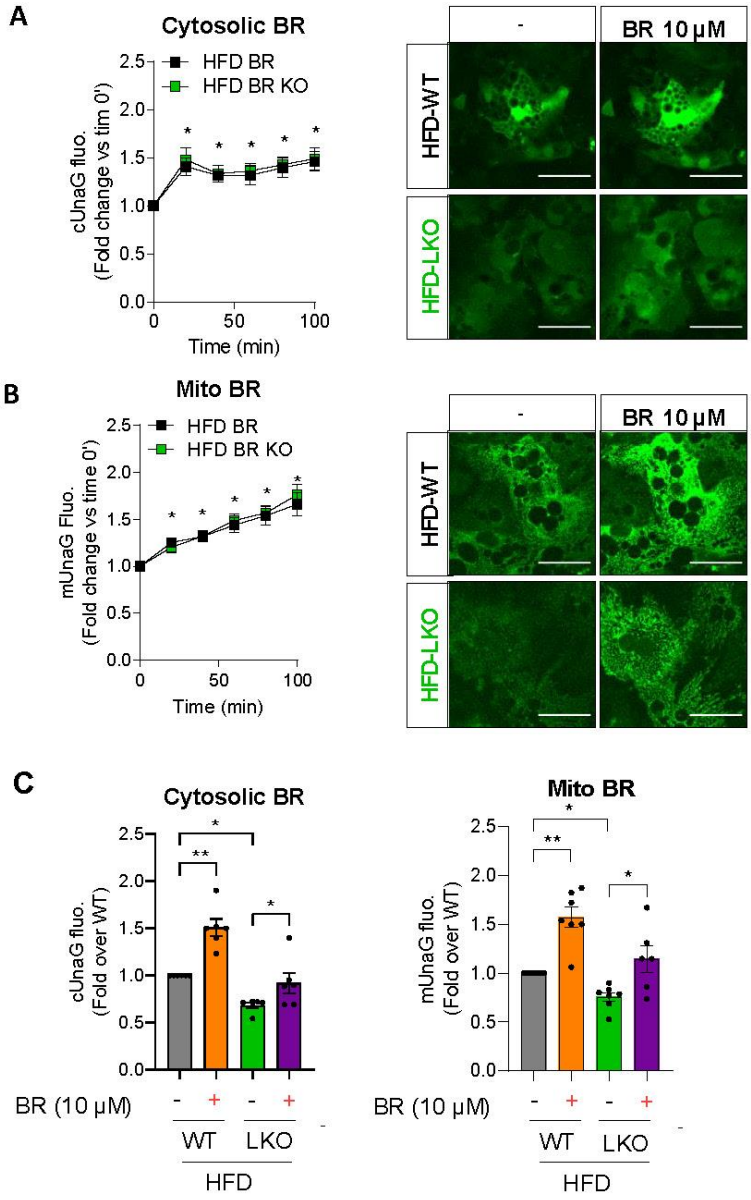

Fig. S4. The response of UnaG fluorescence to bilirubin supplementation in WT and ABCB10 KO hepatocytes. A-C) Average number of WT and ABCB10-LKO male mice fed a high fat diet (HFD) used to isolate hepatocytes ± SEM. n = 4 mice/group. These hepatocytes were transduced with adenovirus encoding cytosolic UnaG (cUnaG), to measure cytosolic bilirubin, or with mitochondrial matrix targeted UnaG (mUnaG), to measure matrix bilirubin. A) Fold increase in cytosolic bilirubin and B) mitochondrial bilirubin after adding bilirubin (10 µM) to the hepatocyte culture media. This same slope supports that the capacity of extracellular bilirubin to reach the cytosol and the mitochondrial matrix is not changed by ABCB10 deletion. *p<0.05 vs. time 0' min. C) Total cytosolic and mitochondrial bilirubin measured in A and B at 100 min normalized by WT concentrations, showing higher accumulation of bilirubin in WT and restoration of bilirubin in LKO. This result is consistent with lower bilirubin synthesis in the LKO. 2-way ANOVA, *p<0.05, **p<0.01 Scale bar, 100 µm.

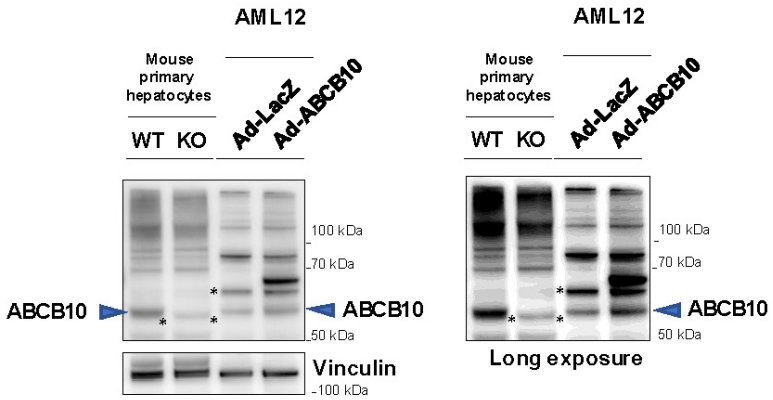

Fig. S5. ABCB10 overexpression in AML12 hepatocytes. AML12 were transduced overnight with Adenovirus (Ad) encoding for LacZ or ABCB10 and analyzed 48h after transduction. Western blots detecting ABCB10 and Vinculin in total lysates from transduced AML12 and from WT and ABCB10 KO mouse primary hepatocytes. The specific ABCB10 band is detected around 60 kDa, which is absent in the KO. One unspecific band* is running very close to ABCB10 in primary hepatocytes as shown in Fig.2 and is marked with an asterisk. An additional band is detected by ABCB10 antibody after ABCB10 overexpression, which migrates at a higher molecular weight. *Unspecific band. Representative gels of 4 different experiments.

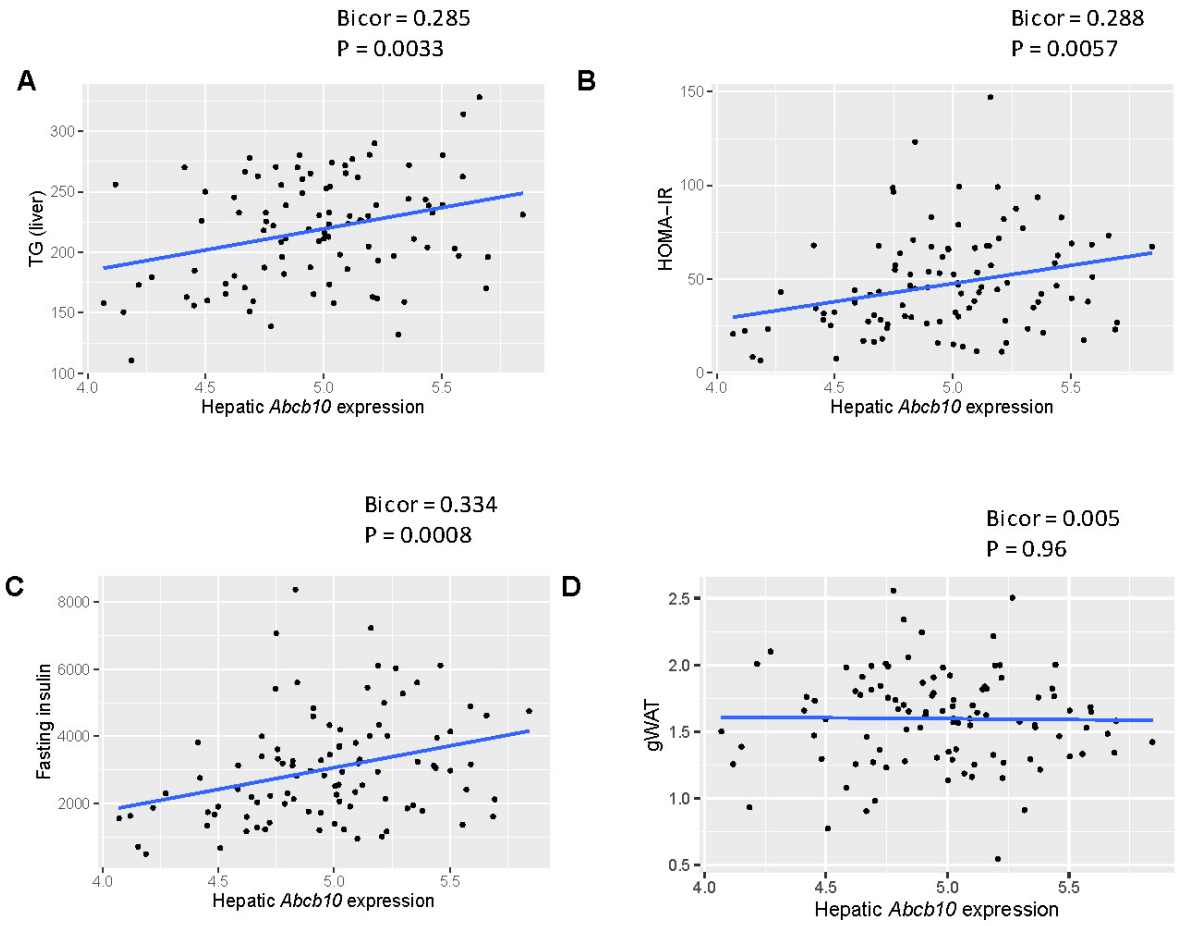

Fig. S6. Correlation plots between hepatic *Abcb10* transcript content and the metabolic traits determined in the HMDP. Biweight midcorrelation (Bicor) plots between hepatic *Abcb10* transcript levels and A) Triglycerides in the liver (TG), B) HOMA-IR (insulin resistance), C) Fasting insulin and D) Gonadal white adipose tissue mass (gWAT). Each dot represents one mouse strain of the HMDP Western diet group, a total of n=102 strains. Values of the Bicor slope and its nominal *P* value shown in each panel.

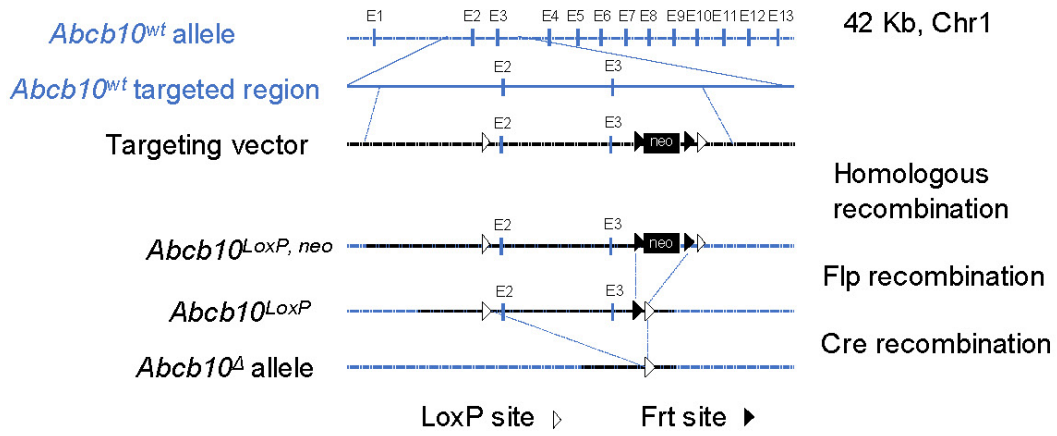

Fig. S7. *Abcb10* targeting strategy to generate ABCB10 LKO mice. ES cells from C57BL/6J were targeted with a vector containing *Abcb10* exon 2 and 3 flanked by LoxP and containing a selection cassette (Neomycin) flanked by FRT sites. Targeted ES cells were generated by genOway. The Neomycin cassette was excised by breeding mice harboring germline transmission of the floxed allele with Flp recombinase transgenic mice. *Abcb10* exons 2 and 3 were excised in hepatocytes by breeding with Albumin Cre transgenic mice.

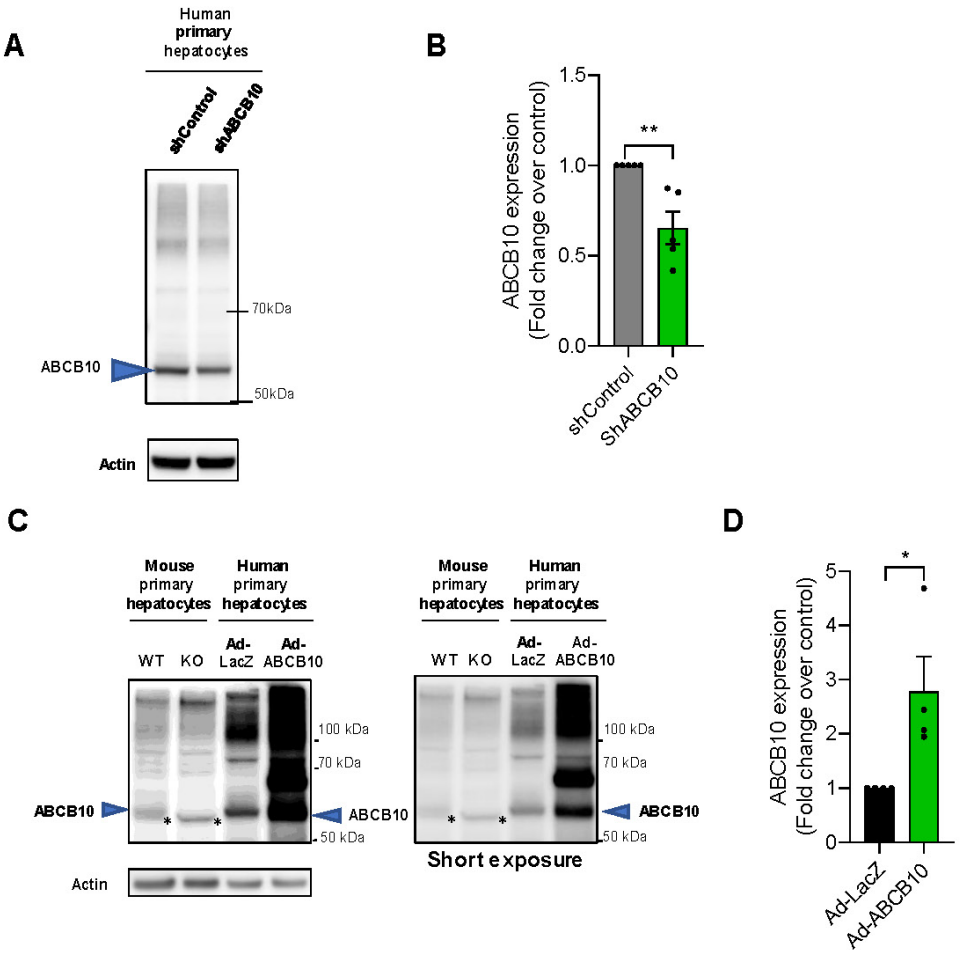

Fig. S8. ABCB10 gain- and loss-of-function approaches in primary human hepatocytes. A) Primary human hepatocytes transduced overnight with Ad-LacZ and Ad-ABCB10 and analyzed 48h after transduction. Western blots detecting ABCB10 and actin in total lysates from human primary hepatocytes, running lysates of mouse primary hepatocytes isolated from WT and ABCB10 LKO mice to validate ABCB10 band (60 kDa). The unspecific band close to ABCB10 is marked with an asterisk (*) and the higher molecular weight band is also observed when ABCB10 is overexpressed in human hepatocytes (see fig. S3). **B)** Primary human hepatocytes were transduced with lentivirus encoding shControl (sh001) or shABCB10. n=5, data are mean ± SEM. **C-D)** Quantification of endogenous ABCB10 band (around 60 kDa) in human hepatocytes transduced with Ad-LacZ and Ad-ABCB10. Student's *t* test; **p<0.01. n=4 SEM. Student's *t* test; *p<0.05.

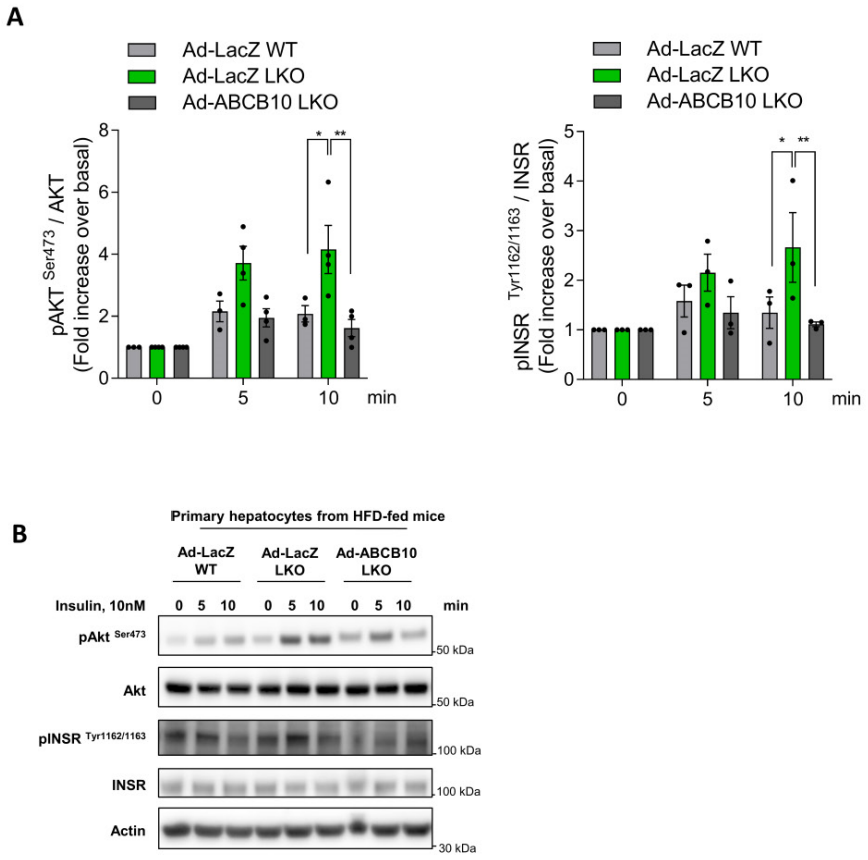

g. S9. Rescuing ABCB10 expression ex vivo reverses the improvement in insulin action seen i BCB10 LKO hepatocytes isolated from HFD-fed mice. A-B) Primary mouse hepatocytes isolate om WT and ABCB10 LKO HFD-fed mice were transduced with Adenovirus (Ad) encoding LacZ c BCB10. Two days after transduction, hepatocytes were treated with or without insulin 10 nM for th dicated minutes (min). **A**) Quantification of $pSer^{473}$ AKT and $pTyr^{1162/1163}$ INSR. **B**) Representativ estern blots of $pSer^{473}$ AKT and $pTyr^{1162/1163}$ INSR, AKT, INSR. Actin was used as loading contro <0.05, **p<0.01 Two-way ANOVA. n=3-4 independent isolations and treatments of WT and K patocyte pairs.

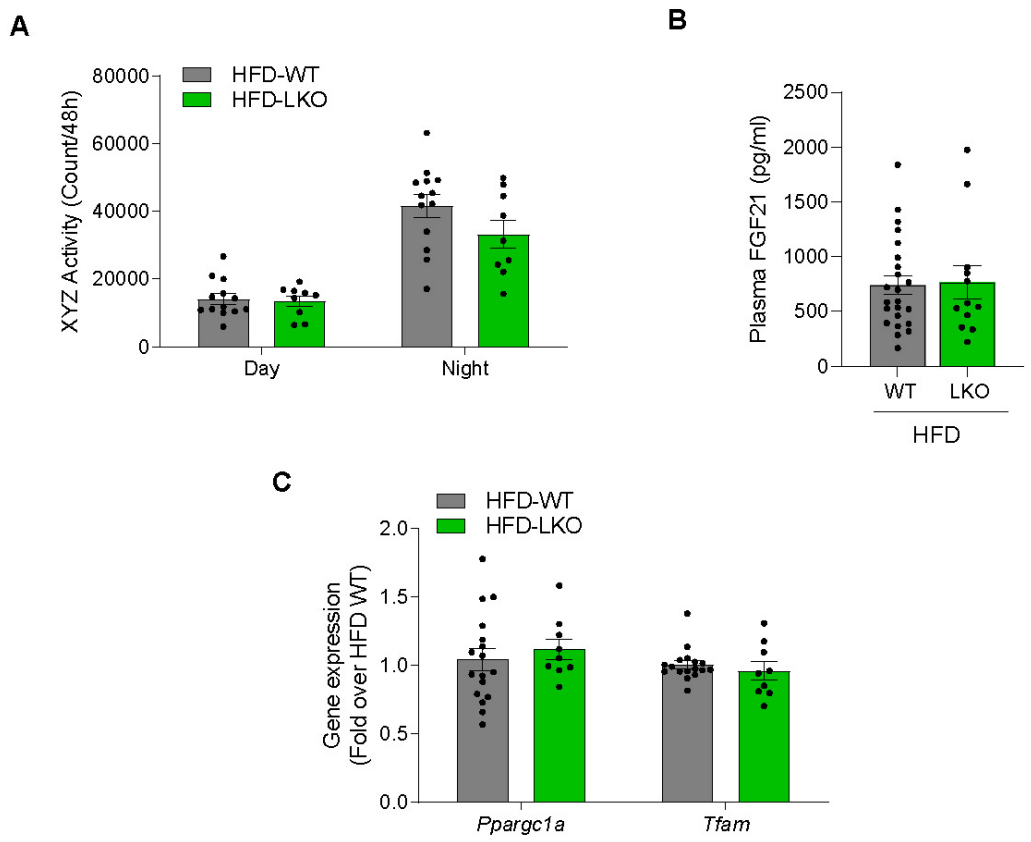

Fig. S10. HFD-fed ABCB10 LKO mice show no differences in physical activity, mitochondrial biogenesis markers in the liver, or plasma fibroblast growth factor 21 (FGF21) concentrations. A-D) Average number of WT and ABCB10-LKO male mice fed a high fat diet (HFD) ± SEM. n = 9-23 mice/ group. **A)** Physical activity as counts of laser beams breaks in XYZ over a 48h period. **B)** Plasma FGF21 and **C)** gene expression of mitochondrial biogenesis markers (*Ppargc1a* aka *Pgc1α* and *Tfam)*.

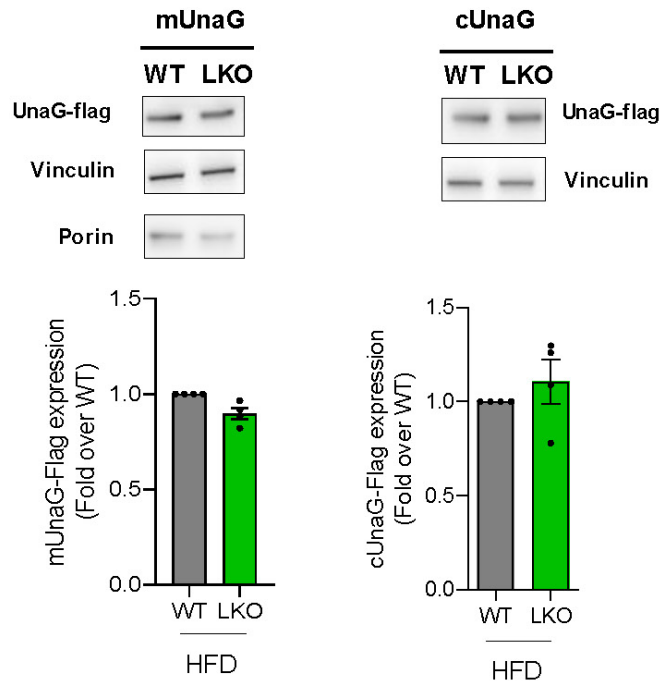

Fig. S11. Total protein content of cytosolic and mitochondrial UnaG is not changed by ABCB10 deletion. Western blot of total UnaG-flag protein expressed in HFD-fed WT and LKO primary hepatocytes, detected with anti-flag. n=4/ group.

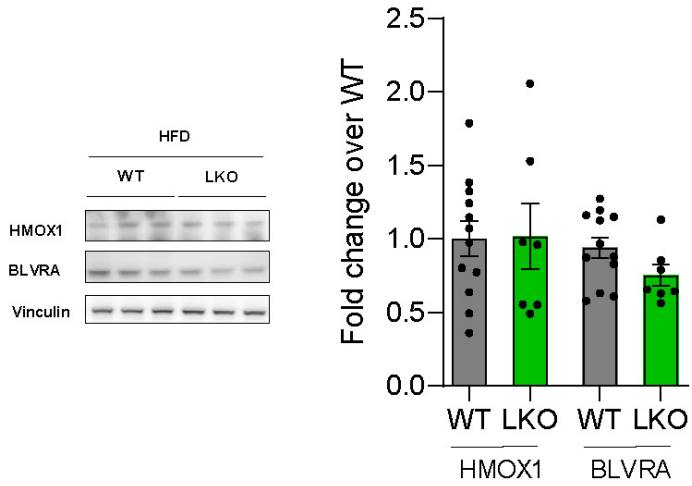

Fig. S12. No differences in hepatic HMOX1 or BLVRA content in HFD-fed ABCB10 LKO mice. Average number of WT and ABCB10-LKO male mice fed a high-fat diet (HFD) ± SEM. n=7-12 mice/group.

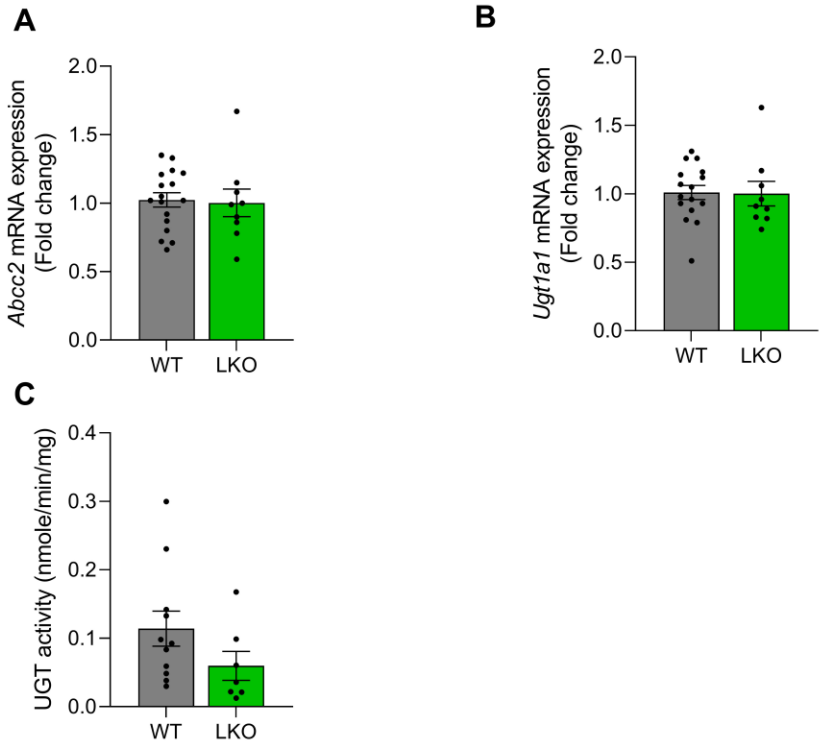

Fig. S13. HFD-fed ABCB10 LKO mice show no changes in the bilirubin exporter ABCC2 or the main enzyme conjugating bilirubin, UGT1A1. A-C) Average number of WT and ABCB10-LKO male mice fed a high-fat diet (HFD) ± SEM. n= 9-16 mice/group. **A)** *Abcc2* mRNA abundance and **B)** *Ugt1a1* mRNA abundance measured in total liver lysates. **C)** UGT activity measured in microsomal fractions from liver.

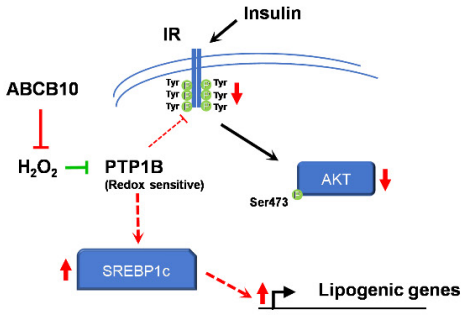

Fig. S14. Summary of PTP1B actions on insulin signaling and lipogenesis and the consequences of PTP1B inactivation by H_2O_2.

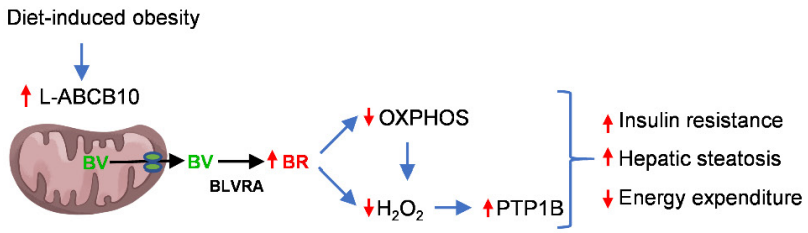

Fig. S15. The role of ABCB10 in hepatic insulin resistance and steatosis in obesity..

Table S1. Primer sequences.

Gene	Forward Primer 5' to 3'	Reverse Primer 5' to 3'
Arbp	AGA AAC TGC TGC TC ACA TC	CAT CAC TCA GAA TTT CAA TGG
Fasn	CTG GCC CCG GAG TCG CTT GAG TAT A	GGA GCC TCC GAA GCC AAA TGA
Ppargc1a	AAG ATG AAG GTC CCC AGG CAG TAG	TGT CCG CGT TGT GTC AGG TC
Pparγ	ACT GCC TAT GAG CAC TTC AC	CAA TCG GAT GGT TCT TCG GA
Scd1	GCC CAC CAC AAG TTC TCA GA	GGG CGA TAT CCA TAG AGA TG
Srebp1c	GCC GGC GCC AG GAC GAG CTG GCC	CAG GAA GGC TTC CAG AGA GGA GGC
Tfam	CAC CCA GAT GCA AAA CTT TCA G	CTG CTC TTT ATA CTT GCT CAC AG

The following data file is available in the online version of the supplement:

Data File S1. Primary data for Figs. 1 to 7 in tabular format.

Chapter 2: The mitochondria biliverdin exporter ABCB10 mitigates the formation of neutrophil extracellular traps in alcoholic hepatitis.

INTRODUCTION

The only effective treatment available for acute liver failure as a result of alcoholic hepatitis (AH) is liver transplantation, which shows the dire need for new therapies to treat AH[1]. Livers of AH patients show a unique molecular signature that separates them from livers of patients with non-alcoholic steatohepatitis (NASH) and even with alcoholic steatohepatitis (ASH)[2]. This AH-specific signature consists of a transcriptional reprogramming in hepatocytes that induces a defective metabolic and redox state, with a concurrent infiltration of neutrophils in the liver parenchyma[2]. Different studies support a "goldilocks" role of these infiltrated neutrophils in AH pathogenesis[3]. Some degree of neutrophil infiltration and activation allows the elimination of damaged hepatocytes and bacteria that entered through a leaky gut caused by alcohol consumption. Neutrophilic activity can thus fight infection and resolve inflammation as well, which is needed to replace dead hepatocytes and prevent fibrosis[3].

However, an overactivation of neutrophils can contribute to liver failure specific of AH[4]. Recent evidence demonstrates that an excessive formation of neutrophil extracellular traps (NETs) by hyperactive neutrophils is a key mechanism contributing to liver failure in AH[5]. Mitigating neutrophil activation and NET formation was sufficient to improve liver function in mice with AH, while increased NETs in humans with AH is

associated with poor prognosis. In this context, whether the selective defects in the metabolic and redox state of hepatocytes induced by AH contribute to the pathogenic hyperactivation of neutrophils to form NETs is unclear.

Our laboratory recently identified a novel mitochondrial mechanism regulating metabolism and redox in hepatocytes in non-alcoholic fatty liver disease (NAFLD)[6]. In mice fed a high fat diet, we found a maladaptive upregulation of the mitochondrial transporter that exports the heme catabolism product biliverdin from the mitochondria to the cytosol: the ATP binding cassette B10 (ABCB10)[6]. This maladaptive increase in ABCB10 function elevated bilirubin synthesis in hepatocytes, as cytosolic biliverdin reductase A can transform exported biliverdin into bilirubin[6]. High intracellular concentrations of bilirubin have a combined effect decreasing both ROS and mitochondrial respiration[6]. Accordingly, hepatocyte-specific deletion of ABCB10 protected from high-fat diet induced hepatic steatosis and insulin resistance, by increasing mitochondrial respiration and restoring ROS-dependent insulin signaling[6]. As a result, the excessive increase in bilirubin production mediated by ABCB10 in high-fat diet fed mice altered hepatocellular metabolism and redox to favor steatosis and insulin resistance[6]. However, the role of hepatic ABCB10 and its redox actions on alcoholic liver disease are completely unknown.

Here, we determined the role of hepatic ABCB10 in ASH and AH. Our results show a selective decrease in hepatic ABCB10 protein content in AH, but not in ASH. Furthermore, we find an anti-inflammatory role of ABCB10 that it is not mediated by changes on mitochondrial respiratory capacity nor by eliminating intrahepatic lipids. Rather, we identify that ABCB10 actions regulating ROS-

mediated actions determine the degree of activation of infiltrated neutrophils to form NETs.

RESULTS

ABCB10 is decreased in livers with alcoholic hepatitis (AH), but not in mice with alcoholic steatohepatitis (ASH).

Hypometabolism with an altered redox state is a hallmark of hepatocytes from human livers with alcoholic hepatitis (AH), which is markedly different from less severe stages of alcoholic steatohepatitis (ASH)[2]. We previously showed that an upregulation of the mitochondrial biliverdin exporter ABCB10 exacerbated non-alcoholic liver disease (NAFLD), by decreasing mitochondrial function and suppressing beneficial ROS-derived signals in hepatocytes[6]. However, the role of ABCB10 redox actions on alcoholic liver disease is unknown.

To determine the role of ABCB10 in alcoholic liver disease, we first measured the effects of ASH and AH on ABCB10 protein content in total liver lysates. We observed a 78% decrease in ABCB10 protein content in human patients with AH, when compared to non-alcoholic donors (Control) (Fig. 2-1A). This is the exact opposite behavior previously published in livers from mice with NAFLD, where ABCB10 protein content was increased[6]. To model human ASH and AH in mice, ethanol binges are administered by oral gavage to effectively induce neutrophil infiltration in the liver parenchyma. The NIAAA model of 10 days of ethanol diet plus a single binge induces steatosis and neutrophil infiltration, but without fibrosis (ASH)[7]. Females under the NIAAA model develop more inflammation and liver damage than males, therefore females recapitulate better some hallmarks of human ASH[7]. On the other hand, the hybrid-binge AH model consists of intragastric

feeding of a high-fat and alcohol diet, plus ad libitum consumption of Western diet for 7 weeks, plus a total of 6 ethanol binges delivered weekly[8,9]. Accordingly, this hybrid-binge AH model induces a higher degree of liver fibrosis, hepatocyte death, severe neutrophil infiltration, ductular reactions and even bilirubin-stasis, resulting in a more severe phenotype similar to moderate AH in humans [8,9]. Only male mice are used in this hybrid-binge AH model, as the higher susceptibility of females to alcohol toxicity causes an excessively high attrition rate[8,9].

As in humans, we observed a significant decrease in liver ABCB10 protein content in male mice with AH induced by the hybrid-binge model (Fig. 2-1B). In marked contrast, ABCB10 content was not decreased in female mice with ASH induced by the NIAAA model (Fig. 2-1C). These data indicate that a decrease in hepatic ABCB10 may contribute to liver damage observed in AH, but not in milder forms of alcoholic liver disease, such as ASH. Furthermore, these data show an opposite behavior of ABCB10 protein in AH versus NAFLD, which strongly supports a specific role of ABCB10 downregulation in AH.

Increasing ABCB10 content in hepatocytes decreases neutrophilic biomarkers in livers from mice with AH.

Close to 90% of ABCB10 mRNA and protein content in the liver is confined to hepatocytes[6] (Fig. 2-2A,B). Therefore, the AH-induced decrease in ABCB10 protein in total liver lysates is mostly due to the loss of ABCB10 in hepatocytes. To determine the contribution of the decrease in ABCB10 protein content in livers with AH, we increased ABCB10 content selectively in hepatocytes of the hybrid-binge AH male mice. This increase was achieved by transducing male mice with adeno-associated virus encoding

for ABCB10, whose expression was controlled by a fragment of the albumin promoter (AAV-ABCB10). Mice transduced with the same AAV8 backbone, but encoding for GFP, were used as controls (AAV-GFP). Transduction was performed 1-2 weeks prior to the start of the hybrid AH diet, which enabled peak ABCB10 transgene expression by the start of the diet.

AAV-ABCB10-transduction caused a 70% increase in ABCB10 protein content in the liver, measured at the final point of the diet (7-8 weeks after transduction) (Fig. 2-2C). Both control and ABCB10 transduced mice showed similar concentrations of alcohol in plasma, supporting the absence of large changes in ethanol detoxification induced by ABCB10 gain-of-function in hepatocytes (Fig. 2-2D). No differences in liver weight-to-body weight ratio (Fig. 2-2E) or in serum AST and ALT (Fig. 2-2D) were observed in AAV-ABCB10-transduced male mice with AH. In marked contrast, we observed a remarkable 80% decrease in total liver myeloperoxidase (MPO) mRNA content in AAV-ABCB10 transduced male mice (Fig. 2-2G). The mRNA content of another neutrophil marker, Neutrophil Elastase (ELANE), showed a 42% decrease as well (Fig. 2-2G). Thus, ABCB10 gain-of-function induced a decrease in MPO and ELANE mRNA content that was not associated with a reduction in hepatocyte detoxification or damage. MPO and ELANE are abundant and essential proteins for neutrophil function that are used as neutrophil markers. To evaluate whether the decrease in MPO and ELANE mRNA content in total liver lysates was explained by a decrease in neutrophil infiltration in the liver, we measured MPO positive foci of cells in liver sections from AAV-ABCB10-transduced mice. We observed a milder decrease in MPO foci (35%) induced by AAV-ABCB10 transduction when compared to the decrease in MPO mRNA, but that did not

reach statistical significance (Fig. 2-2H). These data suggest that hepatic ABCB10 actions may mitigate the exacerbated activity of neutrophils in AH by decreasing MPO and ELANE expression, while potentially showing some mild or no effects decreasing infiltration.

ABCB10 hepatocyte-specific deletion is not sufficient to drive progression from ASH to AH.

The “multiple hit theory” of alcoholic liver disease suggests that progression from simple steatosis to steatohepatitis and ultimately cirrhosis occurs due to complex gene-environment interactions, resulting in a heterogenous pathogenic response to alcohol intake between individuals. The difference in liver ABCB10 content between mouse models of ASH and AH suggest that ABCB10 loss may serve as a critical “hit” in the progression to AH. To determine whether loss of ABCB10 in hepatocytes is sufficient to drive progression from ASH to AH, we induced ASH in hepatocyte-specific ABCB10 KO (L-KO) female mice, by feeding these L-KO females with the NIAAA model (10 days Lieber de Carli + 1 binge). The choice of females was explained by the fact that the NIAAA model induces a higher degree of ASH in females when compared to males, recapitulating human ASH better[7]. Loss of ABCB10 in females did not aggravate hepatomegaly (Fig. 2-3A), triglyceride or NEFA accumulation (Fig. 2-3B,C) or increased serum AST and ALT activity after NIAAA model feeding (Fig. 2-3D). Consistent with the absence of changes in hepatic steatosis induced by ABCB10 loss (Fig. 2-3B,C), ABCB10 L-KO female mice did not show changes in mitochondrial fat expenditure capacity: similar respiration rates were observed in isolated ABCB10 KO mitochondria fueled by palmitoyl-

carnitine (Fig. 2-3E). In addition, no significant changes in complex I- or II-driven respiration were observed, further confirming no impact of ABCB10 loss on mitochondrial oxidative capacity in ASH (Fig. 2-3F,G).

With our previous data showing an anti-inflammatory effect of ABCB10 gain-of-function in mouse livers with AH, we next aimed to determine whether ABCB10 deletion could selectively exacerbate neutrophilic inflammation induced by the NIAAA model. ABCB10 L-KO females fed the Lieber-de Carli diet for 10 days plus one binge (NIAAA model) did not show an increase in total myeloperoxidase (MPO) protein when compared to WT mice (Fig. 2-4A,B). Additionally, we did not observe an increase in oxidative stress in ABCB10 L-KO livers, as no differences in the total content of oxidized lipid adducts with proteins (4-HNE adducts) were observed (Fig. 2-4C). These data indicate that hepatic ABCB10 loss-of-function in females with ASH is not sufficient to drive progression to AH. Consequently, ABCB10 protection from oxidative damage and inflammation might only be required under stresses that induce more liver inflammation and damage than the NIAAA model.

The decrease in neutrophilic inflammatory capacity induced by ABCB10 gain-of-function in mice with AH is not explained by an upregulation in mitochondrial fat expenditure.

We previously published that loss of hepatic ABCB10 in male mice with NAFLD increased mitochondrial respiration and protected from hepatic steatosis[6]. However, ABCB10 deletion had no effects on mitochondrial function in lean mice fed a chow diet[6] or, as shown here, in female mice fed the Lieber-de Carli diet with one binge (NIAAA

model). Thus, the effects of ABCB10 on mitochondrial oxidative capacity appear to be strictly dependent on the metabolic context of the hepatocyte. As a result, it was a possibility that ABCB10 gain-of-function improved mitochondrial function to eliminate pro-inflammatory non-esterified fatty acids (NEFA) in male mice with AH.

To test this possibility, we measured mitochondrial oxidative capacity in male mice fed the hybrid-binge AH diet and transduced with AAV-ABCB10. ABCB10 gain-of-function did not upregulate fatty acid oxidation capacity of liver mitochondria isolated from livers with AH, as shown by similar respiratory rates under palmitoyl-carnitine (Fig. 2-5A). Confirming that overall mitochondrial oxidative capacity was not augmented by ABCB10 gain-of-function, complex I and complex II-driven respiration were not increased (Fig. 2-5B,C). As expected from the lack of changes in mitochondrial fat oxidation capacity, we did not see a decrease in intrahepatic triglycerides (Fig. 2-5D) nor in NEFA content induced by ABCB10 gain-of-function (Fig. 2-5E). These results suggest that improved mitochondrial fat oxidation and decreased lipid accumulation are not the mechanism by which ABCB10 gain-of-function mitigates neutrophilic inflammation in AH.

Hepatic ABCB10 gain-of-function in AH does not alter the expression of cytokines and chemokines that recruit immune cells, nor the content of AH-related PAMPs and DAMPs.

Livers with AH show an increase in the expression of pro- inflammatory cytokines and chemokines, which promote neutrophil recruitment and activation[8,9]. To determine whether ABCB10 gain-of-function mitigated the actions of pro-inflammatory cytokines

produced by hepatocytes in livers with AH, we measured the effects of AAV-ABCB10 transduction on gene expression of these cytokines in livers from male mice fed the hybrid diet AH model. ABCB10 gain-of-function did not downregulate the mRNA content of pro-inflammatory molecules such as TNFalpha, IL-1beta, IL-6 (Fig. 2-6A). Moreover, the expression of anti-inflammatory IL-10 was not increased by hepatic ABCB10 gain-of-function (Fig. 2-6A).

The inflammatory response of liver to AH can involve the recruitment and activation of different immune cells beyond neutrophils, including monocytes and resident macrophages. We found that ABCB10 gain-of-function did not decrease the mRNA content of monocyte chemo-attractants, such as CCL2, CCL3 and CCL4, nor of the macrophage cell surface marker CD68 (Fig. 2-6B). These data indicate that ABCB10 activity in hepatocytes does change the generation of signals attracting monocytes, nor the presence of macrophages in livers from male mice with AH.

Similar to monocytes, neutrophils are recruited to sites of inflammation and damage via cytokine gradients. Alcohol intake in mice induces the expression of neutrophil recruiting chemokines CXCL1, CXCL2, CXCL5 and their receptor CXCR2 in liver. Specifically, hepatic-derived CXCL1 is a neutrophil chemoattractant with a key role in AH[12]. However, hepatic ABCB10 gain-of-function did not decrease the mRNA content of neutrophil-specific cytokines in mice with AH, including CXCL1 (Fig. 2-6C). The lack of decreased CXCL1 expression was also confirmed at the protein level (Fig. 2-7). In addition to cytokine and chemokine gradients attracting inflammatory cells to the liver, neutrophils must transmigrate from liver sinusoids into the parenchyma. Livers with AH were previously demonstrated to have an upregulation in the expression of integrins and

selectins involved in neutrophil transmigration, namely ICAM, VCAM, SELE, SELP, ESL-1 and PSGL-1[13,14]. We did not observe a decrease in the expression of these neutrophil transmigration proteins induced by ABCB10 gain-of-function (Fig. 2-6D). These results further support that decreased neutrophil infiltration is not the mechanism by which ABCB10 mitigates neutrophilic inflammation in AH.

In addition to hepatocyte damage, AH promotes neutrophil activation by damaging the intestinal barrier to enable the infiltration of bacterial PAMPs (pathogen associated molecular pattern) into the portal vein, as well as by hepatocytes rising the production of DAMPs (damage associated molecular patterns), such as HMGB1. Boosted HMGB1 protein production in hepatocytes was demonstrated to exacerbate alcoholic liver disease[15]. Accordingly, HMGB1 deletion in hepatocytes protected from ALD by increasing mitochondrial fat oxidation[15]. To determine whether ABCB10 gain-of-function in hepatocytes could mitigate neutrophil inflammation by decreasing bacterial PAMP content and/or HMGB1, we quantified the content of liposaccharide (LPS, bacterial PAMP) in serum and of HMGB1 protein in liver from mice under the hybrid-AH model and overexpressing ABCB10. No differences were observed in LPS and HMGB1 content (Fig. 2-8A,B), supporting that ABCB10 gain-of-function was not mitigating neutrophilic inflammation by decreasing the content of AH-related PAMPs (LPS) and DAMPs (HMGB1).

Hepatic ABCB10 gain-of-function decreases NET formation and ROS-mediated actions in livers from mice with AH.

Neutrophils form extracellular traps (NETs) as part of their antimicrobial function. These NETs are formed by decondensed chromatin released to the extracellular space, together with MPO and ROS, to trap and kill bacteria[16]. Recent studies showed that a maladaptive and excessive formation of NETs can contribute to liver damage and thus acute liver failure observed in human AH[5]. To determine if hepatic ABCB10 mitigated neutrophilic inflammatory capacity in mice with AH by decreasing NET formation, we quantified the amount of NETs formed in livers of mice with AH and ABCB10 gain-of-function. Histone H3 citrullination in Arg17 (CitrH3) is the key neutrophil-specific process that enables the decondensation of chromatin needed to form NETs[16]. Therefore, by measuring CitrH3 content in liver lysates by Western blot, as well as by visualizing NETs via immunodetection of CitrH3 in liver sections, NET formation can be quantified in the liver. Remarkably, we found that hepatic ABCB10 gain-of-function decreased histone H3 citrullination (CitrH3) in mice with AH, as shown by a 50% decrease in CitrH3/histone H3 ratio (Fig. 2-9A-D) and a decrease in the visualization of CitrH3 positive NETs in liver sections (Fig. 2-9G). These data indicate that hepatic ABCB10 activity modulates the ability of neutrophils to form extracellular traps in AH. The lack of a decrease in total MPO and neutrophil elastase (ELANE) protein in liver induced by ABCB10 gain-of-function (Fig. 2-9E,F), further support a more important role of hepatic ABCB10 in decreasing the function of infiltrated liver neutrophils, when compared to neutrophil infiltration per se.

Oxidative stress is a major activator of NET formation in neutrophils[17–19]. ABCB10 was previously shown to decrease oxidative damage in differentiating erythrocytes and stressed cardiomyocytes[20]. Furthermore, we previously showed that ABCB10 increased

the production of bilirubin within hepatocytes[6], with bilirubin being a lipophilic molecule that decreases H_2O_2 and lipid peroxide content. However, whether hepatocyte-derived pro-oxidants regulated by ABCB10 actions promote NET formation in AH is unknown. To determine whether ABCB10 gain-of-function decreased pro-oxidant actions in AH, we measured the actions of lipid peroxides in livers of mice with AH transduced with AAV-ABCB10. These actions of lipid peroxides, one of them being 4-HNE, can be quantified by measuring the formation of 4-HNE-protein adducts by Western blot. We found that ABCB10 gain-of-function significantly decreased 4-HNE-protein adduct content in mice with AH (Fig. 2-9H). These results suggest that a decrease in pro-oxidant content induced by ABCB10 gain-of-function in hepatocytes can be responsible for the decrease in NET formation in livers of mice with AH.

DISCUSSION

Our study identified that ABCB10 downregulation in liver is a novel metabolic and redox defect of human and mouse livers with AH, with decreased ABCB10 content having an important contribution to the degree of NET formation in livers from mice with AH. To our knowledge, ABCB10 is one of the first redox regulators identified that communicates the hepatocellular redox state to infiltrated neutrophils, to determine the extent of NET formation in AH. Therefore, our findings inform that upregulating hepatocyte-ABCB10 expression could be a novel approach to treat 40% of the patients with AH that do not responding to current treatments (prednisolone)[1], by mitigating the maladaptive formation of pro-inflammatory NETs. In agreement with this expectation, ABCB10 gain-of-function did not completely suppress NET formation: ABCB10 only mitigated NET formation in the

context of excessive neutrophil activation induced by AH. Restoring the endogenous ABCB10 protein lost in a pathogenic state (AH) would be expected to prevent only the excessive formation of NETs. Thus, we believe that restoring ABCB10 expression could not have a strong inhibitory effect blocking NET formation when the neutrophils are directly sensing PAMPs and DAMPs. ABCB10 restoration in hepatocytes would only block excessive formation of NETs occurring on top of and probably independently of direct PAMP and DAMP sensing in neutrophils.

To investigate the exact role of hepatic ABCB10 downregulation in AH, we used a mouse model of AH that recapitulated the downregulation of ABCB10 protein observed in human livers. The widely used NIAAA model of ASH in mice, a 10-day Lieber de Carli diet plus one ethanol binge [7], can induce neutrophil infiltration to the liver parenchyma, recapitulating one hallmark of AH. On the other hand, the hybrid-binge AH model[8,9] of 7-week intragastric ethanol feeding, with *ad libitum* consumption of the Western diet combined with weekly ethanol binges, mimics AH patient drinking and dietary behavior, as well as reproducing key histologic features of clinical AH. When studying the effects of these models, we found that ABCB10 content was only decreased in the hybrid-binge AH model and not in the NIAAA model. Just as Argemi et al.[2] identified unique phenotypic differences between human livers with early ASH and decompensated with AH, we believe that the hybrid-binge AH model recapitulates AH, while the NIAAA model mimics ASH in humans. Altogether, these data indicate that ABCB10 downregulation can be playing a specific role in the development of AH, but not in earlier and milder stages of alcoholic liver disease.

To determine the exact role of ABCB10 downregulation in AH pathogenesis, we studied the effects of hepatocyte ABCB10 gain-of-function on liver inflammation in mice with AH. We discovered that ABCB10 gain-of-function mitigated neutrophilic inflammation in liver, as evidenced by a significant decrease in MPO and neutrophil elastase (ELANE) gene expression with a trend to decreased neutrophil infiltration. Even though MPO is widely used a specific marker of neutrophils and AH is characterized by a marked increase in neutrophil infiltration, MPO can also be expressed in macrophages. However, we did not observe difference in the content of CD68, a specific marker of macrophages, while we also observe a decrease in ELANE expression. These data confirmed that differences in MPO expression and staining induced by ABCB10 gain-of-function stem from infiltrated neutrophils, as expected in livers with AH. In this regard, we provide additional evidence supporting that hepatocyte-ABCB10 is mostly regulating the activity of infiltrated neutrophils, rather than neutrophil infiltration *per se*:

The first evidence is the absence of significant decreases in liver MPO and ELANE protein content induced by ABCB10 gain-of-function, despite the decrease in MPO and ELANE gene expression. MPO and ELANE are highly abundant in neutrophils and are essential for their antibacterial and pro-inflammatory activity, with MPO and ELANE being secreted from activated neutrophils[17,18]. The discrepancy between MPO and ELANE transcript and protein suggests a decrease in MPO and ELANE turnover (i.e. increased storage, decreased release), characteristic of decreased neutrophil secretory activity. The second line of evidence is the absence of differences in the expression of cytokines

and chemokines involved in neutrophil activation and recruitment to the liver. The third line is the lack of changes in the expression of selectins, integrins and other components facilitating transmigration of immune cells to AH livers. The fourth and last line is that ABCB10 gain-of-function was not decreasing HMGB1 protein content in liver, which is a hepatocyte-generated DAMP that promotes ALD by suppressing mitochondrial fat oxidation[15], nor decreasing LPS, a bacterial PAMP whose presence is caused by alcohol-induced damage of the gut. These later set of data is consistent with the absence of changes in mitochondrial fat oxidation and hepatocyte damage when ABCB10 activity was changed in mice with ALD. Thus, the molecular signature of livers with ABCB10-gain-of-function does not support a decrease in the capacity to recruit immune cells or in the presence of DAMPs and PAMPs in livers with AH, but rather a specific change in neutrophil pro-inflammatory activity.

These results indicating that ABCB10 regulated neutrophilic activity, led us to evaluate whether loss of ABCB10 was sufficient to drive the progression from ASH to AH. To this end, we determined the effects of the NIAAA model of ASH on hepatic inflammation and hepatocellular metabolism of liver-specific ABCB10 KO (L-KO) mice. We did not observe that ABCB10 loss worsened liver neutrophil inflammation or metabolism in ASH, as no upregulation in liver MPO content, no decreases in mitochondrial fat oxidation capacity and no exacerbation of hepatic steatosis were observed in ABCB10 L-KO mice under the NIAAA model. These data further support that hepatocellular redox and metabolic function in ASH is not as defective as in AH, such that loss of ABCB10 function in ASH is effectively compensated. As a result, our data indicate

that ABCB10 downregulation has a greater relevance in AH, when hepatocytes are hypometabolic with diminished antioxidant capacity. Indeed, our findings support that the alteration of the expression of multiple genes controlled by the transcriptional factor HNF4□[2], and not just one single gene, is needed to transition from ASH to AH.

NET formation was recently identified as a key process contributing to liver damage in AH[5]. Here, we demonstrate that ABCB10 gain-of-function drastically decreased key processes required for NET formation, such as histone 3 citrullination (CitrH3). This decrease in NET formation induced by ABCB10 gain-of-function coincided with a significant decrease in oxidative damage to proteins mediated by lipid peroxides (4-HNE protein adducts). This effect is consistent with the known role of ABCB10 function producing a lipophilic ROS scavenger in hepatocytes, bilirubin[6]. Given that ABCB10 gain-of-function was selectively induced in hepatocytes, the increased neutrophil-hepatocyte contacts observed in AH may allow neutrophils to uptake bilirubin generated by hepatocytes. When this hepatocyte-generated bilirubin is inside neutrophils, it could scavenge the ROS that were activating NET formation in neutrophils[17–19]. Indeed, previous studies showed that bilirubin can decrease ROS production in neutrophils[21], as well as inactivating ROS-derived from MPO activity[22].

However, patients with AH have a decreased ability to conjugate bilirubin generated in the spleen from red blood cell turnover, causing hyperbilirubinemia[1]. Therefore, it can be challenging to propose that bilirubin availability to neutrophils can be sufficiently limited by a decrease in ABCB10-driven bilirubin synthesis to promote

inflammation in AH. Another possibility is that hepatic ABCB10 may affect the production of pro-inflammatory oxidants in specific subdomains within hepatocytes. Non-enzymatic oxidation of polyunsaturated fatty acids (PUFAs) by H_2O_2 and superoxide generate the stable aldehyde 4-HNE, which can form 4-HNE protein adducts and bioactive oxylipins[23,24]. Once oxylipins and 4-HNE protein adducts are formed, they cannot be reversed or inactivated by bilirubin's ROS scavenging actions (mostly scavenging H_2O_2 and lipid peroxides). Therefore, it is feasible that decreased ABCB10 function resulted in the release of a higher quantity of irreversibly oxidized lipids and protein-adducts that activate NET formation in neutrophils. Consistent with this interpretation, high oxylipins content in liver correlates with the severity of AH[25–27] and are potent inducers of NET formation as well[28–30]. We are currently setting up an *in vitro* system to determine which of these two possibilities can explain how increased ABCB10 function in hepatocytes mitigates NET formation in neutrophils in livers with AH.

In all, we show that ABCB10 gain-of-function in liver is sufficient to mitigate NET formation in mice with alcoholic hepatitis (AH), with ABCB10 protein content being markedly decreased in humans with AH. Thus, our study informs that restoring ABCB10 function in human livers might be a novel strategy to mitigate NET formation and liver inflammation in AH, which are associated with poor prognosis of liver disease.

MATERIALS AND METHODS

Mice

All experiments were approved by IACUC at the University of California, Los Angeles under protocols #2015-121, #2017-061 and at the University of Southern California under protocol 21051-CR004. Constitutive hepatocyte ABCB10 KO mice

(ABCB10 L-KO) were previously generated in C57BL/6J background, by breeding *Abcb10*$^{flox/flox}$ mice with *Alb-Cre+/-* mice procured from Jackson laboratories. *Abcb10*$^{flox/flox}$*; Alb-Cre-/-* and *Abcb10*$^{flox/WT}$;*Alb-Cre-/-* littermates were used as WT controls(Shum *et al*, 2021).

Chronic-plus-binge model of ASH (NIAAA model)

As described by Bertola et al(Bertola *et al*, 2013), twelve- to eighteen-week-old female C57BL/6J mice were fed with a liquid control diet (Bio-Serv F1258SP) for 5 days, followed by a Lieber de Carli diet (Bio-Serv F1258SP + 5% ethanol) administered *ad libitum* for 10 days, using Bio-Serv glass-bottles. Only female mice were used in this NIAAA model of ASH, because males are more resistant to liver damage and inflammation induced by this model(Bertola *et al*, 2013). In the early morning of day 16, mice were delivered 5g ethanol/kg body weight by oral gavage, followed by euthanasia 9 h post-gavage. Control mice were pair-fed with the equivalent number of calories but replacing ethanol with maltodextrin.

Hybrid feeding plus binge model of AH.

As previously described(Ueno *et al*, 2012; Lazaro *et al*, 2015), eight week-old C57BL/6J males procured at Jackson laboratories were fed intra-gastrically an ethanol-containing liquid diet as 60% of their total calorie intake, with the remaining 40% being solid Western diet with high-cholesterol and saturated fat provided *ad libitum*. This hybrid diet was provided for 7 weeks together with weekly ethanol binges commencing in the 2nd week. Ethanol dose was increased gradually over the first three weeks of diet, reaching

peak ethanol intake of 33g/kg body weight by week 3 after diet initiation. Weekly intragastric ethanol binges were performed by withdrawing ethanol infusion for ~4 h, followed by a bolus of ethanol equivalent to the total amount withdrawn. An isocaloric diet replacing ethanol with dextrose was used as a control. Only males were used in this study, because the attrition rates in females fed with the hybrid model of AH before the experimental end- point is excessively high, as published(Ueno *et al*, 2012; Lazaro *et al*, 2015)

AAV generation and transduction of male mice with AH.

AAV with transgene expression restricted to hepatocytes were produced by Vector Biolabs: GFP or mouse ABCB10 were cloned into AAV serotype 8, with their expression controlled by a fragment of the Albumin promoter (AAV8-Alb-ABCB10 and AAV8-Alb-GFP). AAV were titrated by qPCR quantification of AAV genome copies (g.c.). Between 1-2 weeks prior the initiation of the diet and after the implantation of the catheter for intragastric feeding, mice were administered $1x10^{11}$ g.c/per mouse of AAV8-Alb-GFP or AAV8-Alb-ABCB10 via tail vein or retro-orbital injection, allowing for peak transgene expression of the construct by the time of maximal ethanol dose administration.

Human Liver Samples.

Total membrane fractions to analyze ABCB10 protein content were obtained, as previously published(Khanova *et al*, 2018), from human liver biopsies provided by the Clinical Resource for Alcoholic Hepatitis (AH) Investigations at Johns Hopkins University (IRB 00107893 directed by Dr. Zhaoli Sun). Briefly, biopsies were excised from the

explanted livers during liver transplantation in patients with AH, while control samples were wedge biopsies from the healthy livers donated. Five control samples from 2 females and 3 males ranging 32-61 years old, and five AH samples, from 3 males and 2 females, ranging 32-49 years old, all AH patients with liver decompensation and bilirubinemia ranging 14-48 mg/dl.

Serum Liver Enzymes.

Serum AST and ALT activities were measured using IDEXX in mice with AH and with kits from Sigma-Aldrich in mice with ASH.

Seahorse XF96 Respirometry

Mitochondria were isolated via differential centrifugation as published(Shum *et al*, 2021). Mitochondria were diluted in Mitochondrial Assay Solution (MAS: 70 mM sucrose, 220 mM mannitol, 10 mM KH_2PO_4, 5 mM MgCl2, 2 mM HEPES, 1 mM EGTA and 0.2% fatty acid-free BSA, pH 7.2) on ice. Mitochondrial protein fractions were plated in a XF96-well plate in 20 µL of MAS, loading 4µg protein for pyruvate (5mM) + malate (5mM), 2µg for succinate (5mM) + rotenone (4µM) or with 6µg for palmitoyl-carnitine (40µM) +1mM malate-driven respiration. The XF96 plate was centrifuged at 2000xg for 5 min at 4ºC to sediment mitochondria to the bottom of the well. An additional 130 µl MAS was added to each well. The XF96 plate was incubated for 8 min at 37ºC before loading it to the Seahorse XF96 Analyzer for measurement of respiration. ATP-synthesizing respiration was induced after injection of ADP (2mM final), Leak was measured after injection of oligomycin (3 µM final), maximal respiration after injecting

FCCP (4µM final) and antimycin A (4µM final)/rotenone (4µM) was used to block respiration.

Measurements of triglycerides and NEFA in liver

These measurements were realized at the UCLA Lipidomics core. Briefly, a modification of the Bligh and Dyer protocol was used to extract lipids from frozen livers as previously published(Profiling of mouse macrophage lipidome using direct infusion shotgun mass spectrometry). Prior to extraction, an internal standard mixture was added to each sample (AB Sciex 5040156, Avanti 330827, Avanti 330830, Avanti 330828, Avanti 791642). These lipid extracts that included the standards were quantitatively analyzed by Shot Gun Lipidomics, using the Sciex Lipidyzer Platform. The Differential Mobility Device on Lipidyzer was tuned with EquiSPLASH LIPIDOMIX (Avanti 330731). An in-house data analysis platform similar to the Lipidyzer Workflow Manager was used. The total non-esterified or free fatty acids and triglyceride quantitative values were normalized to mg of liver.

Quantitative PCR assay

RNeasy kit (QIAGEN) was used to extract total liver mRNA. cDNA was reverse transcribed using SuperScript VILO cDNA synthesis kit (ThermoFisher) from 2 µg total RNA. qPCR reactions were performed using the TaqMan Fast Advanced Master Mix (ThermoFisher). See Supplementary Table 1 for list of Taqman primers. Results were normalized to hypoxanthine phosphoribosyl transferase (Hprt) within each sample to obtain sample-specific ΔCt values (Ct gene of interest - Ct Hprt). 2_ΔΔCt values were

calculated to obtain fold expression levels, where ΔΔCt = (ΔCt experimental - ΔCt control).

Western Blot Analysis

This protocol was modified from our previous publication(Shum *et al*, 2021). Mouse liver tissues were homogenized in lysis buffer (50 mM Tris pH 7.5, 150 mM NaCl, 2 mM EDTA, 5 mM EGTA, 1% Triton X-100, 1% SDS, 1% sodium deoxycholate, 2 mM sodium orthovanadate, 50 mM sodium fluoride, 5 mM sodium pyrophosphate, 1 mM PMSF, 80 mM sodium β-glycerophosphate). Lysates were centrifuged for 10 min at 10,000xg at 4° C. BCA Protein Assay Kit (Pierce) was used to determine protein concentration. 20-30ug of protein were separated by SDS-PAGE using 4-12% Bis-Tris gels and transferred onto PVDF membrane. Membranes were blocked in 5% (wt/vol.) non-fat milk diluted in Tris pH 7.4 + 0.1% (vol./vol.) Tween (TBS-T) for 1h. Membranes were then incubated with primary antibody overnight at 4°C diluted in 5% (wt/vol.) BSA in TBS-T. See Supplementary Table 2 for list of antibodies.

Immunohistochemistry

Mouse livers were fixed in 10% neutral-buffered formalin for 24 hours then stored in 70% ethanol (HistoPrep). Histology was performed by HistoWiz Inc., with fixed livers being processed, embedded in paraffin, and sectioned at 8μm. Immunohistochemistry was performed on a Bond Rx autostainer (Leica Biosystems) with enzyme treatment (1:1000) using standard protocols. Antibodies used were rabbit polyclonal MPO primary antibody (Abcam, ab9535, 1:50) and mouse anti-rabbit secondary (Vector, 1:100). Bond

Polymer Refine Detection (Leica Biosystems) was used according to the manufacturer's protocol. After staining, sections were dehydrated and film coverslipped using a TissueTek-Prisma and Coverslipper (Sakura). Whole slide scanning (40x) was performed on an Aperio AT2 (Leica Biosystems). Quantification was performed of 10 fields of view per mouse at 10x magnification.

Statistics

Data are shown as average values with standard error of the mean. GraphPad Prism 9 and Excel were used to perform unpaired Student's t-tests and Mann-Whitney U tests.

FIGURES

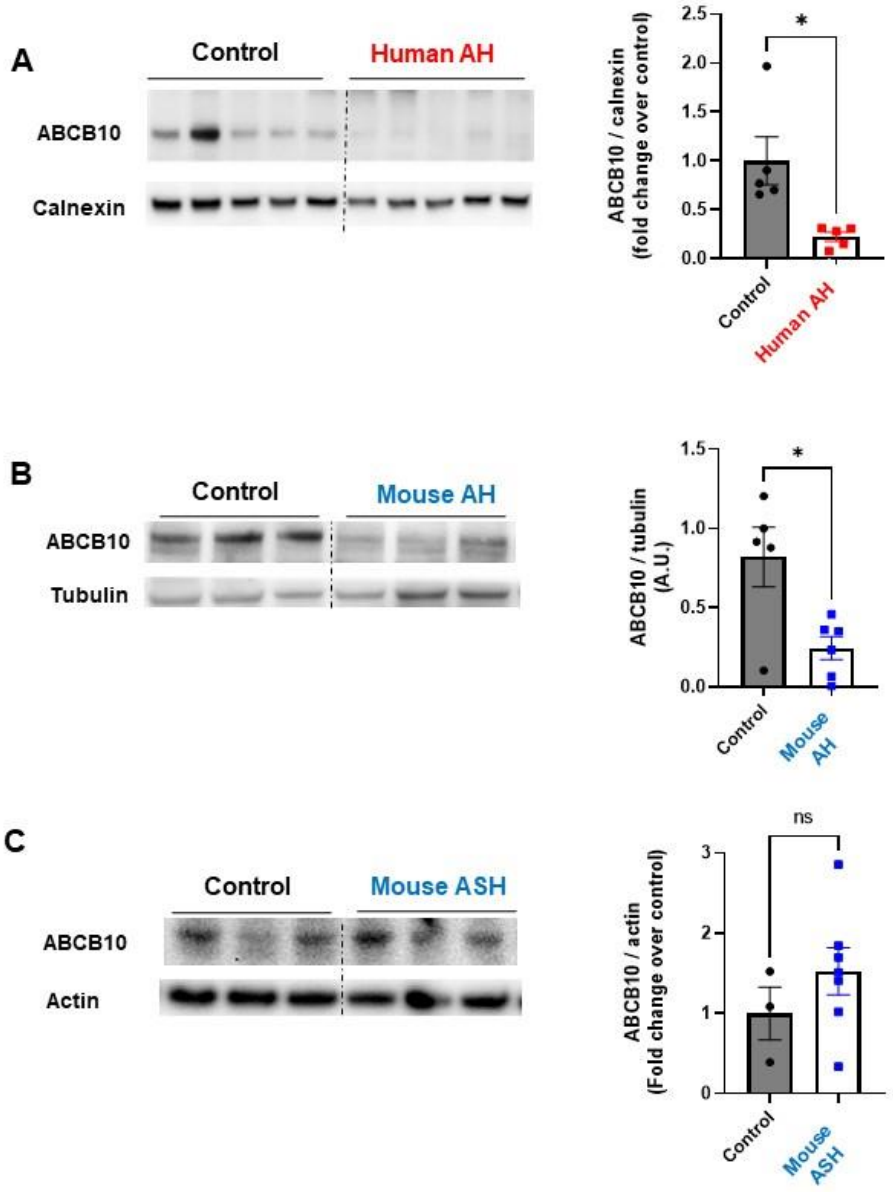

Figure 2-1: ABCB10 protein content is decreased in livers with alcoholic hepatitis (AH), but not in livers with ASH.

(A) Western blot measurements of ABCB10 protein content in total membrane fractions obtained from human livers of non-alcoholic patients (Control) and patients with

alcoholic hepatitis (AH), using the ER membrane protein calnexin as loading control. n= 5 per group **p<0.01 Student's t-test. **(B)** ABCB10 protein content in total liver lysates from male mice fed the hybrid diet plus ethanol binges to induce alcoholic hepatitis (AH) and fed with an isocaloric diet without ethanol as control (Control). Tubulin is used as loading control. n= 5-6 per group. *p<0.05 Student's t-test. **(C)** ABCB10 protein content in total liver lysates from female mice with ASH induced by the NIAAA model (10 days Lieber-de Carli plus one ethanol binge) or an isocaloric diet without ethanol as control (Control). Actin is used as loading control. n= 3-6 per group (n.s. Student's t-test). Data expressed as mean ± SEM.

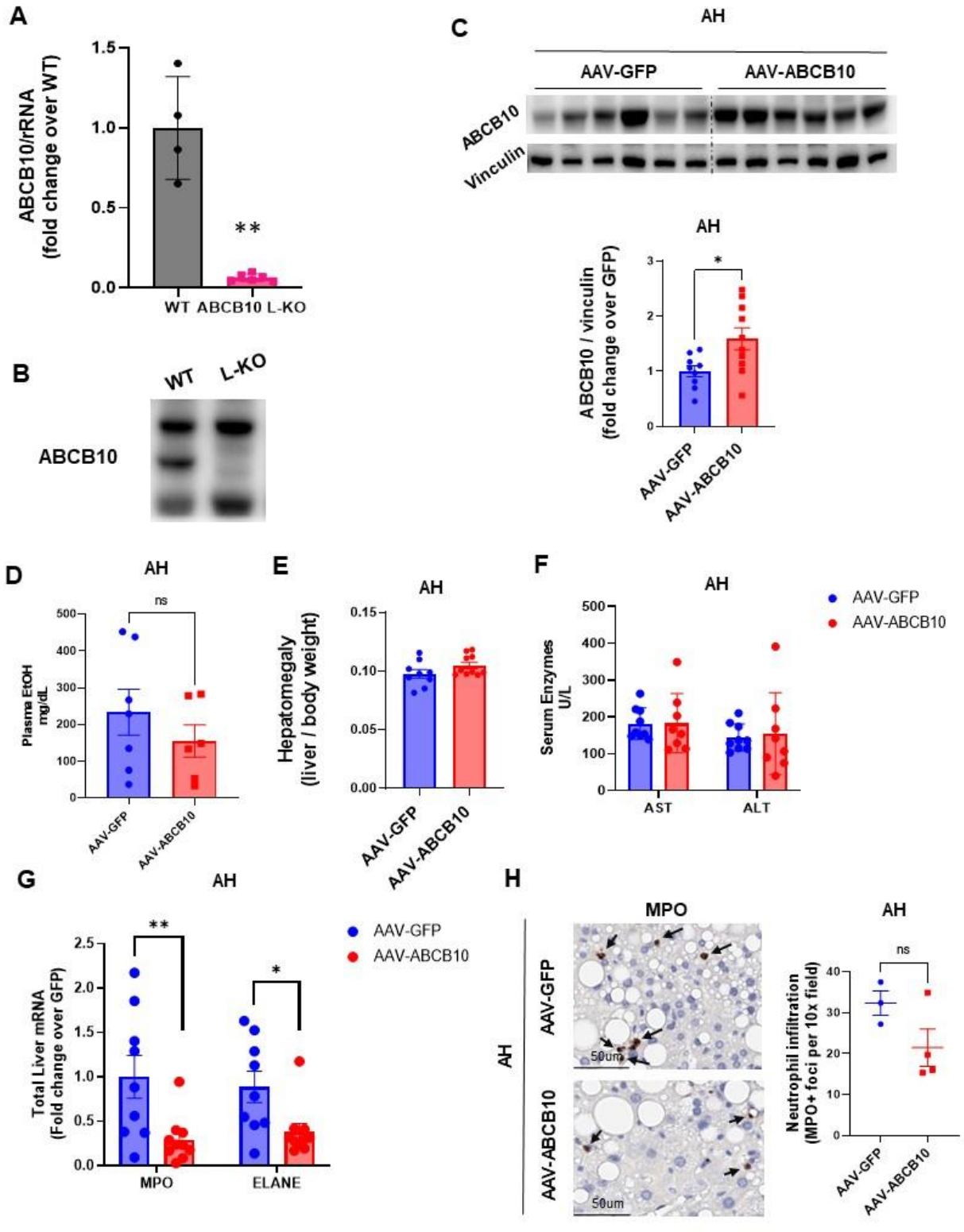

Figure 2-2: Increasing ABCB10 content in hepatocytes decreases neutrophil

biomarkers without mitigating hepatocyte damage in livers from mice with AH.

(A) qPCR measurements of total liver mRNA and **(B)** Western blot detecting ABCB10 in total liver lysates from WT and ABCB10 L-KO female mice. L-KO mice were generated by breeding *Abcb10*$^{flox/flox}$ mice with *Alb-Cre*+/- mice, to delete ABCB10 in hepatocytes. n=4-6 mice per group, error bars SEM. **p=0.0095 Mann-Whitney U. Male mice with AH, induced by hybrid diet feeding plus ethanol binges, and transduced with AAV-ABCB10 or- GFP as transduction control were analyzed for: **(C)** ABCB10 protein content in total liver lysates n=9-10 per group, (D) plasma thanol measured with a fluorometric assay (Sigma-Aldrich MAK076-1KT) in plasma diluted 1/100 n=6-7 per group ns represents p>0.05 unpaired Student's t test., **(E)** liver-to-body weight ratio n=9-10 per group, **(F)** serum AST and ALT n=8-9 per group, **(G)** MPO and neutrophil elastase (ELANE) gene expression measured by qPCR in mRNA isolated from liver. n=9-10 per group *p<0.05, **p<0.01 Student's t-test. **(H)** Immunohistochemistry detecting the neutrophil marker MPO in liver sections. Representative MPO staining shown at 40x digital slide magnification, with arrows indicating MPO^{+} and ELANE^{+} cell foci. Quantification of MPO^{+} cell foci per 10x field of liver sections. n= 3-4 per group (n.s. Student's t-test). Data expressed as mean ± SEM.

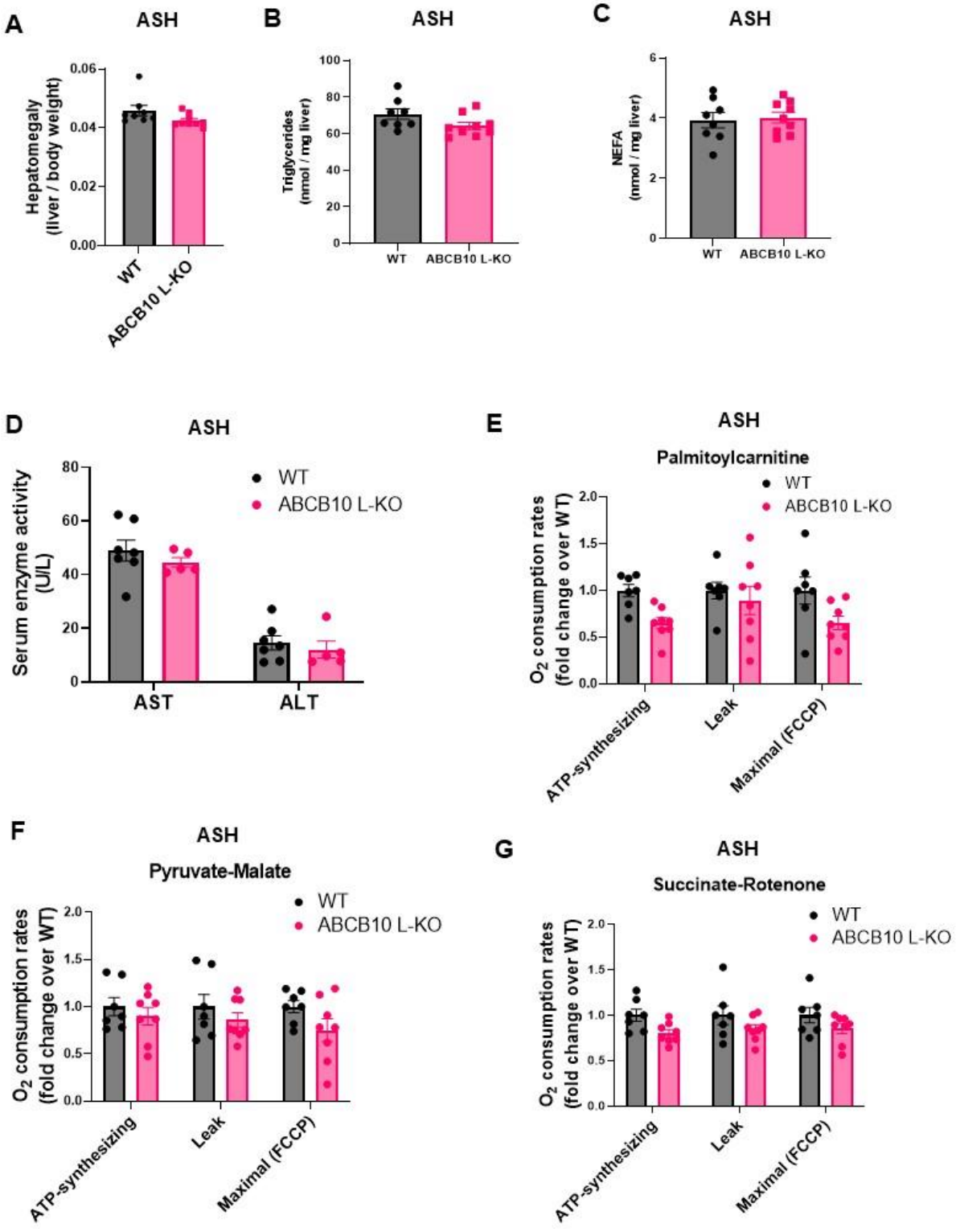
A
ASH
Hepatomegaly (liver / body weight)
0.06
0.04
0.02
0.00
WT
ABCB10 L-KO
B
ASH
Triglycerides (nmol / mg liver)
100
80
60
40
20
0
WT
ABCB10 L-KO
C
ASH
NEFA (nmol / mg liver)
6
4
2
0
WT
ABCB10 L-KO
D
ASH
Serum enzyme activity (U/L)
80
60
40
20
0
WT
ABCB10 L-KO
AST
ALT
E
ASH
Palmitoylcarnitine
WT
ABCB10 L-KO
O2 consumption rates (fold change over WT)
2.0
1.5
1.0
0.5
0.0
ATP-synthesizing
Leak
Maximal (FCCP)
F
ASH
Pyruvate-Malate
WT
ABCB10 L-KO
O2 consumption rates (fold change over WT)
2.0
1.5
1.0
0.5
0.0
ATP-synthesizing
Leak
Maximal (FCCP)
G
ASH
Succinate-Rotenone
WT
ABCB10 L-KO
O2 consumption rates (fold change over WT)
2.0
1.5
1.0
0.5
0.0
ATP-synthesizing
Leak
Maximal (FCCP)

Figure 2-3: ABCB10 hepatocyte-specific deletion is not sufficient to drive progression from ASH to AH.

(A) Liver -to-body weight ratio of wild-type (WT) and ABCB10 L-KO female mice with ASH induced by the NIAAA model (10 days Lieber-de Carli diet + 1 ethanol binge). n=8-9 per group (n.s. Student's t-test). **(B-C)** lipids were extracted from their livers of WT and ABCB10 L-KO female mice with ASH to perform Shot-gun lipidomics and quantify intrahepatic triglyceride and non-esterified fatty acids (NEFA) content. Each individual point represents one mouse, and error bars, SEM. **(D)** Serum AST and ALT activity from WT and ABCB10 L-KO female mice with ASH. n=5-7 per group (n.s. Student's t-test) **(E-G)** Respiration in isolated liver mitochondria from WT and ABCB10 L-KO female mice with ASH. Oxygen consumption rates were measured under **(E)** palmitoyl-carnitine, **(F)** pyruvate-malate or **(G)** succinate-rotenone. ATP-synthesizing, leak, and maximal respiration were calculated as fold change relative to WT respiration. n=7-8 per group (n.s. Student's t-test)

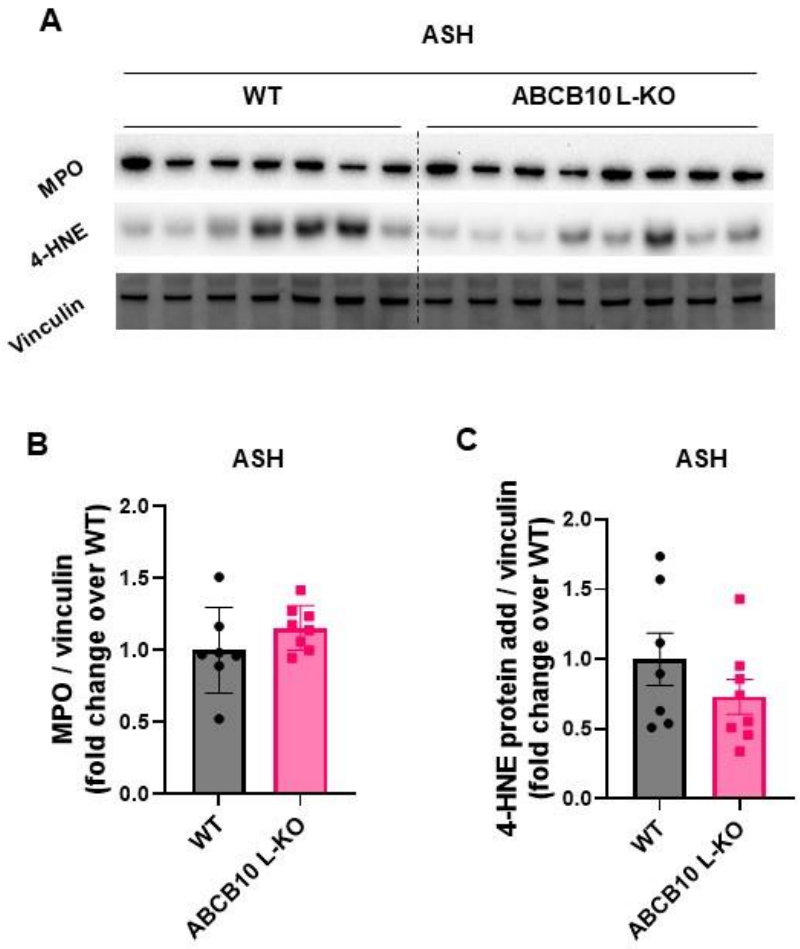

Figure 2-4: ABCB10 hepatocyte-specific deletion does not induce neutrophil inflammation or increased oxidative stress in ASH

(A) Representative immunoblot of MPO and 4-HNE-protein adducts content in total liver lysate of WT and ABCB10 L-KO female mice with ASH, with Vinculin used as loading control. **(B-C)** Immunoblot quantification of **(B)** MPO and **(C)** 4-HNE-protein adducts. n=7-8 per group (n.s. Student's t-test). Data expressed as mean ± SEM.

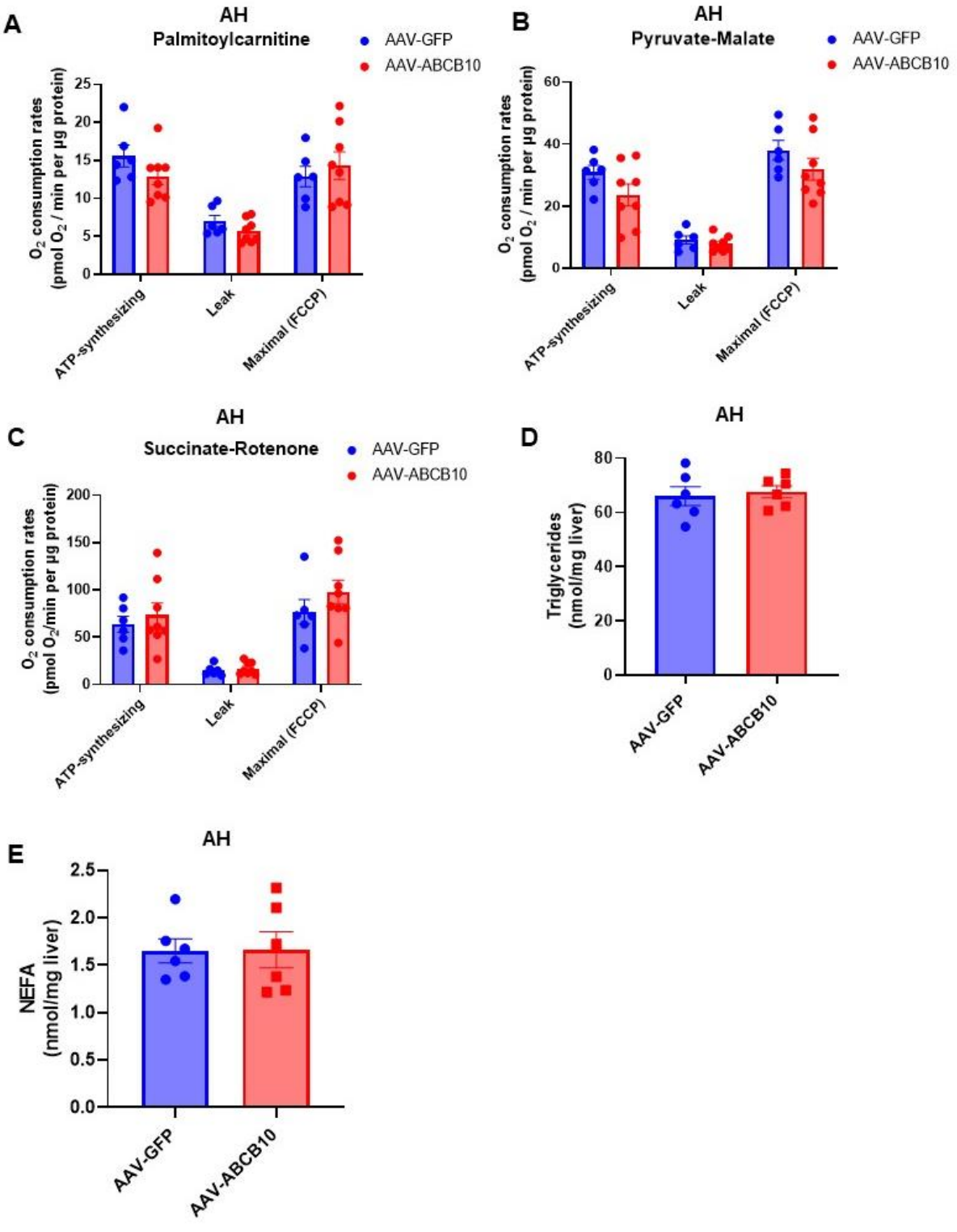

Figure 2-5: Increasing ABCB10 content in hepatocytes does not improve mitochondrial function and does not decrease steatosis in mice with AH

(A-C) Respiration in mitochondria isolated from livers of male mice with AH, induced by the hybrid diet plus ethanol binges, and transduced with AAV-ABCB10 or GFP (control). Oxygen consumption rates were measured under **(A)** palmitoyl-carnitine, **(B)** pyruvate-malate, or **(C)** succinate-rotenone. ATP-synthesizing, leak, and maximal respiration were calculated for each substrate. n=6-8 per group (n.s. Student's t-test). (**D**-**E**) Shot-Gun lipidomics quantification of **(D)** triglycerides and **(E)** NEFA in total lipid extracts obtained from male mouse livers with AH and transduced with AAV-ABCB10 or -GFP. n=6 per group (n.s. Student's t-test). Data expressed as ean ± SEM.

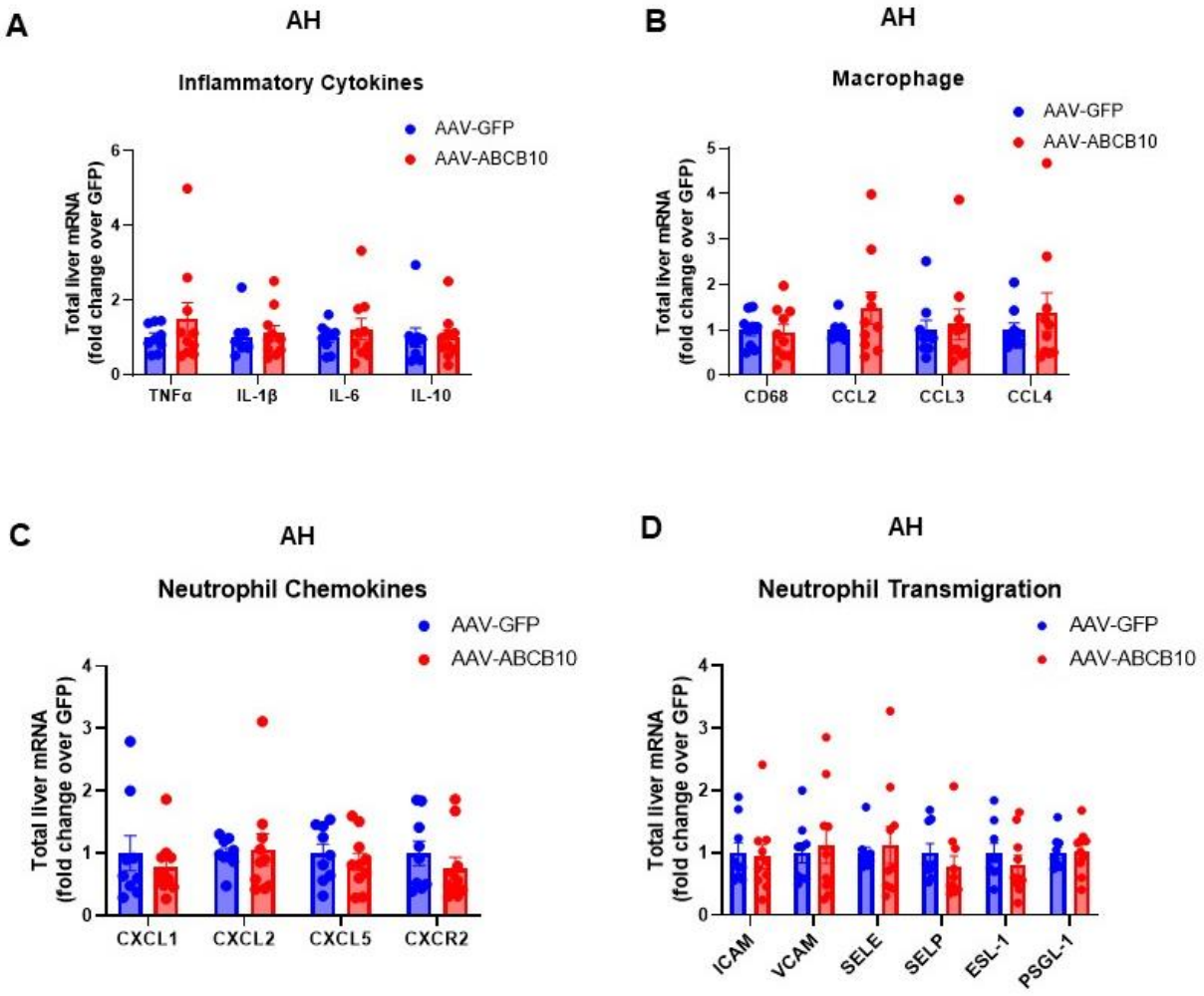

Figure 2-6: Hepatocyte ABCB10 gain-of-function in mice with AH does not decrease the expression of cytokines, chemokines and proteins involved in neutrophil activation, recruitment and transmigration.

(A-D) Gene expression analyses of livers from male mice with AH transduced with AAV-ABCB10 or -GFP (control), measuring mRNA content of **(A)** pro- and anti-inflammatory cytokines, **(B)** monocyte chemo-attractants & macrophage markers, **(C)** neutrophil chemokines and **(D)** proteins mediating neutrophil transmigration to the liver parenchyma. *Hprt* expression used as housekeeping control and data are expressed as fold change of

delta-delta-CT over AAV-GFP. N=9-10 per group (n.s. Student's t-test). Data expressed as mean ± SEM.

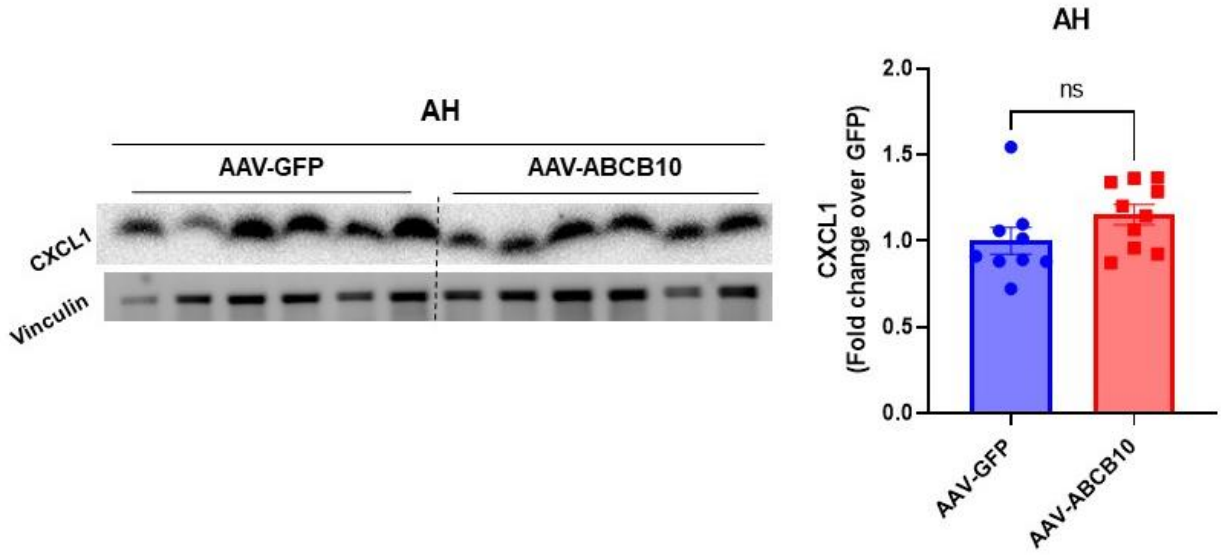

Figure 2-7: CXCL1-protein content is not changed by ABCB10 gain-of-function in mice with alcoholic hepatitis (AH).

Western blot quantifying CXCL1 protein content in total liver lysates from male mice under the hybrid diet AH model and overexpressing ABCB10 in hepatocytes via AAV transduction, using AAV-GFP-transduced mice as controls. Each individual lane and data points represents one mouse, error bars are SEM.

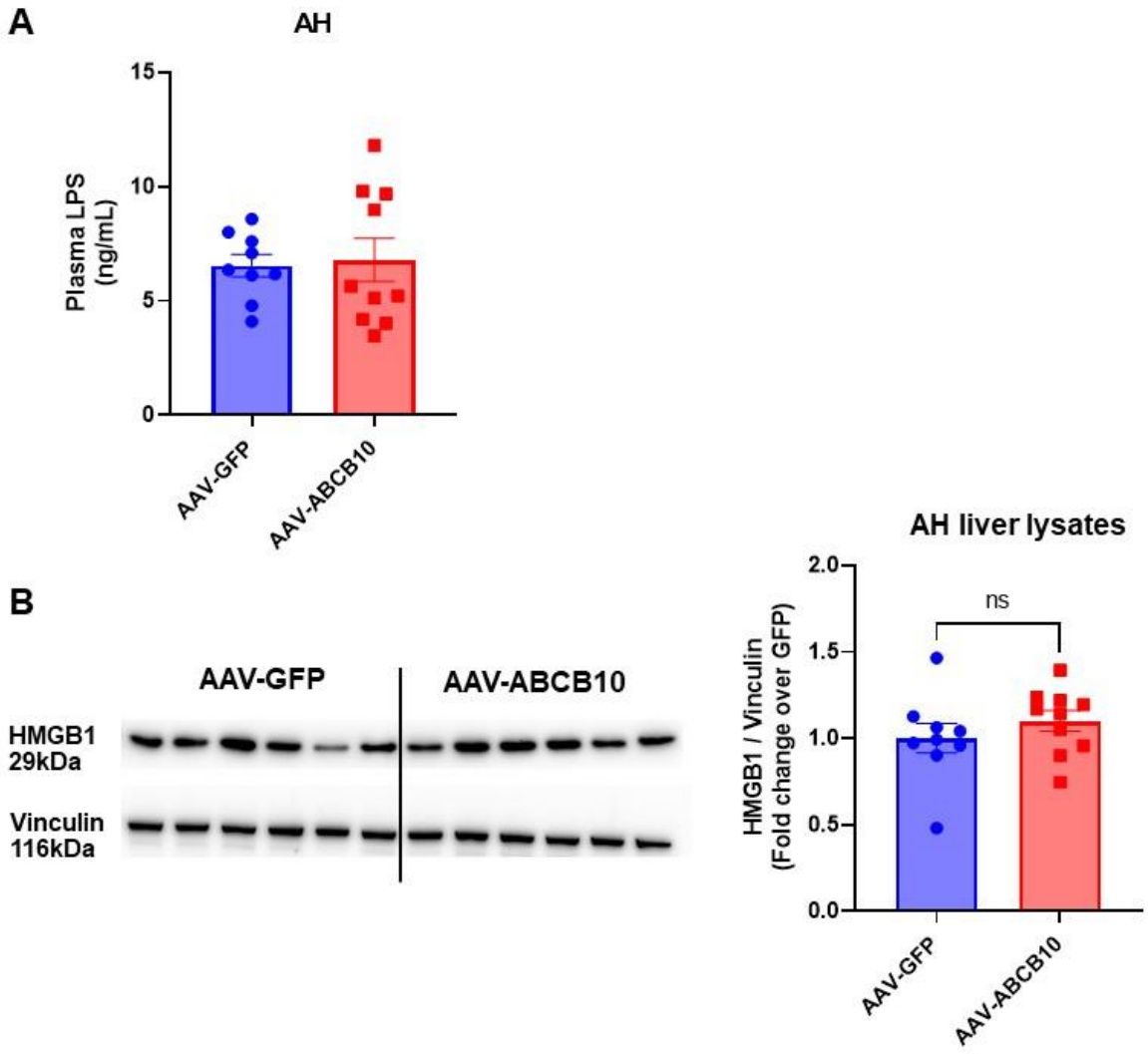

Figure 2-8: Bacterial lipopolysaccharide (LPS) in plasma and HMGB1-protein content in liver are not changed by ABCB10 gain-of-function in male mice with alcoholic hepatitis (AH).

(A) Chromogenic LAL assay quantifying bacterial LPS in plasma from male mice under the hybrid diet AH model and overexpressing ABCB10 in hepatocytes via AAV transduction, using AAV-GFP transduced mice as controls. **(B)** Western blot quantifying HMGB1 protein content in total liver lysates from the same AH mice as in panel A. Each

individual data point and lane represents one mouse, error bars represent SEM, and ns $p>0.05$ in Student's t test.

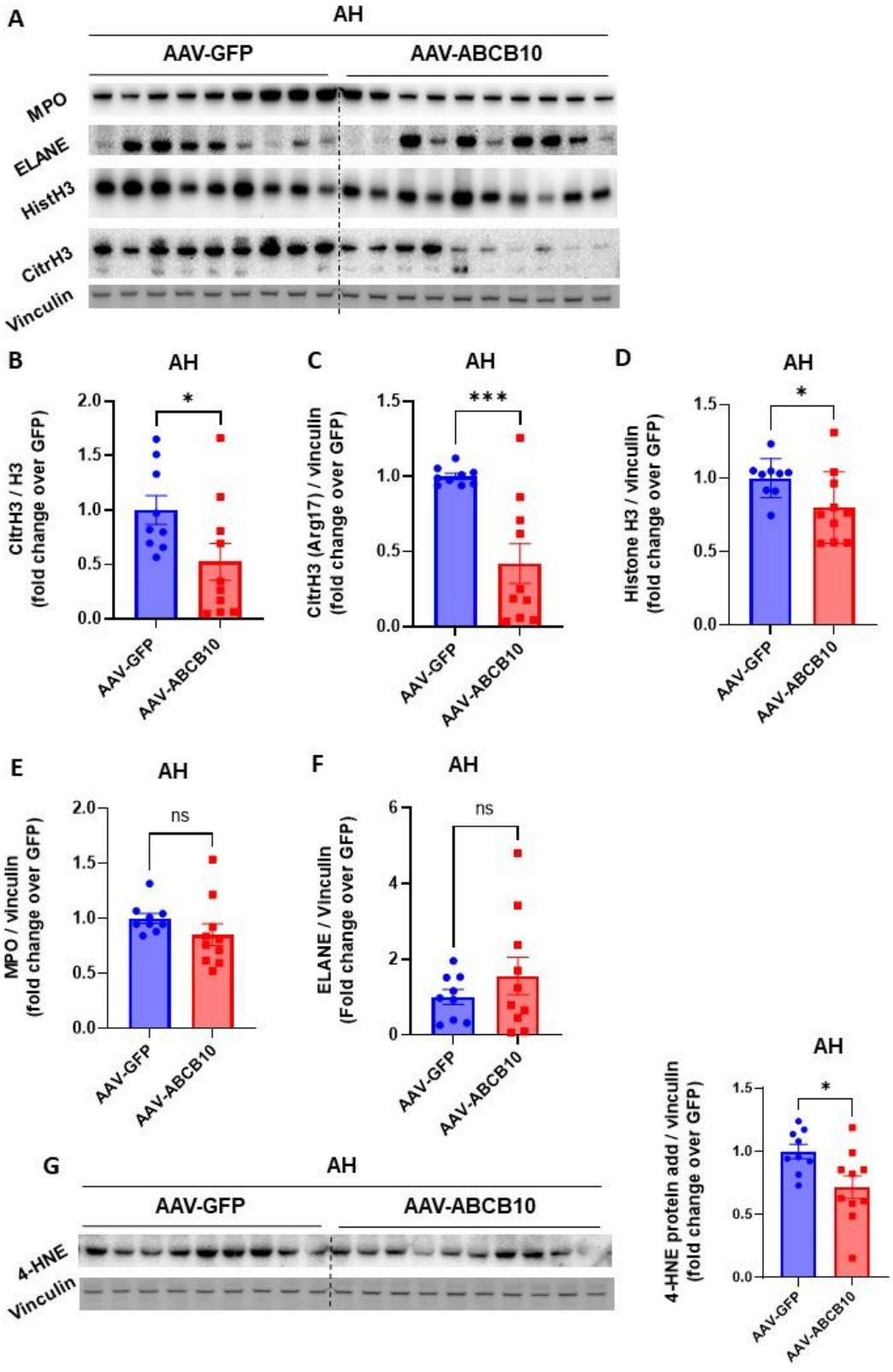
A
AH
AAV-GFP
AAV-ABCB10
MPO
ELANE
HistH3
CitrH3
Vinculin
B
AH
CitrH3 / H3
(fold change over GFP)
*
AAV-GFP
AAV-ABCB10
C
AH
CitrH3 (Arg17) / vinculin
(fold change over GFP)
***
AAV-GFP
AAV-ABCB10
D
AH
Histone H3 / vinculin
(fold change over GFP)
*
AAV-GFP
AAV-ABCB10
E
AH
MPO / vinculin
(fold change over GFP)
ns
AAV-GFP
AAV-ABCB10
F
AH
ELANE / Vinculin
(Fold change over GFP)
ns
AAV-GFP
AAV-ABCB10
G
AH
AAV-GFP
AAV-ABCB10
4-HNE
Vinculin
AH
4-HNE protein add / vinculin
(fold change over GFP)
*
AAV-GFP
AAV-ABCB10

Figure 2-9: Hepatic ABCB10 gain-of-function decreases NET formation and ROS-mediated actions in livers of mice with AH.

(A) Immunoblot of neutrophil specific proteins and markers of NET formation in total liver lysates of male mice with AH transduced with AAV-ABCB10 or -GFP. **(B-F)** Quantifications the immunoblots measuring **(B)** citrullinated histone H3 in Arg 17 [CitrH3] to histone 3 [H3] content ratio, **(C)** total [CitrH3], **(D)** total [H3] content, **(E)** total MPO and (**F**) neutrophil elastase [ELANE]. Vinculin was used as a loading control. **(G)** Immunoblot and quantification of 4-HNE-protein adducts content in total liver lysates from male mice with AH transduced with AAV-ABCB10 or GFP as control mice, with Vinculin used as loading control. n=9-10 per group *p<0.05 ***p<0.001 Student's t-test. Data expressed as mean ± SEM.

Taqman Gene Expression Assay	Manufacturer	Catalog #
ABCB10	ThermoFisher Scientific	Mm00497926_m1
CCL2	ThermoFisher Scientific	Mm00441242_m1
CCL3	ThermoFisher Scientific	Mm00441259_g1
CCL4	ThermoFisher Scientific	Mm00443111_m1
CD68	ThermoFisher Scientific	Mm03047343_m1
CXCL1	ThermoFisher Scientific	Mm04207460_m1
CXCL2	ThermoFisher Scientific	Mm00436450_m1
CXCL5	ThermoFisher Scientific	Mm00436451_g1
CXCR2	ThermoFisher Scientific	Mm00438258_m1
ELANE	ThermoFisher Scientific	Mm00469310_m1
Eukaryotic 18s rRNA	ThermoFisher Scientific	4333760
Glg1 (ESL-1)	ThermoFisher Scientific	Mm00486029_m1
Hprt	ThermoFisher Scientific	Mm00446968_m1
ICAM-1	ThermoFisher Scientific	Mm00516023_m1
IL-1b	ThermoFisher Scientific	Mm00434228_m1
IL-6	ThermoFisher Scientific	Mm00446190_m1
IL-10	ThermoFisher Scientific	Mm00439614_m1
MPO	ThermoFisher Scientific	Mm01298424_m1
SELE	ThermoFisher Scientific	Mm00441278_m1
SELP	ThermoFisher Scientific	Mm01295931_m1
Sytl1 (PSGL-1)	ThermoFisher Scientific	Mm00473300_m1
TNFa	ThermoFisher Scientific	Mm00443258_m1
VCAM-1	ThermoFisher Scientific	Mm01320970_m1

Table 1. List of Taqman primers used for qPCR

Manufacturer	Primary Antibody	Species	Primary Dilution	Secondary Dilution
Invitrogen MA5-27570	4HNE	Ms	1:1000	1:2000
ProteinTech 14628-1-AP	ABCB10	Rb	1:1000	1:2000
Abcam ab8227	Actin	Rb	1:5000	1:10,000
Abcam ab22595	Calnexin	Rb	1:5000	1:10,000
Cell Signaling 97272	Citrullinated Histone H3	Rb	1:1000	1:2000
Thermofisher PA1-29220	CXCL1	Rb	1:1000	1:2000
Cell Signaling 4499	Histone H3	Rb	1:1000	1:2000
Cell Signaling 6893	HMGB1	Rb	1:1000	1:2000
Cell Signaling 14569	MPO	Rb	1:1000	1:2000
Cell Signaling 89241	Neutrophil Elastase	Rb	1:1000	1:2000
Abcam ab14734	VDAC/Porin	Ms	1:1000	1:2000
Sigma V9131	Vinculin	Ms	1:5000	1:5000
ThermoFisher A-21121	Goatanti-Mouse AlexaFluor488	---	---	---
Cell Signaling 7076	Anti-mouse HRP-IgG	---	---	---
Cell Signaling7074	Anti-rabbit HRP-IgG	---	---	---

Table 2. List of antibodies used for Western blots.

REFERENCES

1. Lucey, M. R., Mathurin, P. & Morgan, T. R. Alcoholic Hepatitis. *N Engl J Med* **360**, 2758–2769 (2009).

2. Argemi, J. *et al.* Defective HNF4alpha-dependent gene expression as a driver of hepatocellular failure in alcoholic hepatitis. *Nat Commun* **10**, 3126 (2019).

3. Cho, Y. & Szabo, G. Two Faces of Neutrophils in Liver Disease Development and Progression. *Hepatology* **74**, 503–512 (2021).

4. Mookerjee, R. P. *et al.* Neutrophil dysfunction in alcoholic hepatitis superimposed on cirrhosis is reversible and predicts the outcome. *Hepatology* **46**, 831–840 (2007).

5. Cho, Y. *et al.* Neutrophil extracellular traps contribute to liver damage and increase defective low-density neutrophils in alcohol-associated hepatitis. *Journal of Hepatology* **78**, 28–44 (2023).

6. Shum, M. *et al.* ABCB10 exports mitochondrial biliverdin, driving metabolic maladaptation in obesity. *Science Translational Medicine* **13**, eabd1869 (2021).

7. Bertola, A., Mathews, S., Ki, S. H., Wang, H. & Gao, B. Mouse model of chronic and binge ethanol feeding (the NIAAA model). *Nat Protoc* **8**, 627–637 (2013).

8. Ueno, A. *et al.* Mouse intragastric infusion (iG) model. *Nat Protoc* **7**, 771–781 (2012).

9. Lazaro, R. *et al.* Osteopontin deficiency does not prevent but promotes alcoholic neutrophilic hepatitis in mice. *Hepatology* **61**, 129–140 (2015).

10. Khanova, E. *et al.* Pyroptosis by caspase11/4-gasdermin-D pathway in alcoholic hepatitis in mice and patients. *Hepatology* **67**, 1737–1753 (2018).

11. Profiling of mouse macrophage lipidome using direct infusion shotgun mass spectrometry. https://star-protocols.cell.com/protocols/359.

12. Chang, B. *et al.* Short- or long-term high-fat diet feeding plus acute ethanol binge synergistically induce acute liver injury in mice: An important role for CXCL1. *Hepatology* **62**, 1070–1085 (2015).

13. Chronic plus Binge Ethanol Feeding Synergistically Induces Neutrophil Infiltration and Liver Injury: a Critical Role for E-selectin - PMC. https://www.ncbi.nlm.nih.gov/pmc/articles/PMC3726575/.

14. Blaya, D. *et al.* Endothelial dysfunction markers predict short-term mortality in patients with severe alcoholic hepatitis. *Hepatol Int* **15**, 1006–1017 (2021).

15. Ge, X. et al. High Mobility Group Box-1 (HMGB1) Participates in the Pathogenesis of Alcoholic Liver Disease (ALD). *Journal of Biological Chemistry*, 33, 22672-22691 (2014)

16. Honda, M. & Kubes, P. Neutrophils and neutrophil extracellular traps in the liver and gastrointestinal system. *Nat Rev Gastroenterol Hepatol* **15**, 206–221 (2018).

17. Stoiber, W., Obermayer, A., Steinbacher, P. & Krautgartner, W.-D. The Role of Reactive Oxygen Species (ROS) in the Formation of Extracellular Traps (ETs) in Humans. *Biomolecules* **5**, 702–723 (2015).

18. Björnsdottir, H. *et al.* Neutrophil NET formation is regulated from the inside by myeloperoxidase-processed reactive oxygen species. *Free Radical Biology and Medicine* **89**, 1024–1035 (2015).

19. Douda, D. N., Khan, M. A., Grasemann, H. & Palaniyar, N. SK3 channel and mitochondrial ROS mediate NADPH oxidase-independent NETosis induced by calcium influx. *Proceedings of the National Academy of Sciences* **112**, 2817–2822 (2015).

20. Liesa, M., Qiu, W. & Shirihai, O. S. Mitochondrial ABC transporters function: The role of ABCB10 (ABC-me) as a novel player in cellular handling of reactive oxygen species. *Biochimica et Biophysica Acta (BBA) - Molecular Cell Research* **1823**, 1945–1957 (2012).

21. Arai, T. *et al.* Bilirubin Impairs Bactericidal Activity of Neutrophils through an Antioxidant Mechanism in Vitro. *Journal of Surgical Research* **96**, 107–113 (2001).

22. Boon, A. C., Hawkins, C. L., Coombes, J. S., Wagner, K. H. & Bulmer, A. C. Bilirubin scavenges chloramines and inhibits myeloperoxidase-induced protein/lipid oxidation in physiologically relevant hyperbilirubinemic serum. *Free Radic Biol Med* **86**, 259–268 (2015).

23. Yadav, U. C. S. Oxidative Stress-Induced Lipid Peroxidation: Role in Inflammation. in *Free Radicals in Human Health and Disease* (eds. Rani, V. & Yadav, U. C. S.) 119–129 (Springer India, 2015). doi:10.1007/978-81-322-2035-0_9.

24. Gabbs, M., Leng, S., Devassy, J. G., Monirujjaman, M. & Aukema, H. M. Advances in Our Understanding of Oxylipins Derived from Dietary PUFAs12. *Adv Nutr* **6**, 513–540 (2015).

25. Warner, D. R. *et al.* Ethanol and unsaturated dietary fat induce unique patterns of hepatic ω-6 and ω-3 PUFA oxylipins in a mouse model of alcoholic liver disease. *PLOS ONE* **13**, e0204119 (2018).

26. Gao, B. *et al.* Serum and fecal oxylipins in patients with alcohol-related liver disease. *Dig Dis Sci* **64**, 1878–1892 (2019).

27. Warner, D. *et al.* Linoleic Acid-Derived Oxylipins Differentiate Early Stage Alcoholic Hepatitis From Mild Alcohol-Associated Liver Injury. *Hepatology Communications* **5**, 947–960 (2021).

28. Douda, D. N., Grasemann, H., Pace-Asciak, C. & Palaniyar, N. A Lipid Mediator Hepoxilin A3 Is a Natural Inducer of Neutrophil Extracellular Traps in Human Neutrophils. *Mediators of Inflammation* **2015**, 1–7 (2015).

29. Alarcón, P. *et al.* Oleic and Linoleic Acids Induce the Release of Neutrophil Extracellular Traps via Pannexin 1-Dependent ATP Release and P2X1 Receptor Activation. *Frontiers in Veterinary Science* **7**, (2020).

30. Surmiak, M. *et al.* LTB4 and 5-oxo-ETE from extracellular vesicles stimulate neutrophils in granulomatosis with polyangiitis. *J Lipid Res* **61**, 1–9 (2020).

CONCLUSIONS AND FUTURE DIRECTIONS

Oxidative stress has been shown to play a role in pathogenesis of both NAFLD and ALD as both demonstrate altered electron transport function, decreased antioxidant defense mechanisms, and increased oxidative damage to macromolecules[1,2]

It is equivocal whether NAFLD increases or decreases mitochondrial function, which. It has been shown that diet-induced obesity in mice lower respiration of isolated hepatocytes. It is thought that defects in mitochondria calcium homeostasis lead to increase mitochondrial ROS and disrupt respiration leading to increased steatosis. In this same manner, insulin resistance is promoted by ROS-mediated c-Jun-N-terminal kinase (JNK) activation leading to hyperglycemia[3]. However, isolated liver mitochondria from ob/ob mice with steatosis did not demonstrate defects in respiration but rather increased beta-oxidation capacity[4]. This increase in respiration can also contribute to increased ROS impairment of phosphatases like PTP1B. This increase in ROS in NAFLD can be seen in increases of lipid oxidation/peroxidation products such as malondialdehyde (MDA) and 4-hydroxy-nonenal (4-HNE) as well as well oxidation of mitochondrial DNA leading to decrease copy number and increase mutation rate[5].This pro-oxidant milieu is further complicated by decreased antioxidant mechanisms. Patients with NAFLD have been shown to have decreased hepatic glutathione levels in addition to decreased hepatic antioxidants such as super oxide dismutase and catalase [5].

In chapter 1, we demonstrate that ABCB10 is maladaptively increased in NAFLD. While hepatic ABCB10 is dispensable for normal hepatocyte function, we found that hepatic ABCB10 deletion counteracts diet-induced obesity by increasing mitochondrial respiration and thus decreasing hepatic steatosis. Additionally, we found that increased hepatic ABCB10 expression in NAFLD increases intracellular antioxidant BR content, altering H_2O_2-redox signaling and leading to insulin resistance. These findings suggest that decreased mitochondrial respiration in NAFLD is deleterious, leading to increased steatosis, while increased respiration is protective in that lipotoxicity is prevented. Additionally, we show demonstrate that despite noted increases in ROS in patients and mouse models of NAFLD, not all antioxidants are equal. While antioxidant protection is necessary to prevent damage to macromolecules and further organellar dysfunction or cell death, there is an essential level of ROS needed maintain signaling cascades in NAFLD. While excess BR secondary to obesity-induced increases in hepatic ABC10 may seem beneficial, we demonstrate that disproportionate hepatic ABCB10-driven BR production leads to hyperactivation of PTP1B, dephosphorylation of insulin receptor, and subsequent insulin resistance and steatosis.

Similarly to NAFLD, studies of isolated hepatic mitochondrial respiration in ALD have shown equivocal results. Rat models of ALD have shown decreases in oxidative phosphorylation[6]. Evaluation of hepatic mitochondrial subunits shows this impairment in respiration is linked with decreased damage to mitochondrial DNA as well as the machinery of protein synthesis[7]. Conversely, isolated liver mitochondria from mice fed oral and intragastric ethanol have demonstrated increases in complex I and complex II respiration as well as increased beta oxidation[8]. This increase in mitochondrial respiration

is most likely adaptive to enhance alcohol metabolism as increased PGC1alpha and ETC complexes have been demonstrated, suggesting increased mitochondrial biogenesis. However, stimulation of mitochondrial respiration, coupled with alcohol catabolism by alcohol dehydrogenase and induction of detoxification by cytochrome P450 2E1, contribute to the characteristic hypermetabolic state of hepatocytes as well as increased ROS production[9]. Though species-specific differences in respiratory response to alcohol metabolism have been noted, alterations in mitochondrial respiration occurs despite increased oxidative damage to protein and mitochondrial DNA in both rats and mice[6,10]. Hypermetabolism in ALD produces excess reducing equivalents, facilitating increased electron transfer and subsequent production of super oxide anion as well as reductive stress. Studies of mitochondrial super oxide dismutase have also been equivocal, though homozygous SOD mutations lead to increased risk for severe ALD[11]. Mitochondrial glutathione, critical to eliminating H_2O_2, is shown to be decreased in rodents fed alcohol, which is not restored by glutathione precursor n-acetylcsyteine[12,13].

In chapter 2 we demonstrate that hepatic ABCB10 content is maladaptively diminished in a mouse model of severe AH, similar to that seen in patients with AH and in contrast to the increase in hepatic ABCB10 seen in NAFLD. Hepatic ABCB10 content is unchanged in a less severe ALD model of ASH homozygous hepatic ABCB10 deletion did not induce disease progression in mice as mitochondrial respiration, steatosis, hepatocellular damage, and neutrophil inflammation were not significantly worsened. Unique phenotypic differences have been noted in liver biopsies of patients with early ASH vs fulminant liver failure secondary to AH. Patients with AH display a distinct hypometabolism, altered redox state, and massive neutrophil inflammation.

While hepatic ABCB10 may not play a significant role in the pathological mechanisms of a milder form of ALD in ASH, we did demonstrate a role for hepatic ABCB10 in the more severe model of AH. We expected that increasing hepatic ABCB10 in mice with AH would improve mitochondrial respiration and steatosis but we did not observe differences in mitochondrial respiratory capacity or steatosis. However, we did discover that hepatic ABCB10 alters the inflammatory phenotype in ASH. Though we found that hepatic ABCB10 in NAFLD can regulate metabolism, we did not find that hepatic ABCB10 contributes to the hypometabolism previously noted. Interestingly hepatic ABCB10 in severe AH mitigates NET formation as seen by decreased citrullinated histone H3 (Arg17), a specific marker of NETs, without altering: 1) inflammatory cytokines and chemokines 2) integrins and selectin involved in immune cell diapedesis and transmigration or 3) decreasing hepatocyte DAMPs or bacterial PAMPs.

Though our data suggest hepatic ABCB10 has disease-specific roles in NAFLD and ALD, we have shown hepatic ABCB10 consistently alters hepatic redox. Healthy mitochondria produce H_2O_2 and have sufficient levels of antioxidants, such as peroxiredoxins and glutathione peroxidases, to mitigate potential oxidative damage due to excess[14]. Mitochondrial tend to be preferentially oxidized at cysteine residues[15], which contain reversibly oxidizable thiol groups allowing for rapid signal titration necessary for cellular and mitochondrial stress response. Nevertheless, H_2O_2 remains a toxic by-product especially in the context of decreased antioxidant buffering capacity seen in both NAFLD and ALD. The ability of cells to tightly regulate redox under homeostatic conditions is aided by the compartmentalization of H_2O_2 synthetic and degradative enzymes. This is supported by data demonstrating that hepatocyte-specific deletion of

mitochondrially localized glutathione peroxidase 1 (Gpx1), leading to increased H_2O_2 production and inactivation of PTP1B via cysteine residue oxidation decreasing phosphatase activity[16]. Deletion of HO1, upstream of ABCB10 in the heme degradation pathway, produces a similar phenotype to Gpx1 deletion[17]. Our data suggests that this may be achieved through reduction in BR production as evinced in our high-fat diet fed hepatocyte-specific ABCB10 knockout mice. Mitochondria from insulin resistant mice demonstrate tight interactions with the endoplasmic reticulum, which can also associate with cytosolic BLVR. Thus, ABCB10-mediated export of BV can allow for rapid conversion to BR at this contact sites, allowing for a microdomain of BV-BR trafficking into and out of the mitochondria. It is notable that studies of antioxidants in NAFLD have focused on hydrophilic species, further suggesting compartment specific roles of hydrophilic vs lipophilic antioxidants.

We further demonstrate the importance of redox microdomains in our study of ALD. While livers of mice and patients with severe AH demonstrate an ~70% reduction in ABCB10, the hepatocytes are not at a loss for BR. As ALD progresses to AH, hepatocytes tend to de-differentiate decreasing normal hepatocyte function as well as increasing the risk of hepatocellular carcinoma (HCC). This loss of hepatocyte function includes, but is not limited to, decreased production of albumin, decreased production of clotting factors, and decreased ability to conjugate BR. However, patients with ALD have marked hyperbilirubinemia and still develop hepatitis, as do mouse models of AH[18]. This is likely why we do not see altered mitochondrial function in our AH ABCB10 gain-of-function study; the high concentrations of BR have altered mitochondria respiratory function sufficiently that they are not affected by further ABCB10-mediated increases in

BR. What our data indicate is that hepatocyte-specific BR, and more likely further BR sub-cellular localization, is necessary for the protective effect we see of ABCB10 to decrease lipid peroxidation and mitigate deleterious NET formation in AH.

Understanding the disease-specific role of ABCB10 in hepatocytes offers insights not only into the differential pathogenesis of NAFLD and ALD but also highlights the role of ABCB10-mediated BR-sensitive redox microdomains Though ABCB10 is abundant in hematopoietic cells, cardiomyocytes, and hepatocytes, it is expressed in a multitude of tissues, such as pancreatic beta cells, macrophages, and skeletal muscle. Investigating the role of ABCB10 in these tissues, for which ABCB10 function has yet to be described, may reveal further insight into the role of BR antioxidant protection and signaling function in normal physiology and disease.

REFERENCES

1. Shum M, Ngo J, Shirihai OS, Liesa M. Mitochondrial oxidative function in NAFLD: Friend or foe? *Mol Metab*. 2020;50:101134. doi:10.1016/j.molmet.2020.101134

2. Teschke R. Alcoholic Liver Disease: Alcohol Metabolism, Cascade of Molecular Mechanisms, Cellular Targets, and Clinical Aspects. *Biomedicines*. 2018;6(4). doi:10.3390/biomedicines6040106

3. Arruda AP, Pers BM, Parlakgül G, Güney E, Inouye K, Hotamisligil GS. Chronic enrichment of hepatic ER-mitochondria contact sites leads to calcium dependent mitochondrial dysfunction in obesity. *Nat Med*. 2014;20(12):1427-1435. doi:10.1038/nm.3735

4. Brady LJ, Brady PS, Romsos DR, Hoppel CL. Elevated hepatic mitochondrial and peroxisomal oxidative capacities in fed and starved adult obese (ob/ob) mice. *Biochem J*. 1985;231(2):439-444.

5. Arroyave-Ospina JC, Wu Z, Geng Y, Moshage H. Role of Oxidative Stress in the Pathogenesis of Non-Alcoholic Fatty Liver Disease: Implications for Prevention and Therapy. *Antioxidants (Basel)*. 2021;10(2):174. doi:10.3390/antiox10020174

6. Cunningham CC, Coleman WB, Spach PI. The effects of chronic ethanol consumption on hepatic mitochondrial energy metabolism. *Alcohol Alcohol*. 1990;25(2-3):127-136. doi:10.1093/oxfordjournals.alcalc.a044987

7. Venkatraman A, Landar A, Davis AJ, et al. Modification of the mitochondrial proteome in response to the stress of ethanol-dependent hepatotoxicity. *J Biol Chem*. 2004;279(21):22092-22101. doi:10.1074/jbc.M402245200

8. Han D, Ybanez MD, Johnson HS, et al. Dynamic Adaptation of Liver Mitochondria to Chronic Alcohol Feeding in Mice: BIOGENESIS, REMODELING, AND FUNCTIONAL ALTERATIONS. *J Biol Chem*. 2012;287(50):42165-42179. doi:10.1074/jbc.M112.377374

9. Ceni E, Mello T, Galli A. Pathogenesis of alcoholic liver disease: Role of oxidative metabolism. *World J Gastroenterol*. 2014;20(47):17756-17772. doi:10.3748/wjg.v20.i47.17756

10. Han KH, Hashimoto N, Fukushima M. Relationships among alcoholic liver disease, antioxidants, and antioxidant enzymes. *World J Gastroenterol*. 2016;22(1):37-49. doi:10.3748/wjg.v22.i1.37

11. Degoul F, Sutton A, Mansouri A, et al. Homozygosity for alanine in the mitochondrial targeting sequence of superoxide dismutase and risk for severe alcoholic liver disease. *Gastroenterology*. 2001;120(6):1468-1474. doi:10.1053/gast.2001.24051

12. Hirano T, Kaplowitz N, Tsukamoto H, Kamimura S, Fernandez-Checa JC. Hepatic mitochondrial glutathione depletion and progression of experimental alcoholic liver disease in rats. *Hepatology*. 1992;16(6):1423-1427. doi:10.1002/hep.1840160619

13. Guidot DM, Brown LA. Mitochondrial glutathione replacement restores surfactant synthesis and secretion in alveolar epithelial cells of ethanol-fed rats. *Alcohol Clin Exp Res*. 2000;24(7):1070-1076.

14. Korshunov SS, Skulachev VP, Starkov AA. High protonic potential actuates a mechanism of production of reactive oxygen species in mitochondria. *FEBS Lett*. 1997;416(1):15-18. doi:10.1016/s0014-5793(97)01159-9

15. van der Reest J, Lilla S, Zheng L, Zanivan S, Gottlieb E. Proteome-wide analysis of cysteine oxidation reveals metabolic sensitivity to redox stress. *Nat Commun*. 2018;9:1581. doi:10.1038/s41467-018-04003-3

16. Merry TL, Tran M, Dodd GT, et al. Hepatocyte glutathione peroxidase-1 deficiency improves hepatic glucose metabolism and decreases steatohepatitis in mice. *Diabetologia*. 2016;59(12):2632-2644. doi:10.1007/s00125-016-4084-3

17. Jais A, Einwallner E, Sharif O, et al. Heme Oxygenase-1 Drives Metaflammation and Insulin Resistance in Mouse and Man. *Cell*. 2014;158(1):25-40. doi:10.1016/j.cell.2014.04.043

18. Morgan TR. Management of Alcoholic Hepatitis. *Gastroenterol Hepatol (N Y)*. 2007;3(2):97-99.